1971

Effects of variable zinc and oxygen concentrations on the optical properties of gallium phosphide single crystals

Tommy Dennis Gambrel
Lehigh University

EFFECTS OF VARIABLE ZINC AND OXYGEN CONCENTRATIONS ON THE OPTICAL PROPERTIES OF GALLIUM PHOSPHIDE SINGLE CRYSTALS

BY

TOMMY DENNIS GAMBREL

Abstract

The optical properties of solution grown p-type gallium phosphide single crystals were studied as a function of the concentrations of zinc and Ga_2O_3 added to the melt. Two series of crystals were considered in this work. One contained variable zinc with constant oxygen while the other contained variable oxygen with constant zinc.

The samples were annealed for five hours at 600°C. This time and temperature were chosen to maximize the formation of Zn-O complexes, which would thus maximize the photoluminescence efficiency of the crystals. The total external quantum efficiency, the photoluminescence spectra, and the absorption spectra were measured for each sample before and after annealing. The individual components of red and infrared external efficiencies were separated using the information contained in the total efficiency and photoluminescence spectra measurements. The absorption spectra measurements were used to qualitatively determine how the Zn-O complex and unpaired substitutional oxygen (O^+) concentrations changed during annealing. These concentrations were then related to the red and infrared external efficiencies.

For constant Ga_2O_3 doping (0.02 mole %), the optimum Zn doping concentration was found to be 0.02 mole %. For constant Zn doping (0.07 mole %), the optimum Ga_2O_3 doping concentration was found to be 0.04 mole %. The average photoluminescence efficiency at 0.02 mole % Ga_2O_3 and 0.02 mole % Zn was about twice as large as the average

photoluminescence efficiency at 0.07 mole % Zn and 0.04 mole % Ga_2O_3.

The total photoluminescence efficiency and the red external efficiency were found to increase in all cases after annealing. The infrared external efficiency increased in the majority of the samples upon annealing but in some cases either decreased in value or remained constant. For constant oxygen doping, both the Zn-O complex and O^+ concentrations increased after annealing.

A correlation was seen to exist between the red external efficiency and the concentration of Zn-O complexes, as well as between the infrared external efficiency and the O^+ concentration. The correlation was not direct, however, and the existence of other factors that affect the radiative processes was evident. These other factors include thermalization of electrons out of the Zn-O centers into the conduction band, the existence of a shunt path, the exciton emission decay time, and the bound-to-free transition decay time.

Experimental evidence was also found indicating the presence of a latent reservoir of oxygen in the crystals that becomes active in the recombination processes with annealing. This was concluded by observing that both the Zn-O center and O^+ concentrations increased after annealing in many of the samples. It was concluded also that oxygen is present in the crystals even in the absence of any intentional oxygen doping.

EFFECTS OF VARIABLE ZINC AND OXYGEN CONCENTRATIONS ON THE OPTICAL PROPERTIES OF GALLIUM PHOSPHIDE SINGLE CRYSTALS

BY

TOMMY DENNIS GAMBREL

A Thesis

Presented to the Graduate Committee

of Lehigh University

in Candidacy for the Degree of

Master of Science

in

Metallurgy and Materials Science

Lehigh University

1971

CERTIFICATE OF APPROVAL

This thesis is accepted and approved in partial fulfillment of the requirements for the degree of Master of Science.

May 17, 1971
Date

Michael R. Notis
Professor in Charge

G. L. Liard Dr
Chairman of the Department of
Metallurgy and Materials Science

Acknowledgements

This work was completed with the aid, advice, and assistance of several people.

The advice and guidance of Dr. M. R. Notis of Lehigh University throughout the course of this work is deeply appreciated. A special thanks is extended to Dr. J. M. Donahue of the Western Electric Engineering Research Center for invaluable aid in the experimental sections of this work, as well as for providing advice and assistance at all times. The support provided by Dr. A. E. Dugan, Research Leader of the group in which this work was performed, is also appreciated. Above all, gratitude is extended to these three people for the confidence they showed in the author.

Appreciation is also extended to Dr. J. M. Dishman and Dr. R. Caruso of Bell Telephone Laboratories for supplying the crystals for this study and to Dr. Dishman for his many stimulating and informative conversations. The aid of Dr. S. Y. Lien, S. J. Buzash, B. Menichelli, and E. Paulsen, all of Western Electric, is also acknowledged.

The author further wishes to thank Miss Bonnie Landis for her attitude and efficiency in the typing of this thesis.

Finally, the author is indebted to his wife, Mary, and children, Jennifer and Lance, for the time they gave for this work.

Table of Contents

List of Tables

List of Figures

Abstract

The optical properties of solution grown p-type gallium phosphide single crystals were studied as a function of the concentrations of zinc and Ga_2O_3 added to the melt. Two series of crystals were considered in this work. One contained variable zinc with constant oxygen while the other contained variable oxygen with constant zinc.

The samples were annealed for five hours at 600°C. This time and temperature were chosen to maximize the formation of Zn-O complexes, which would thus maximize the photoluminescence efficiency of the crystals. The total external quantum efficiency, the photoluminescence spectra, and the absorption spectra were measured for each sample before and after annealing. The individual components of red and infrared external efficiencies were separated using the information contained in the total efficiency and photoluminescence spectra measurements. The absorption spectra measurements were used to qualitatively determine how the Zn-O complex and unpaired substitutional oxygen (O^+) concentrations changed during annealing. These concentrations were then related to the red and infrared external efficiencies.

For constant Ga_2O_3 doping (0.02 mole %), the optimum Zn doping concentration was found to be 0.02 mole %. For constant Zn doping (0.07 mole %), the optimum Ga_2O_3 doping concentration was found to be 0.04 mole %. The average photoluminescence efficiency at 0.02 mole % Ga_2O_3 and 0.02 mole % Zn was about twice as large as the average

photoluminescence efficiency at 0.07 mole % Zn and 0.04 mole % Ga_2O_3.

The total photoluminescence efficiency and the red external efficiency were found to increase in all cases after annealing. The infrared external efficiency increased in the majority of the samples upon annealing but in some cases either decreased in value or remained constant. For constant oxygen doping, both the Zn-O complex and O^+ concentrations increased after annealing.

A correlation was seen to exist between the red external efficiency and the concentration of Zn-O complexes, as well as between the infrared external efficiency and the O^+ concentration. The correlation was not direct, however, and the existence of other factors that affect the radiative processes was evident. These other factors include thermalization of electrons out of the Zn-O centers into the conduction band, the existence of a shunt path, the exciton emission decay time, and the bound-to-free transition decay time.

Experimental evidence was also found indicating the presence of a latent reservoir of oxygen in the crystals that becomes active in the recombination processes with annealing. This was concluded by observing that both the Zn-O center and O^+ concentrations increased after annealing in many of the samples. It was concluded also that oxygen is present in the crystals even in the absence of any intentional oxygen doping.

I. Introduction

A. General

Solids can emit visible light in a variety of ways. A solid raised to sufficiently high temperature will emit light, a principle that is used in the tungsten incandescent lamp[1]. But practical considerations limit the efficiency and reliability of such a lamp. In electroluminescence, however, electronic energy is converted directly into light, and in principle, there is nothing to prevent this process from being efficient even in a device operating at room temperature. Since a large part of the electrical energy in this process is converted into heat rather than light, it is difficult to achieve efficiencies that are even remotely near the maximal theoretical values.

Semiconductor light emitting diodes (LED's) possess an interesting combination of properties[2]. They operate at low voltage and relatively low current, can emit visible radiation, and have fast switching times. Also, since they are semiconductor devices, the diodes are small, rugged, reliable, and have a long life. These features are useful in visual information displays, data processing and special opto-electric applications. The devices are particularly well suited to the telephone industry, because the power for semiconductor lamps can be supplied by a telephone line.

A p-n junction is fabricated for the light emitting devices because forward biasing of a p-n junction is the most efficient manner to obtain luminescence[2]. Further, it permits use of the same high

volume and inexpensive methods for construction that are used to build modern semiconductor diodes and transistors.

The material must be doped (impurity atoms introduced) so that it can behave as both an n-type or p-type semiconductor to be useful as a p-n junction light source [3]. The material must also be stable, so that it will not decompose in a normal moist-air environment. These two requirements limit the number of elements that can be used as light sources. In addition, the all-important problems involved in growing single crystals with controlled concentrations of impurities must be considered. Finally, the device must be reasonably efficient. When all of these factors are considered, GaP emerges as an excellent material for use as a semiconductor light source.

The primary function of light emitting diodes is the conversion of electrical energy into light. Various quantities can be used to measure this conversion [4]. For instance, the power efficiency is the ratio of the optical power output to the electrical power input. The external quantum efficiency is the ratio of the external photon current to the net charge current passing through the p-n junction. The internal quantum efficiency is the ratio of the number of photons generated by the electron-hole recombination in the p-n junction to the number of charge carriers passing through the junction.

If none of the photons generated in the junction are lost by absorption in the crystal prior to escaping through the diode surfaces,

then the external and internal quantum efficiencies are equivalent. However, the generated photons do experience absorption losses which are amplified by multiple reflections at the diode surfaces before escaping. The internal and external efficiencies are related through the absorption coefficient, the crystal volume, the emitting surface areas of the crystal, and the transmission coefficient.

The addition of zinc and oxygen to gallium phosphide creates a crystal which can be stimulated to emit red light at room temperature with reasonably high efficiencies. The simultaneous presence of the zinc and oxygen impurities introduces two deep radiative recombination centers in GaP[5]. Isolated oxygen is a deep donor approximately 0.9 ev below the conduction band[6]. Infrared radiative recombination occurs when electrons trapped at oxygen donors recombine with holes trapped on isolated zinc acceptors (D-A recombination); or when the trapped electrons at oxygen recombine with free holes in the valence band (B-F recombination)[7]. The peak energy of the infrared emission corresponds to about 1.37 ev (9100A°). The isoelectronic center formed by a zinc acceptor and an oxygen donor on nearest neighbor sites (Zn-O complex) also acts as a deep electron trap approximately 0.2 to 0.3 ev below the conduction band[8,9]. Red luminescence with a peak energy of about 1.77 ev (7000A°) originates from these Zn-O centers by one of two processes: pair recombination or recombination of bound excitons. Pair recombination occurs when the electrons at the Zn-O complex

recombine with holes on distant Zn acceptors.

An exciton is formed in the following manner (Figure 1): when zinc and oxygen occupy adjacent lattice sites, an electrically neutral or isoelectronic complex results. This complex acts as a deep electron trap in GaP [10]. This is assumed to be due primarily to the less effective shielding of the positive nuclear charge in O compared with P [10]. Therefore, electrons are attracted to this Zn-O complex and holes are subsequently trapped by Coulombic attraction, thereby creating a bound exciton[11].

Thus, there are two mechanisms that account for the red luminescence (exciton recombination and pair recombination) and two mechanisms that account for the infrared luminescence (donor-acceptor pair recombination (D-A), and bound electron to free hole (B-F) recombination). At room temperature, the red luminescence is essentially excitonic[9] and the infrared luminescence is essentially bound to free[7].

The various mechanisms that will be referred to in this work can be seen on a more descriptive basis by referring to Figures 1 and 2. Figure 2 shows the competing processes at the Zn-O energy level and at the oxygen energy level.

Bhargava[12] found that both the quantum efficiency of the exciton emission (7000A°) and the B-F emission (9100A°) increased after annealing. Annealing was performed at 600°C for five hours

in a N_2 gas atmosphere. Thermalization of electrons out of the Zn-O complex was postulated to be an important factor at room temperature, which reduced the exciton emission. Further, Bhargava suggested that changes in the ratio of intensities of exciton and B-F emission should not be related solely to changes in the densities of Zn-O complexes and substitutional oxygen. The author concluded this from the observation of other factors that changed after annealing, such as the exciton emission decay time, the B-F transition decay time, and the electron capture time for the Zn-O complex.

Casey and Trumbore[10] report that the luminescence intensity is a function of the Ga_2O_3 and Zn doping concentrations. The intensity was found to reach a maximum, then decrease at higher concentrations of both dopants. The authors proposed that the decrease in efficiency at high zinc values was due to screening by the holes or by Auger processes. The efficiency decrease at high oxygen doping was thought to indicate a lower solubility limit for oxygen than had been previously reported by Foster and Scardefield[13].

According to Dishman, DiDomenico, and Caruso[5], a low infrared efficiency generally implies a low red efficiency and vice versa. This suggested to Dishman et al. that the shunt path was the major variable factor influencing the efficiency at constant doping levels.

The low infrared efficiency resulted from the low capture cross section for oxygen, which was much lower than for Zn-O. The red efficiency was found to be limited by Auger recombination and by thermalization of the electrons out of the Zn-O centers.

B. General Annealing Effects

Several workers have commented on the effects of annealing on GaP crystals or diodes. No in-depth reports are available that consider all of the aspects of annealing. In this section, the results will be given on the annealing studies to date.

In 1963, Thomas et al.[14], studied the photoluminescence spectra of GaP solution grown crystals at measurement temperatures of 20°K and below. They annealed the crystals in an attempt to detect ion pairing effects. Annealing for 16 hours at 400°C, 16 hours at 700°C, and 44 hours at 800°C did not produce any marked changes in the pair spectra corresponding to recombination involving donors and acceptors on the same and on opposite lattice sites.

Logan et al.[15] studied the effects of heat treatment on p-n junctions in compensated solution grown GaP. They found that the photoluminescence efficiencies of the p-n junctions degraded with the heat treatment at 600°C for 5 minutes used to alloy ohmic contacts. They attributed the degradation to the diffusion of Zn to dislocations where it formed precipitates.

In a later study, Logan et al.[16] observed the effects of heat treatment on p-n junctions, grown by liquid-phase epitaxy, containing 0.07 mole % Zn and 0.02 mole % Ga_2O_3 and deposited on solution grown substrates. They found that the photoluminescence efficiency reached a maximum value after heat treatment for about 16 hours at temperatures in the range 400°C to 725°C, and remained approximately

constant with longer annealing times. The increase of efficiency with time of annealing was relatively insensitive to temperature in the indicated range.

The dependence of photoluminescence efficiency on the heat treatment of GaP (Zn, O) diodes was studied by Onton and Lorenz[17]. Their investigation revealed that the infrared and red electroluminescent peaks were related. Further, they found that recombination which resulted in infrared radiation subtracted from the total possible red emission. The efficiency was found to decrease after annealing at 900°C for 2 minutes, and returned to its former value following heating at 600°C for less than 30 minutes. Subsequent heat treatment at 900°C shifted a considerable part of the total emission into the infrared and further heating at 600°C returned the emission to the red. Thus, they were able to shift emission from the red to the infrared by heat treating the diode at high temperatures, and to return the emission into the red with a heat treatment at lower temperatures. These results suggested that a low temperature heat treatment could optimize the visible light output of GaP "red" diodes.

Following the work of Onton and Lorenz, Toyama et al.[18] observed heat treatment effects on diffused GaP diodes doped with Te and Ga_2O_3. Their results substantiated the results of Onton and Lorenz and revealed more information on annealing conditions and doping concentrations.

Toyama et al. also found that neither the overall lifetime of electrons in the p-region nor the ratio of red-to-infrared emission depended on the Ga_2O_3 concentration over the range of 0.004 to 0.2

mole % in the gallium melt. This was in contrast with the fact that the electroluminescence efficiency varied with the Ga_2O_3 concentrations.

C. Absorption Effects

Gershenzon et al.[19] reported that the maximum photoluminescence efficiency was obtained in solution grown crystals from Ga containing 0.1 atomic % Zn and 0.01 atomic % Ga_2O_3. Cuthbert et al.[20] found that 0.01 atomic % Zn and 0.01 atomic % Ga_2O_3 gave the maximum photoluminescence efficiency. However, they noted that the Zn-O exciton absorption of crystals doped with 0.01, 0.1, and 1.0 atomic % Zn increased up to 1.0 atomic % Zn although the efficiency dropped rapidly in this region. The Zn-O exciton absorption also increased with the amount of Ga_2O_3 in the Ga solution.

Dishman et al.[5] performed experiments which included the determination of the concentrations of the deep Zn-O and O centers. They showed that the concentrations of these centers could be determined from a series of five optical measurements:

1. Impurity absorption below the band gap energy
2. Internal photoluminescence quantum efficiency for below gap excitation
3. Internal photoluminescence quantum efficiency for above gap excitation
4. Photoluminescence saturation
5. Decay time of luminescence

They studied solution grown GaP (Zn,O) with doping levels of 0.07 mole % Zn and 0.02 mole % Ga_2O_3. Using the five optical measurements outlined above, Zn-O and O concentrations were found to be typically of the order 10^{16} and 10^{17} cm^{-3}, respectively. They found that annealing the samples at 400°C and 600°C increased the Zn-O complex concentration

by as much as a factor of five, but nonradiative recombination also increased by a comparable factor to limit the overall luminescent efficiency. It was difficult to achieve a unique separation of the Zn-O and O absorption bands due to the long low-energy tails on each peak. They noted that the red luminescence could not be excited preferentially because the absorption band for direct photoexcitation of the Zn-O level was overlapped entirely by the absorption band for oxygen. Also, a correlation could not be found in their work between the red and infrared efficiencies and the amount of oxygen doping. From this observation they concluded that the incorporation of oxygen into the GaP lattice during solution growth was uncontrolled.

Finally, they noted that the substitutional oxygen concentration increased with annealing at 600°C for 5 hours in three of the five crystals investigated. For the samples in which the concentration decreased, the magnitude of the decrease was not accounted for by the concentration of additional Zn-O pairs. An understanding of the mechanism for the change in substitutional oxygen concentration with annealing was not understood but was postulated to have involved the background oxygen in the lattice.

Recent work by Lacey[27] has been performed with optical measurements similar to those used in the present investigation. However, no work has been found which relates absorption measurements to photoluminescence efficiency or annealing effects.

D. Purpose

Because of major inconsistencies in previous studies, it appeared that there was a need for a comprehensive study of annealing effects on the optical properties of GaP as a function of variable doping concentrations. The purpose of this study is therefore:

1. To observe the effects of variable Zn and Ga_2O_3 doping on the photoluminescence efficiency of GaP single crystals.

2. To find the optimum doping concentrations of Zn and Ga_2O_3 in GaP.

3. To observe the effects of annealing on the photoluminescence efficiency in (Zn-O) - doped GaP.

4. To relate the changes in photoluminescence efficiency after annealing to the changes in the red-to-infrared integrated intensity ratio, as well as to the changes in the Zn-O complex concentration and unpaired substitutional oxygen concentration.

5. To study the existence of other factors that can affect the radiative recombination processes.

II. Theoretical Equations

Separation of Red and Infrared External Efficiencies

Two of the major parameters involved in studying the emission from GaP crystals are the red and infrared external quantum efficiencies. Because the two emission bands overlap, it is difficult to separate the two components in efficiency measurements. As a result, the total (red plus infrared) external quantum efficiency is measured. It would be beneficial to be able to determine the individual contributions of the red and infrared efficiencies to the total efficiency in order to monitor the red and infrared efficiencies independently. Thus, some quantitative measure of each efficiency would provide more information towards an understanding of the radiative processes. In this section, equations are derived which permit the determination of these individual components.

List of Symbols

η_x^T: Total external quantum efficiency

η_x^R: Red external quantum efficiency (7000A°)

η_x^{IR}: Infrared external quantum efficiency (9100A°)

η_i^T: Total internal quantum efficiency

η_i^R: Red internal quantum efficiency (7000A°)

η_i^{IR}: Infrared internal quantum efficiency (9100A°)

A: Red-to-infrared integrated intensity ratio

F: Correlation factor relating internal to external efficiency

$\bar{\alpha}$: Average absorption coefficient

V: Crystal volume

S: Emitting surface area of the crystal

T: Transmission coefficient

α_1: Absorption coefficient at 7000A°

α_2: Absorption coefficient at 9100A°

x: Thickness of sample

Derivation

We may define the total quantum efficiencies as:

$$\eta_x^T = \eta_x^R + \eta_x^{IR} \qquad (1)$$

$$\eta_i^T = \eta_i^R + \eta_i^{IR} \qquad (2)$$

and the ratio of the red and infrared internal quantum efficiencies as:

$$\frac{\eta_i^R}{\eta_i^{IR}} = A \qquad (3)$$

The total internal quantum efficiency may also be related to the total external quantum efficiency by the relation:

$$\eta_i^T = F\left(\eta_x^T\right) \qquad (4)$$

where:

$$F = 1 + \frac{4\,\bar{\alpha}\,V}{ST} \qquad (5)$$

Equations (4) and (5) are relations quoted by Lorenz[4,21] from the work of Cheroff, Stern and Triebwasser[22].

Using Equations (1) and (2), Equation (4) becomes:

$$\eta_i^R + \eta_i^{IR} = F\left(\eta_x^R + \eta_x^{IR}\right) \qquad (6)$$

We assume from Equation (6) that:

$$\eta_i^R = F\left(\eta_x^R\right) \qquad (7a)$$

$$\eta_i^{IR} = F\left(\eta_x^{IR}\right) \qquad (7b)$$

That is, we assume that the factor F, which relates internal to external efficiency, is approximately equal for the red and infrared emission. The implications of this assumption will be treated later.

Using Equations (7a) and (7b), Equation (1) can be written:

$$\eta_x^T = \frac{\eta_i^R}{F} + \frac{\eta_i^{IR}}{F} \qquad (8)$$

Substituting for η_i^{IR} from Equation (3), this becomes:

$$\eta_x^T = \frac{\eta_i^R}{F} + \frac{\eta_i^R}{AF} \qquad (9)$$

Collecting terms in Equation (9) gives:

$$\eta_x^T = \frac{\eta_i^R}{F}\left(\frac{1+A}{A}\right) \qquad (10)$$

Solving this for η_i^R we get:

$$\eta_i^R = \eta_x^T \,(F)\left(\frac{A}{1+A}\right) \qquad (11)$$

Using Equation (3) we see that:

$$\eta_i^{IR} = \eta_x^T \,(F)\left(\frac{1}{1+A}\right) \qquad (12)$$

Equations (11) and (12) may be substituted back into Equations (7a) and (7b), respectively, to give:

$$\eta_x^R = \eta_x^T\left(\frac{A}{1+A}\right) \qquad (13)$$

and

$$\eta_x^{IR} = \eta_x^T\left(\frac{1}{1+A}\right) \qquad (14)$$

which are the desired equations to determine the individual contributions of the red and infrared efficiencies to the total efficiency.

Therefore, by measuring the total external quantum efficiency (η_x^T) and the red-to-infrared integrated intensity ratio (A) at room temperature, the individual red and infrared efficiencies can be found.

The analysis is further simplified by using the algorithm of Dishman, Di Domenico and Caruso[5] to determine the value of the red-to-infrared integrated intensity ratio (A). Accordingly, the above-band gap excited internal efficiencies of the two emission bands can be found by an algorithm expressing the areas of the bands in terms of their peak heights. Thus, if P_R and P_{IR} are the values of the maxima of the red and infrared bands, then the room temperature internal quantum efficiencies of the emission bands are given by:

$$\eta_i^R = 0.263\, P_R \qquad (15)$$

$$\eta_i^{IR} = 0.236\, (P_{IR} - 0.0135 P_R) \qquad (16)$$

It was mentioned earlier that the assumption $F_R = F_{IR}$ was made. To examine this assumption, recall from Equation (5) that:

$$F = 1 + \frac{4\,\bar{\alpha}\,V}{ST}\,.$$

Assuming $F_R = F_{IR}$, then:

$$1 + 4\,\frac{\alpha_1 V}{ST_1} = 1 + 4\,\frac{\alpha_2 V}{ST_2} \qquad (17)$$

Equation (17) reduces to:

$$\frac{\alpha_1}{T_1} = \frac{\alpha_2}{T_2} \qquad (18)$$

but according to Moser and Urbach[23],

$$T_1 \approx e^{-\alpha_1 x}$$

$$T_2 \approx e^{-\alpha_2 x} .$$

Equation (18) then becomes:

$$\frac{\alpha_1}{e^{-\alpha_1 x}} = \frac{\alpha_2}{e^{-\alpha_2 x}} \qquad (19)$$

Obviously, Equation (19) is valid only when $\alpha_1 = \alpha_2$. Therefore, the assumption made in Equations (7a) and (7b) only requires that $\alpha_1 = \alpha_2$. Thus, for the assumption to be valid, the absorption coefficient at 7000A° must be approximately equal to the absorption coefficient at 9100A°. For 21 of 25 crystals measured, these absorption coefficients are, in fact, similar in this range and the assumption appears to be valid. The difference between α_1 and α_2 was typically 1-2 cm^{-1} out of 25-30 cm^{-1}. The assumption is less valid at very high zinc doping contents (0.11 mole % Zn and above) where free carrier absorption becomes more prevalent and the curve develops a long low-energy tail.

Two plausibility arguments are extended in conjunction with the above rationalization. First, accurate and reliable measurements of absorption coefficients are difficult to obtain. The error involved

in assuming $\alpha_1 = \alpha_2$ should not be much greater than the error in the actual measured quantities. Second, it is felt that the error involved in assuming $\alpha_1 = \alpha_2$ is <u>less than</u> the total error in actually measuring all of the quantities involved in calculating F; ie., the volume of the crystal, the average absorption coefficient, the emitting surface area, and the transmission coefficient.

III. Experimental Details

A. Measurements and Equipment

1. Photoluminescence Efficiency

The schematic of Figure 3 illustrates the experimental arrangement used to measure the total external quantum efficiency.* The sample was placed on a transparent platform in the middle of a reflective cavity that was enclosed in a light-tight black box. The laser beam entered the black box and struck a semi-reflective prism that split the beam into two parts. The first part of the beam was directed to a calibrated silicon solar cell used to monitor the intensity of the laser. The second part of the laser beam impinged on the sample. The luminescent energy emitted by the sample was measured by a calibrated silicon solar cell panel consisting of thirty individual solar cells.

The total external quantum efficiency is determined from the equation:

$$\eta_x^T = \frac{\text{number of photons emitted}}{\text{number of photons absorbed}}$$

which is, for the efficiency test set used:

$$\eta_x^T = 1.83 \frac{(\text{V solar panel} - \text{V background})}{\text{V laser monitor}}$$

where V represents a recorded voltage and the value of 1.83 represents the calibration factor for our efficiency test set. The calibration factor accounts for losses of the reflecting cavity, the solar cell

---

* This system was designed at Bell Telephone Laboratories and set up by Drs. J. M. Donahue and H. D. Pruett of Western Electric.

panel calibration, and the solar cell monitor calibration. It was found by measuring a diode of known efficiency in the test set.

All of the above voltages were measured with a Model 419A Hewlett Packard D.C. Null Voltmeter. The null voltmeter was connected to a Model 8100A Fluke Digital Multimeter to give accurate digital readouts of the voltages. For each sample, three individual measurements of efficiency were taken both before and after annealing and the average used as the recorded value of the efficiency. The source of excitation for these measurements was the 4880A° line of an argon ion laser (2 watt, Model 52 from Coherent Radiation).

Since the efficiency varies over the surface of the sample, care was taken to properly align each sample in the test set. The laser beam was first located visually inside the test set and the micrometer X-Y drive was used to place the front edge of the transparent platform under the laser beam. The sample was then placed on the platform directly behind the laser beam and the platform was moved so that the entire surface of the sample could be scanned in order to find the area of maximum efficiency. Visual inspection of the location of the laser beam on the sample then revealed the position of this area. The desired area was then marked on a photograph of the sample. With the aid of these photographs, each sample could be removed from the test set and remeasured later without loss of alignment. This procedure greatly reduced the time required to locate the maximum efficiency areas of the samples on subsequent measurements. All of these measurements were performed at room temperature.

2. Photoluminescence Spectra

The schematic of Figure 4 illustrates the experimental arrangement used to measure the photoluminescence spectra. As in the efficiency measurements, the source of excitation was the 4880A° line of an argon ion laser. The output power was monitored by a Model 235 Coherent Radiation Light Sampler.

When the laser beam strikes the crystal, energy is absorbed by the crystal resulting in the emission of red and infrared light. The emitted light is passed through a filter which prevents any laser light (5500A°) from reaching the monochromator. This stray excitation could result in "ghosts" in the spectra. A "sharp cut" Corning CS 3-69 filter was used for this purpose. Since it is possible for this filter to luminesce, a Signal Yellow Corning CS 3-76 filter was placed between the sharp cut filter and the laser to negate any harmful luminescence from the sharp cut filter. The lens was used to focus the sample emission onto the slit entrance of the monochromator.

The monochromator was a Spex 1800, 3/4 meter from Czerny Turner. The slit width used for all photoluminescence spectra was 2500 microns and the slit height was 5 millimeters. A stepping motor allowed the emission intensity to be scanned in steps of 25A°. For the undoped samples, 1000 photons per data point were counted. In all of the other samples, 10,000 photons per data point were counted.

An ITT FW 118 photomultiplier tube was used in conjunction with

a photon counting system* to detect the intensity of the light emitted from the sample. The useful range of the photomultiplier tube extends beyond the 6000A° - 10,000A° range used in experimentation.

The monochromator started at the initial wavelength of 6000A° and an electronic counter was turned on to initiate a cycle. The data acquisition system consisted of a Hewlett Packard 2547A data coupler and a Kennedy magnetic tape recorder. When the pre-set number of counts of 10,000 had been reached, the electronic counter sent a "print" command to the data acquisition coupler which recorded the time on a magnetic tape. A signal was simultaneously sent to the pre-set counter in order to control the monochromator stepping motor (the motor advanced the monochromator in 25A° steps). Hold-off commands were sent to the counter when data was being recorded and when the monochromator was being advanced. Once the hold-off command had been removed, the next signal pulse initiated a new cycle. This process continued until the 6000A° - 10,000A° spectral range had been recorded.

Since time cannot be measured directly with an electronic counter, the number of time units that were 10^{-5} seconds long in a given period (n_2) were counted for the length of time it took to count 10,000 signal pulses (n_1) from the photomultiplier tube. The value of n_2 was recorded on magnetic tape which was mounted on the

---

*This system was designed and built by Dr. H. D. Pruett of the Western Electric Engineering Research Center.

data acquisition system. This data on the magnetic tape was used as input data for a Fortran IV program. The program calculated the light intensity (photons/sec) from the relation:

$$r_s = \frac{f_2 \; n_1}{n_2} - r_d = \frac{(10^5)(10^4)}{n_2} - r_d = \frac{10^9}{n_2} - r_d$$

where r_s is the signal rate, f_2 is the electronic counter time base which was equal to 10^5Hz, n_1 is the number of signal counts made, and r_d is the dark count rate. After every spectral run, the dark current was recorded by removing the laser light from the sample. This number was inserted into the program by cards and it was converted to r_d using the relation:

$$r_d = \frac{f_2 \; n_1}{n_2}$$

The program also corrects for the non-uniform spectral response of the filters and monochromator as well as for the spectral sensitivity of the photomultiplier tube. After each data point had been adjusted and the intensity calculated, the program normalized the data. A punched paper tape that contained this normalized data was then obtained from an IBM-360 computer. The information on the paper tape was inserted into a Digital Equipment Corporation PDP-10 computer so that a Calcomp plotter could be used to generate graphs of the data.

Before making spectral measurements, the laser optics and the system optics were adjusted for maximum luminescence. The output

power of the laser was then adjusted so that the counter would count approximately 500,000 pulses/second (this included dark current pulses and pulses due to sample luminescence) at a wavelength of 7000A°, the peak intensity. If the number of pulses being counted in a short time interval is too large, pulse pile-up could occur, resulting in some of the pulses not being counted. On the other hand, if the number of pulses being counted in a short time interval is too small, it would take an unreasonable length of time to scan the spectrum. By using 500,000 counts/second, there were less than 2 percent of the pulses not counted as determined by the relation:

$$F = 1-e^{-ta}$$

where F is the fraction of pulses not counted, t is the rise time of the counter (40 nanoseconds), and a is the number of pulses being counted (500,000 pulses/second)[24].

3. Absorption Spectra

The schematic of Figure 5 shows the experimental arrangement used to measure the absorption spectra. The tungsten lamp is used as a very stable broad-band source. Using a tungsten lamp instead of a laser, the crystals will not receive enough energy to emit their characteristic radiation. Thus, the photomultiplier tube will see the light that is transmitted through the samples.

A Jarrell-Ash Monochromator is used to scan the wavelength region from 5500A° to 8700A°. The 5500A° wavelength corresponds roughly to the band gap energy of GaP. The photomultiplier detects the intensity of the light as a function of the wavelength (λ).

The absorption measurements are performed using the sample-in sample-out technique. The wavelength range is scanned for each of these two conditions, and both the incident and transmitted intensities are recorded every 20A°.

One of the two filters placed between the monochromator and the sample is to prevent the second-order spectrum from impinging on the sample. The second filter is used to reduce the intensity of the light from the source.

In order to enhance light-tightness in the system, black cloth covers were used. Since it was desired to actually place the sample as close as possible to the detector, a fiber optics tube was placed inside the photomultiplier housing. This served to collect the light from the source.

An ITT FW 130 photomultiplier tube served as the detector. The bandpass of the monochromator was 16.5A°. The accuracy of the system

was determined by a comparison technique with a Cary 14 Spectrophotometer. The optical density of two Corning filters was measured on the Cary 14, then the absorption coefficient as a function of wavelength was determined. These same filters were then measured on the absorption set-up and the system was aligned to given absorption coefficient values comparable to those obtained on the Cary 14. The error between the two different absorption coefficient measurements was less than one percent.

In the normal data runs, after the two monochromator scans were taken to obtain the incident and transmitted intensities as a function of wavelength, the data recorded on the magnetic tape was then fed into an IBM 360 computer along with a Fortran IV program to compute the absorption coefficient every 20A° over the 5500A° - 8700A° range. A Calcomp plotter was used to generate the absorption spectra plots of absorption coefficient as a function of wavelength. The Fortran IV program calculated the absorption coefficients from the equation:

$$T = \frac{I_t}{I_o} = \frac{(1 - R)^2 \quad (e^{-\alpha x})}{1 - (R^2) \quad (e^{-2\alpha x})}$$

from Kleinman and Spitzer[25], Dean and Thomas[26], and Lacey[27]. In this equation, I_t and I_o represent the measured values of the transmitted and incident intensities, respectively. The sample thickness is denoted by (x), the reflectivity by (R), the absorption coefficient by (α) and the transmission coefficient by (T).

B. Sample Preparation and Character

Two groups of solution grown GaP crystals, supplied by Dr. J. M. Dishman and Dr. R. Caruso of Bell Telephone Laboratories, were used for this study. One group was doped with a constant Ga_2O_3 and a variable zinc content (Table I) and the other group had constant zinc at variable Ga_2O_3 doping (Table II). The amount of each impurity covered a very broad range, as can be seen from Tables I and II. In addition,two undoped samples were included, resulting in a total of twenty-five samples used in this work.

Since the supplied crystals were in the form of raw chunks, some initial preparation was necessary. The crystals were first rough lapped with Linde M302 (20 micron) Al_2O_3 abrasive, then fine lapped with Linde M305 (15 micron) Al_2O_3 abrasive. Following this, the samples were rough polished and fine polished with Linde A (0.1 micron) and Linde B (0.05 micron) Al_2O_3 polish respectively. The samples were then rinsed in separate baths of acetone, methanol and deionized water in that order. A metallograph and a light microscope were used throughout the procedure to inspect for surface appearance, inclusions and inhomogeneities.

After annealing, the samples were given a very light etch (to remove any surface film) in a solution of one part H_2SO_4 (concentrated), one part 3% H_2O_2, and three parts deionized water for about three minutes. The amount of material removed by this process is negligible - 0.01 micron/minute when the etchant contains three parts H_2SO_4. There was no detectable difference in the surface quality of the samples after this etching step.

C. Annealing

The samples were annealed in an argon atmosphere at 600°C for five hours. A Marshall Combustion Tube Furnace (Model 1147) with a four-inch flat zone was used for this purpose. The annealing time and temperature were chosen to maximize the concentration of Zn-O complexes[5]. Cold tap water was used after annealing to quench in the high-temperature-created Zn-O complexes. After the quench and etch steps, the samples were again cleaned in acetone, methanol and deionized water.

IV. Results and Discussion

As was previously mentioned, the main objective of this work was to study the effects of variable zinc and Ga_2O_3 doping concentrations on the optical properties of gallium phosphide single crystals. To do this, the samples were annealed at 600°C for five hours. Measurements of the total external quantum efficiency, the photoluminescence spectra and the absorption spectra were taken both before and after annealing. All measurements were performed at room temperature. Using only room temperature measurements permits a direct comparison of the data by ensuring that the same mechanisms for the red and infrared emission are operative in each measurement. Bhargava[7] has shown that D-A pair emission dominates below 100°K and B-F emission begins to dominate above 160°K. Thus, at room temperature, we can speak of the red emission due to exciton recombination and the infrared emission due to bound-to-free recombination.

The values given in Table I are the measured total external quantum efficiencies, the measured integrated intensity ratios, and the calculated red and infrared external efficiencies at variable zinc doping with a constant doping content of Ga_2O_3. Table II represents the same parameters at variable Ga_2O_3 doping with a constant doping content of zinc. The quantities from Table I are plotted as a function of the mole % zinc added to the melt in Figures 23-29. The number of samples at each doping concentration

is shown in Table I and the points on each of the curves in Figures 23-29 represent an average value for those cases in which more than one sample was available at a particular doping concentration. The quantities from Table II are plotted as a function of the mole % Ga_2O_3 added to the melt in Figures 30-36. Average values were also used in these figures. Values for the typical carrier concentrations at each of the various doping levels are given in Table III.

A. Representative Cases of Photoluminescence Spectra and Absorption Spectra

Typical curves of the measured photoluminescence spectra are shown in Figures 6 through 13. These eight figures were chosen as representative cases from the photoluminescence spectra taken in this study. Figure 6 shows the photoluminescence spectra for an undoped sample. As shown, the emission was almost entirely in the infrared with no visible red emission. In Figure 7, the same sample is shown after annealing. The red emission peak at 7000A° increased but was still not visible. More scatter is present in Figures 6 and 7 than in the other curves because only 1000 photons per data point were counted (due to the low emission) as compared to 10,000 in all other cases.

Figures 8 and 9 show a typical spectrum before and after annealing, respectively, for a sample doped with 0.07 mole % Zn-0.10 mole % Ga_2O_3. The red-to-infrared integrated intensity ratio (ratio of the area under each peak) increased after annealing. All of the samples, with the exception of the undoped samples and the samples doped 0.50 mole % Zn-0.02 mole % Ga_2O_3, had curves similar to these figures.

Curves for the samples containing a very high Zn doping content (0.50 mole % zinc) are shown in Figures 10 and 11. As indicated by Figure 11, the intensity ratio decreased after annealing, which was opposite behavior to all other samples. The values given in Table I for η_x^R and η_x^{IR} indicate that the ratio decreased

because of a twofold increase in the infrared efficiency.

Another typical case is shown in Figures 12 and 13. These curves represent two identically doped samples with different total efficiencies. In comparing these two figures, the sample with the highest efficiency also had the highest intensity ratio. Regarding Figure 12, the total efficiency was 2.84% and the ratio was 2.12. In Figure 13, the total efficiency was 4.76% and the ratio was 4.62. This relationship between total efficiency and intensity ratio for samples of the same doping concentrations existed for every case without exception. Observation of Table I shows, for these two samples, that the sample with the highest total efficiency and the highest intensity ratio also had the highest red efficiency and the lowest infrared efficiency.

Results of representative cases of the absorption spectra measurements are shown in Figures 14 to 22. Figure 14 is the curve for an undoped sample. No structure is apparent in this curve and Figure 15 shows the curve to be of the same shape after annealing with a slight shift in the absorption coefficient at all wavelengths.

A more typical spectrum is shown in Figures 16 and 17. Annealing has caused the shape of the curve to change, the most notable change occurring around 5840A°. This peak is attributed[5] to Zn-O complexes, and it may be seen that this peak has increased upon annealing.

The curves of Figures 18 and 19 show a more "desired spectrum". The peak at 5840A° (due to Zn-O pairs[5]) was increased on annealing and the broad band around 7100A° (due to unpaired substitutional

oxygen[5]) decreased with annealing. These curves indicate that annealing causes the formation of more Zn-O pairs using the oxygen present substitutionally in the lattice for this case. Figure 20 is a much more graphic display of the difference between Figures 18 and 19. By plotting the magnitude of the difference between the unannealed and annealed absorption coefficients versus wavelength, the differences are maximized and the peaks at 5840A° and 7100A° are clearly visible. It should be noted that the peak at 7100A° actually represents a decrease in the absorption coefficient for the sample under consideration. However, for other samples, a similar curve could depict an increase in O^+.

The last case is shown in Figures 21 and 22. Represented here is the sample doped with 0.50 mole % Zn-0.02 mole % Ga_2O_3 and it may be noted that the shape of the curve is unchanged after annealing. The most dominant factor in these curves is the long low-energy tail (high wavelength) due to free carrier absorption that begins around 6700A° and extends into the infrared. Although the Zn-O peak is very distinct, this sample had the lowest total efficiency of the entire group. This result is surprising if it is believed that a direct relation exists between the Zn-O concentration and the efficiency. To be more explicit, if the absorption curves of two samples were compared, it might be expected that the sample with the highest efficiency would have the highest, or most prominent, Zn-O peak. This would be thought to indicate a larger concentration of Zn-O centers with a subsequent higher

efficiency. But this is not the case. For example, if the absorption curves of Figures 16 and 17 are compared to those of Figures 21 and 22, it is seen that the latter represents a much better Zn-O peak. However, the sample represented by Figures 16 and 17 has an efficiency almost ten times greater than the sample represented by Figures 21 and 22. This is strong support for the model extended by Bhargava[12] that the density of complexes is not directly related to the exciton emission. It also supports the theory presented by Dishman et al.[5] that other factors (thermalization, shunt path, lifetimes) have a very large effect on the emission processes.

B. Variable Zinc Doping

1. Photoluminescence Spectra and Efficiency Results

The results for the group of samples that contained a varying amount of zinc dopant with a constant level of Ga_2O_3 dopant are, as mentioned, represented by Table I and Figures 23 to 29. Comparison of these figures reveal some interesting general trends in the data as well as some special cases.

The variation in the total external efficiency with zinc doping content is shown in Figure 23. This efficiency reached a maximum at the doping level of 0.02 mole % Zn-0.02 mole % Ga_2O_3, then decreased as the amount of zinc doping was increased. The average total efficiency at the maximum was about 5.4 % before annealing and about 6.7 % after annealing. The total efficiency increased for all samples after annealing.

Figure 24 indicates the red-to-infrared integrated intensity ratio increased with annealing except for the samples containing a very high zinc doping content (0.50 mole % Zn-0.02 mole % Ga_2O_3). Thus, with this exception, the increases in total efficiency with annealing were accompanied by increases in the intensity ratio. Table I shows that the intensity ratio decreased for the samples doped 0.50 mole % Zn because the infrared efficiency increased to over twice its original value.

The sample doped with 0.07 mole % Zn exhibited a very large increase in the intensity ratio with annealing as shown in Figure 24. Inspection of Figures 25 and 26 indicates that the red external

efficiency increased and the infrared external efficiency decreased with annealing in this case. Thus, the large increase in intensity ratio was due to an increase in the red external efficiency along with a decrease in the infrared external efficiency. All of the other samples showed an increase in the red external efficiency (Figure 25) after annealing while the infrared external efficiency (Figure 26) either increased in value or remained relatively constant. One of the significant factors from these results is the fact that the red external efficiency was improved at the expense of the infrared external efficiency for only one case. In general, the red and infrared external efficiencies were both improved by the annealing cycle.

Comparing Figure 23 to Figure 25, it is noted the shape of the curves are very similar. This was expected since the red external efficiency represented 92% to 98% of the total external efficiency in the usual case. Comparison of Figure 25 to Figure 26 reveals a correlation between the red and infrared external efficiency. The highest red external efficiencies were at the doping levels of 0.007 mole % Zn and 0.02 mole % Zn. The highest infrared external efficiencies occurred at these same doping levels. Thus, a high red efficiency implied a high infrared efficiency. Above the doping level of 0.02 mole % Zn, these figures also show a low red efficiency correlates with a low infrared efficiency.

2. Absorption Spectra Results

If the variables in Smakula's Equation[28] could be determined, this equation could be used to find the concentrations of Zn-O centers and unpaired substitutional oxygen. The equation is:

$$N_o = K \alpha_m W$$

where N_o = impurity concentration (Zn-O or O^+)

α_m = absorption coefficient at peak of the impurity band

W = half-width of impurity absorption band

$$K = \frac{1.29 \times 10^{17}}{f} \quad \frac{n}{(n^2 + 2)^2}$$

and n = index of refraction

f = oscillator strength of the electronic transition

Since data are not available to calculate or estimate values for K and W, the impurity concentrations cannot be determined in this work. However, the values of α_m have been measured, and since the impurity concentration is proportional to α_m, changes in this parameter with annealing may be assumed to indicate changes in the impurity concentration. This assumes the other parameters (K and W) do not change after annealing. The absorption coefficient at the peak of the Zn-O band at 5840A° will be referred to as α_R since the Zn-O centers are responsible for red emission. The absorption coefficient at the peak of the oxygen band at 7100A° will be called α_{IR}, since unpaired substitutional oxygen is responsible for infrared emission.

Changes in the peak absorption coefficients are shown in Figures 27, 28, and 29. Figure 27 shows the variation of α_R with zinc doping content, Figure 28 shows the variation of α_{IR} with zinc doping content, and Figure 29 shows the variation in the ratio of α_R to α_{IR} with zinc doping content. Since it is noted that α_R and α_{IR} either both increase or both decrease after annealing, the ratio is used to qualitatively determine which quantity experienced the largest change due to annealing.

The curves shown in Figure 27 indicate the absorption coefficient at 5840A° increased after annealing for every sample except the one that was doped 0.07 mole % Zn-0.02 mole % Ga_2O_3. The curves shown in Figure 28 for the absorption coefficient at 7100A° indicate the same results. It may be recalled that the sample containing 0.07 mole % Zn also had the largest increase in red-to-infrared integrated intensity ratio upon annealing, which was due in part to a decrease in the infrared external efficiency. Thus, the decrease in α_{IR} with annealing correlates with the decrease in infrared external efficiency. For all other cases in the absorption measurements, an increase in α_R was accompanied by an increase in α_{IR}.

The above results indicate that the annealing procedure enhanced the formation of Zn-O centers as well as the amount of unpaired substitutional oxygen. This infers a source of oxygen is present in the crystals that is not substitutional since it would be expected that the unpaired substitutional oxygen concentration would decrease when the Zn-O center concentration increased.

Using these absorption results, it is possible to account for the observed changes in the red and infrared external efficiencies. First, it is recalled that the red external efficiency increased with annealing in every case. The increase in this efficiency is correlated with increases in the number of Zn-O centers as seen in the absorption measurements. Similarly, increases in the infrared external efficiency are correlated with increases in the unpaired substitutional oxygen concentration.

3. Comparison of Variable Zinc Doping Results to Theory

The optimum doping concentration as found in the measurements of the total efficiency (Figure 23) agrees well with that found by other workers[9, 19, 29]. For this group of samples, the optimum was found to be 0.02 mole % Zn and 0.02 mole % Ga_2O_3.

As previously mentioned, Figure 25 shows the variation in red external efficiency with zinc doping content and Figure 26 shows the variation in infrared external efficiency with zinc doping content. Comparison of these two figures showed that a low red external efficiency was correlated with a low infrared external efficiency and vice versa. This result was also found by Dishman, Di Domenico and Caruso[5] for the relation between the internal red and infrared efficiencies. They theorized[5] that this correlation suggested the shunt path (γ_{ns} in Figure 2) was the major variable influencing the efficiency at constant doping levels. The correlation found in this work was for variable doping levels of zinc.

Bhargava[12] has stated that annealing will cause both the red and infrared efficiency to increase. Other experimenters such as Onton and Lorenz[17] have felt that an increase in the red efficiency meant a decrease in the infrared. That is, as more Zn-O complexes form to promote exciton recombination, the bound-to-free recombination paths should be fewer in number due to oxygen moving to nearest-neighbor sites. The results found here for variable zinc doping indicate the red can improve without a decrease in the infrared. This infers that other mechanisms are present which affect the red and

infrared efficiencies (such as thermalization of electrons out of the Zn-O complex, or the shunt path) that are less prevalent after annealing. In fact, for the majority of the samples considered, the infrared was a small contribution to the total efficiency.

Another factor to consider regarding the increase in both the red and infrared efficiency is the total oxygen concentration. If a latent reservoir of oxygen were present in the crystals, such as at interstitials or precipitates, then both the number of Zn-O pairs and the number of unpaired substitutional sites could increase upon annealing. This would account for the increase in both the red and infrared efficiency. The possibility of a source of nonsubstitutional oxygen in the crystals has been previously suggested by Dishman et al.[5]. Kowalchik et al.[29] have found Ga_2O_3 precipitates in GaP (Zn,O) layers grown by liquid-phase epitaxy, which experimentally indicates a source of nonsubstitutional oxygen.

Foster and Scardefield[13] have noted that low concentrations of Zn-O centers in optimally doped GaP could be due to trace impurities that degrade the luminescent process. The impurities could compete for the electron bound to the Zn-O complex and introduce alternate decay paths. The fact that the Zn-O concentration decreased for the sample doped with 0.07 mole % Zn-0.02 mole % Ga_2O_3, with an increase in the red efficiency, could be due to a decrease in these nonradiative competing processes.

The curves of Figure 25 for the red external efficiency vs. mole % zinc show the efficiency reaching a peak at 0.02 mole % Zn-0.02 mole % Ga_2O_3, then decreasing as the impurity concentration was increased. Angelova et al.[30] obtained essentially the same type of curves for the dependence of the intensity of the red band on the zinc content in the melt. For a Ga_2O_3 content of 0.035 mole %, they found a peak intensity at 0.03 atomic % zinc. They theorized the decrease in intensity with zinc doping could be due to an increase in imperfections at the higher doping levels or an increase in nonradiative transitions. Sinha and DiDomenico[11] also report the photoluminescence intensity for Zn-O emission as reaching a maximum and decreasing at high concentrations of zinc.

C. Variable Ga_2O_3 Doping

1. Photoluminescence Spectra and Efficiency Results

The results for the group of samples that contained a varying amount of Ga_2O_3 dopant with a constant level of zinc dopant are represented by Table II and Figures 30 to 36.

The total efficiency, red-to-infrared integrated intensity ratio and red external efficiency are represented by Figures 30, 31 and 32, respectively, as a function of the Ga_2O_3 doping content. These figures indicate that every sample exhibited an increase in these three parameters after annealing. Also, a maximum in all three parameters under question occurred at a doping concentration of 0.07 mole % Zn-0.04 mole % Ga_2O_3. Thus, the total efficiency and the integrated intensity ratio were both enhanced by annealing and an increase in the red external efficiency was seen to partially account for the improvement in these two parameters.

The total efficiency at the optimum doping concentration for this group of samples was about 2.2% before annealing and about 3.2% after annealing. Recalling the total efficiency results at the optimum in variable zinc doping (5.4% before annealing and 6.7% after annealing), it is seen that the actual optimum doping concentration is 0.02 mole % Zn-0.02 mole % Ga_2O_3. That is, the total efficiency at the optimum in variable zinc doping (0.02 mole % Zn-0.02 mole % Ga_2O_3) is approximately double the total efficiency at the optimum in variable Ga_2O_3 doping (0.07 mole % Zn-0.04 mole % Ga_2O_3).

The infrared external efficiency as a function of the Ga_2O_3 doping content is shown in Figure 33. This efficiency was seen to either increase or decrease after annealing, depending on the doping concentration. It is significant from this data that the samples containing the optimum doping concentration (0.07 mole % Zn-0.04 mole % Ga_2O_3) exhibited an increase in the infrared efficiency with annealing. Thus, the red efficiency was not improved at the expense of the infrared efficiency at the optimum doping level. However, the red efficiency was improved at the expense of the infrared efficiency for several other samples, as indicated in Figures 32 and 33.

Another point of interest concerns the sample that contained no intentional oxygen doping (0.07 mole % Zn-0.00 mole % Ga_2O_3). This sample had a total efficiency comparable to the samples at other doping levels and the total efficiency improved with annealing. This infers the undoped sample actually contained some oxygen since the Zn-O pairing was enhanced.

2. Absorption Spectra Results

Results of the absorption measurements are shown in Figures 34, 35 and 36. Figure 34 shows the variation in α_R with Ga_2O_3 doping, Figure 35 shows the variation in α_{IR} with Ga_2O_3 doping and Figure 36 shows the variation in α_R/α_{IR} with Ga_2O_3 doping.

For the sample doped 0.07 mole % Zn-0.00 mole % Ga_2O_3, both α_R and α_{IR} increased with annealing. The ratio of these two values shows α_{IR} increased more than α_R increased. Thus, the increase in red efficiency agrees with the increase in α_R (or the number of Zn-O centers). Since the infrared efficiency remained constant while α_{IR} increased, this indicates something else occurred to prevent more infrared radiation from the higher ionized oxygen concentration.

For the samples doped 0.07 mole % Zn-0.01 mole % Ga_2O_3, α_R increased while α_{IR} decreased. Remembering that the red efficiency increased while the infrared decreased, the results are seen to be favorable in terms of a model which predicts increases in the red efficiency with increases in the number of Zn-O centers and decreases in the infrared efficiency with decreases in the ionized oxygen content.

Another representative case occurred for the samples doped 0.07 mole % Zn-0.02 mole % Ga_2O_3. The values of α_R and α_{IR} decreased with α_{IR} decreasing the largest amount. Coupled with the knowledge that the red efficiency increased and the infrared decreased, and the assumption that the absorption coefficients are proportional to

the defect concentration, it is proposed that the efficiency changes are not solely related to changes in the Zn-O and ionized oxygen contents.

The samples at any given doping content can be viewed in the manner above by observation of Figures 30 to 36. Proceeding in this manner for each sample, it is apparent that no direct correlation can be found to apply in all cases between the efficiencies and the number of recombination centers.

3. Comparison of Variable Ga_2O_3 Doping Results to Theory

Some of the results found for the group of samples that contained variable Ga_2O_3 doping levels are similar to the results found for the group of samples that contained variable zinc doping levels. However, additional information can be obtained from the results of the group of samples that contained variable Ga_2O_3 doping levels. The main results for these samples are considered in this section.

One sample in this study was not intentionally doped with oxygen. However, the sample had a reasonably high efficiency and indicated an increase in both Zn-O and O^+ concentration in the absorption measurements after annealing. Obviously, the sample must have contained oxygen for this to occur. It has been found that oxygen is inevitably incorporated into GaP during the growth process even in the absence of intentional oxygen doping. Miyauchi et al.[31] indicate the source of this oxygen is the quartz ampoules used for growing the crystals.

Dishman, Di Domenico and Caruso[5] studied solution grown samples that were doped with 0.07 mole % Zn-0.02 mole % Ga_2O_3. They found that the unpaired substitutional oxygen concentration could increase with annealing at 600°C for 5 hours. From this result they inferred a source of nonsubstitutional oxygen was present in the crystals. In this study, it was also found that the O^+ concentration could increase with annealing at 600°C for 5 hours. This also indicates a latent source of oxygen can be present in the crystals. Similar results were found at variable zinc doping levels.

The existence of factors other than the Zn-O and O^+ concentrations that affect the luminescence are also present in this data. For example,

some samples showed an increase in the red external efficiency while the Zn-O concentration decreased. The infrared external efficiency and O^+ concentrations were also found to vary oppositely in some cases. These cases thus indicate the presence of other competing processes such as thermalization of electrons out of the Zn-O complex or a changed in the shunt path, as suggested by Dishman et al.[5].

The red external efficiency increased for all of the samples at variable Ga_2O_3 doping. However, the infrared external efficiency either increased or decreased in value depending on the doping level. For the samples doped 0.07 mole % Zn-0.04 mole % Ga_2O_3, both the red and infrared efficiencies were improved by annealing. This result does not agree with the results of Hughes[32], who performed annealing experiments on samples doped with 0.07 mole % Zn-0.04 mole % Ga_2O_3. Hughes (in agreement with Onton and Lorenz[17]) stated that at this composition, the red emission was enhanced at the expense of the infrared emission. However, the differences between the two studies can be attributed to a difference in the doping levels used in the crystal growth procedures. Investigation of Table I shows, for a range of zinc doping levels, that the infrared efficiency can remain relatively constant after annealing. Changes in the red efficiency are seen to be the dominant factor in Table I. Figure 26 also shows that the infrared experienced only small changes with annealing. Thus, although the present investigation disagrees with the interpretation that the red efficiency is enhanced at the expense of the infrared efficiency, it has no influence on the validity of the Zn-O ion pairing model that Hughes used in his work.

V. Conclusions

Following are the conclusions of this investigation relating to the luminescence of gallium phosphide single crystals:

1. Although undoped GaP crystals do not emit any visible light, the crystals can emit visible red light when doped only with zinc. Since oxygen is necessary to form Zn-O pairs for exciton recombination, this infers that oxygen is present in the crystals as a residual impurity, presumably from the solution grown process.
2. The total efficiency of GaP is improved by doping the crystals with Zn and Ga_2O_3. For a constant doping concentration of 0.02 mole % Ga_2O_3, the optimum Zn doping concentration is 0.02 mole % Zn. For a constant doping concentration of 0.07 mole % Zn, the optimum Ga_2O_3 doping concentration is 0.04 mole % Ga_2O_3.
3. To obtain the highest total efficiency, the crystals should be doped with about 0.02 mole % Zn and 0.02 mole % Ga_2O_3. A lower concentration of Zn (0.007 mole % Zn) at the same Ga_2O_3 concentration will also produce very high efficiencies.
4. The total external efficiency is normally composed of 92% to 98% red emission, with infrared constituting the remainder of the total value.
5. It was found in this work, as well as in the work of Dishman et al., that a low red efficiency generally implies a low infrared efficiency and vice versa. Dishman et al. indicates that this infers the shunt path is a major variable factor influencing the efficiency. This work, which indicates that the Zn-O center

and O^+ concentrations as determined from the absorption measurements may not correlate directly with the efficiency, also leads to the same conclusion.

6. At a constant doping level of 0.02 mole % Ga_2O_3 with a Zn doping range of 0.007 to 0.50 mole % Zn, the efficiency of the red emission can be improved by annealing at 600°C for five hours. This annealing cycle also enhances the red emission at a constant doping level of 0.07 mole % Zn with a Ga_2O_3 doping range of 0.00 to 0.10 mole % Ga_2O_3.

7. Annealing at 600°C for five hours can improve the efficiency of the infrared emission as well as the efficiency of the red emission. Normally, both efficiencies are improved by annealing at this time and temperature. Thus, the efficiency of the red emission is not usually enhanced at the expense of the infrared emission. At two of the doping concentrations used commonly in past experimental work (0.07 mole % Zn-0.04 mole % Ga_2O_3 and 0.02 mole % Zn-0.02 mole % Ga_2O_3), the red emission was not enhanced at the expense of the infrared emission.

8. An increase in the red-to-infrared integrated intensity ratio is correlated with an increase in the red external efficiency. A decrease in this intensity ratio is correlated with an increase in the infrared external efficiency.

9. At variable Zn doping, an increase in the red external efficiency is accompanied by an increase in the number of Zn-O centers. Also, an increase in the infrared external efficiency correlates

with an increase in the unpaired substitutional oxygen (O^+) concentration. At variable Ga_2O_3 doping, these direct relations do not seem to exist.

10. The efficiency of the red emission can improve with an apparent decrease in the number of Zn-O centers. Also, the efficiency of the infrared emission can improve with an apparent decrease in the O^+ concentration. This suggests the red and infrared efficiencies are not solely dependent upon the concentrations of Zn-O centers and unpaired substitutional oxygens. Thus, other factors must be involved in the recombination processes (thermalization, shunt path, lifetimes).

11. For any given crystal, the concentrations of both the Zn-O centers and unpaired substitutional oxygens can increase upon annealing. This implies a source of nonsubstitutional oxygen can be present in the crystals and the oxygen moves to substitutional sites during the heat treatment.

VI. Suggestions for Further Study

The amount of zinc and oxygen in GaP crystals is not necessarily equivalent to the amount of Zn and Ga_2O_3 doping concentrations. The carrier concentrations can be different in equally doped samples which will result in different values of efficiencies. Measurement of these carrier concentrations would give more information to account for the difference in total efficiencies between equally doped samples. However, since the optimum doping concentrations seem to be well defined with agreement between several independent sources, future work should consider the physics of the recombination processes under these optimum conditions.

Further annealing studies could be beneficial to quantitatively relate the red efficiency to the Zn-O center concentration and the infrared efficiency to the O^+ concentration. With this information, more knowledge on the nonradiative processes associated with the Zn-O and O^+ energy levels would be available to further understand the emission processes. Additional effort to improve the efficiency would probably be most fruitful if directed toward these nonradiative processes (thermalization, shunt path, lifetimes) since it appears the efficiencies are not directly related to the Zn-O and O^+ concentrations.

ENERGY LEVEL DIAGRAM OF Zn-O IN GaP

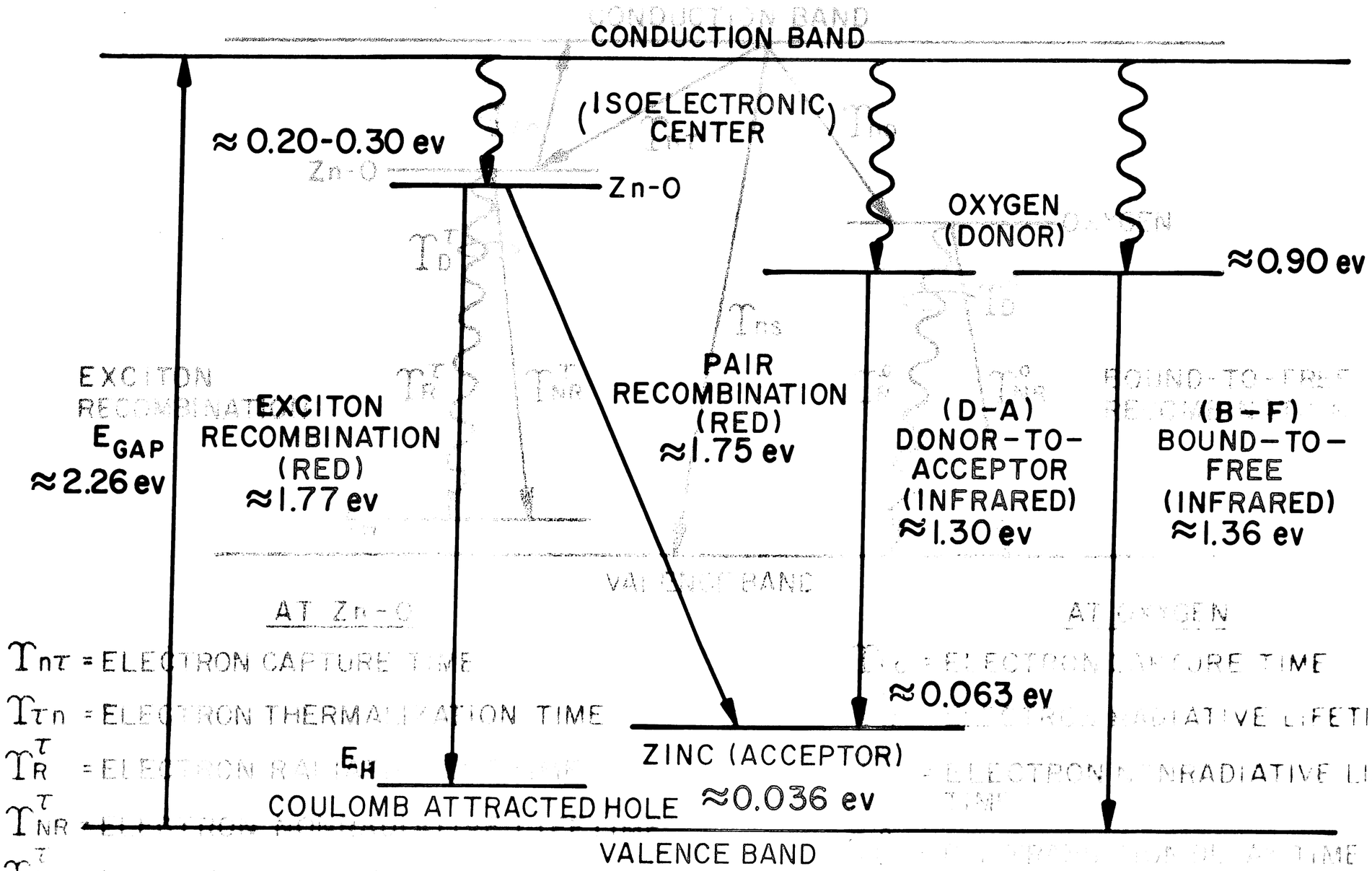

FIGURE 1

ENERGY LEVEL DIAGRAM OF Zn-O IN GaP

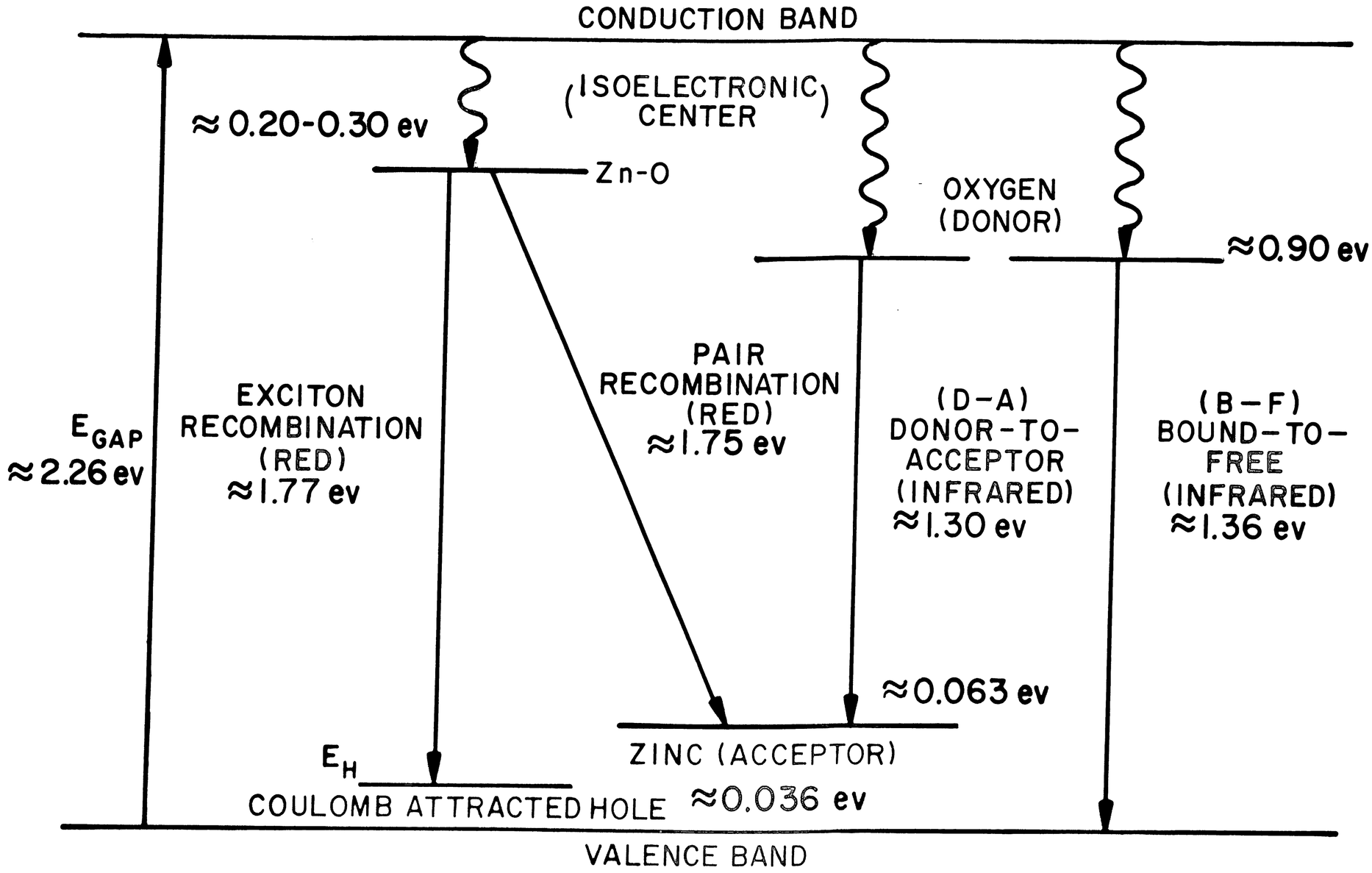

FIGURE 1

ENERGY LEVEL DIAGRAM SHOWING LIFETIME FACTORS

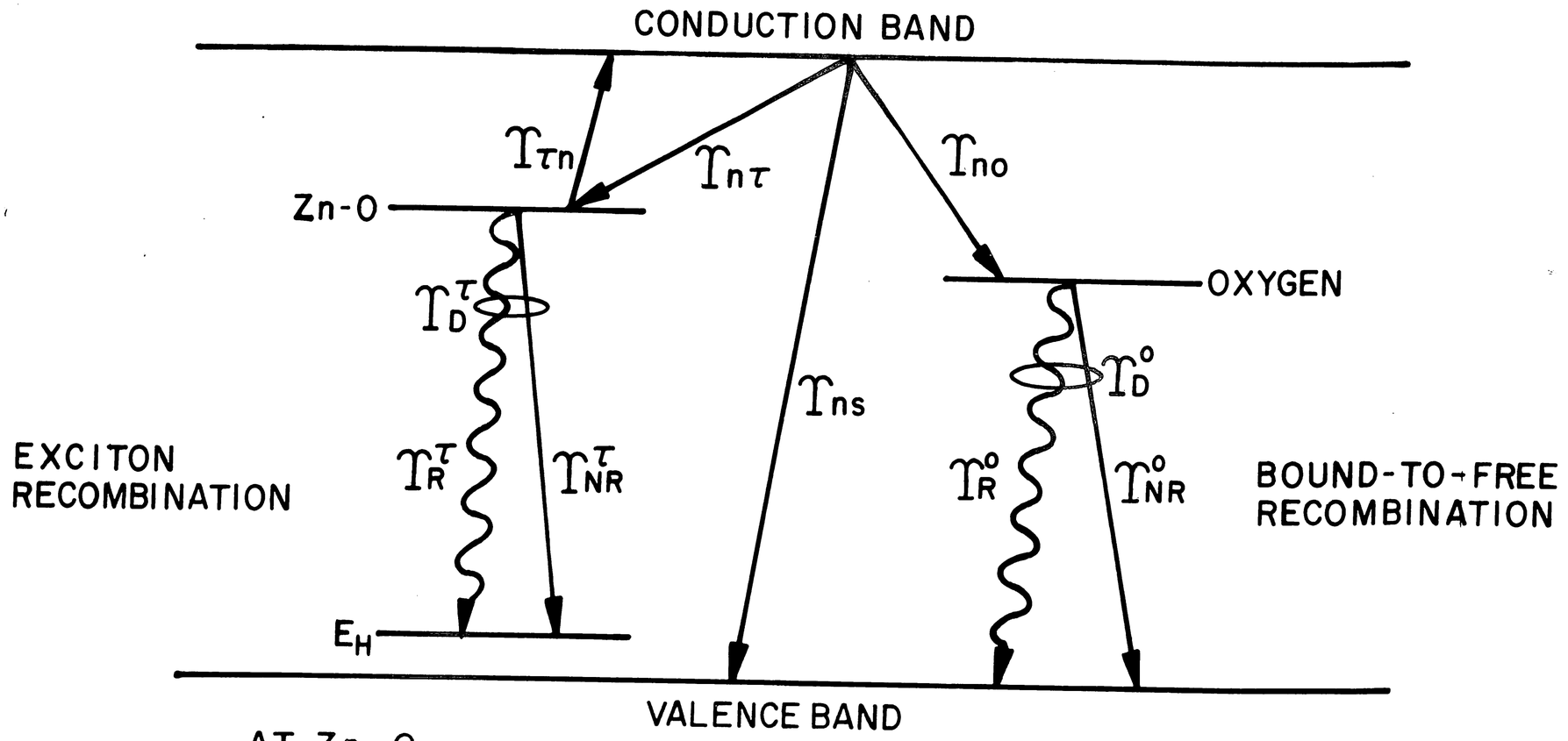

57.

AT Zn-O

$\Upsilon_{n\tau}$ = ELECTRON CAPTURE TIME

$\Upsilon_{\tau n}$ = ELECTRON THERMALIZATION TIME

Υ_R^τ = ELECTRON RADIATIVE LIFETIME

Υ_{NR}^τ = ELECTRON NONRADIATIVE LIFETIME

Υ_D^τ = EXCITON EMISSION DECAY TIME

AT OXYGEN

Υ_{no} = ELECTRON CAPTURE TIME

Υ_R^o = ELECTRON RADIATIVE LIFETIME

Υ_{NR}^o = ELECTRON NONRADIATIVE LIFETIME

Υ_D^o = B-F TRANSITION DECAY TIME

Υ_{NS} = ELECTRON SHUNT PATH LIFETIME

FIGURE 2

PHOTOLUMINESCENCE EFFICIENCY TEST SET

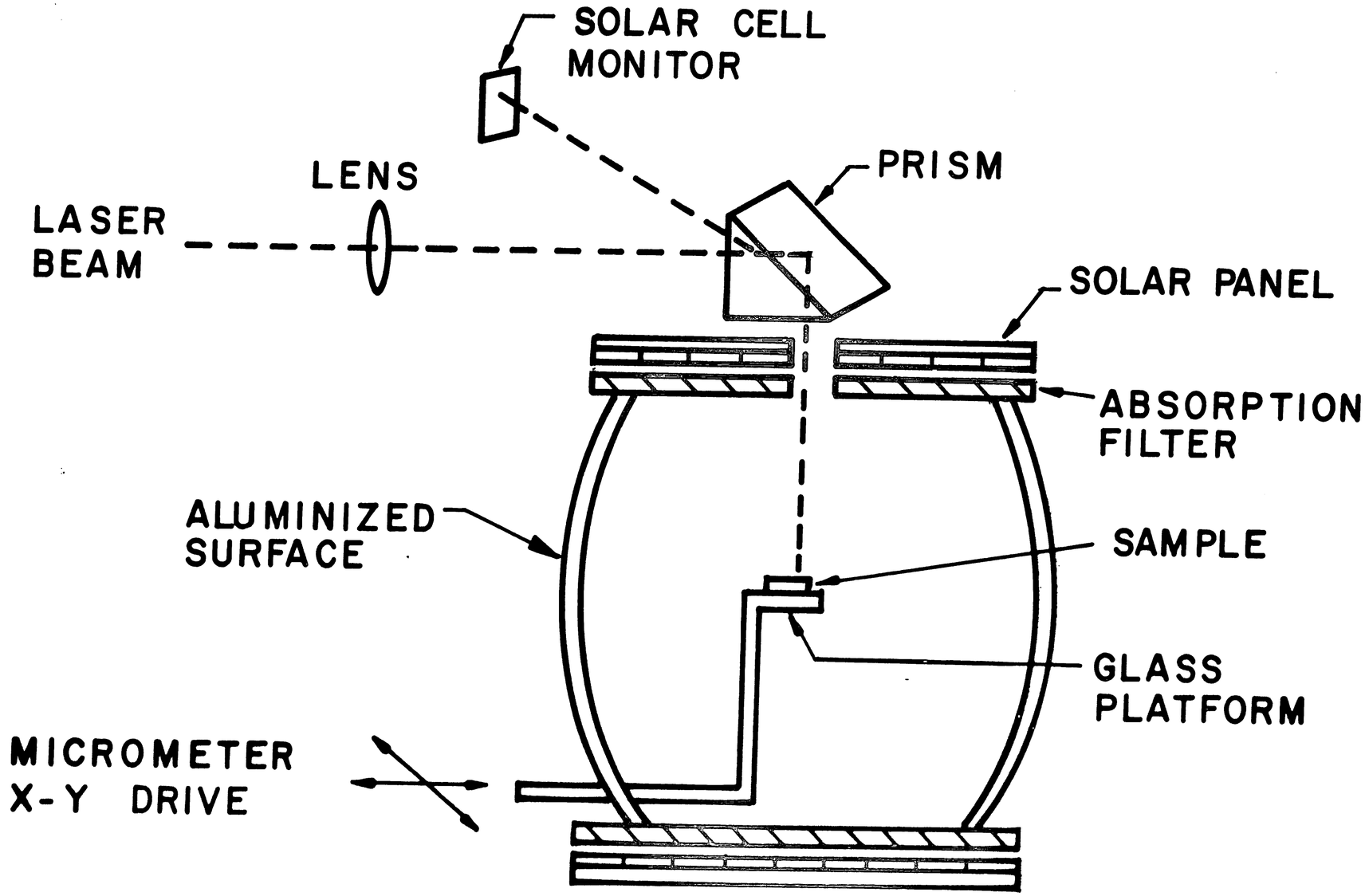

FIGURE 3

EXPERIMENTAL SETUP FOR PHOTOLUMINESCENCE SPECTRA MEASUREMENTS

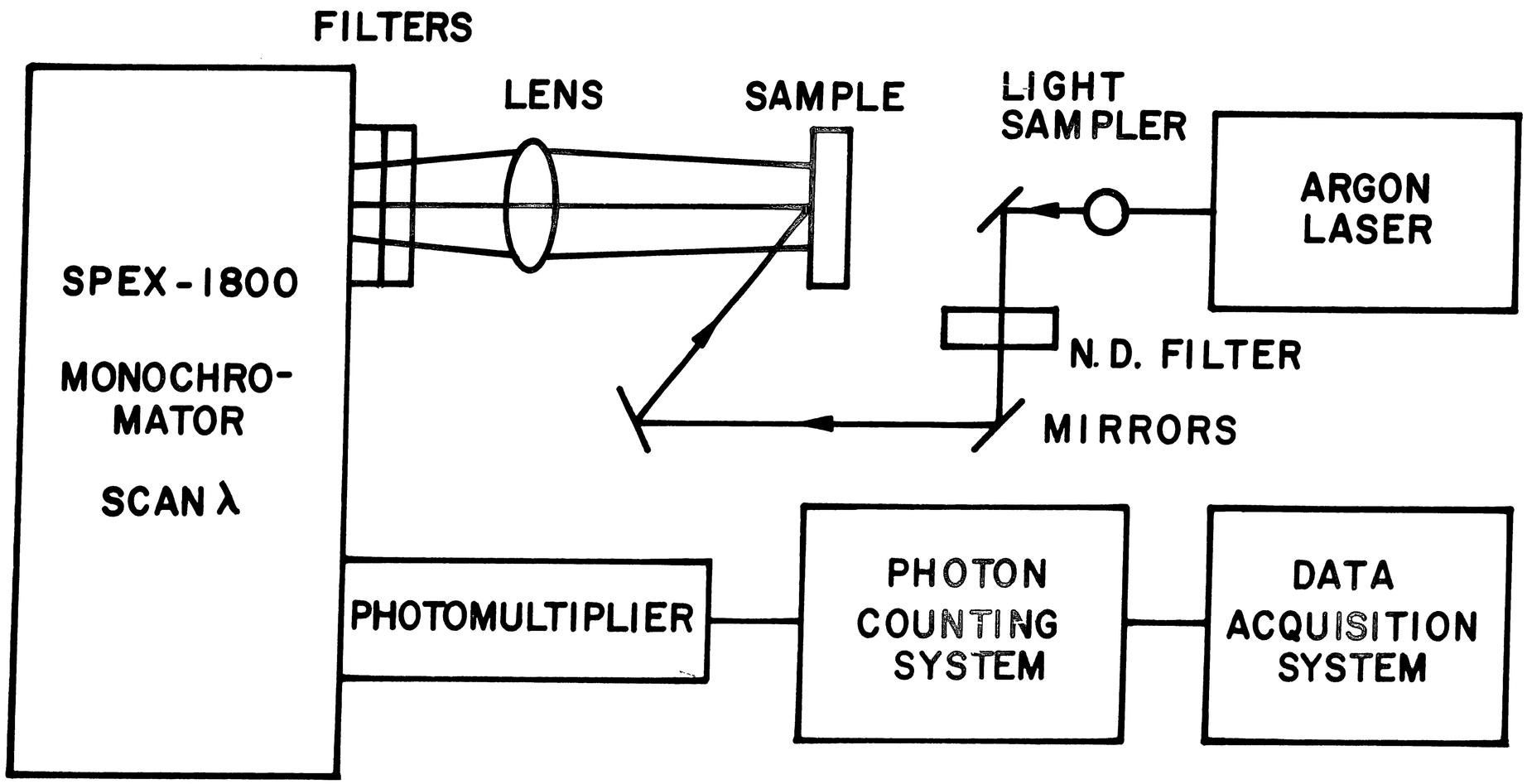

FIGURE 4

EXPERIMENTAL SETUP FOR ABSORPTION SPECTRA MEASUREMENTS

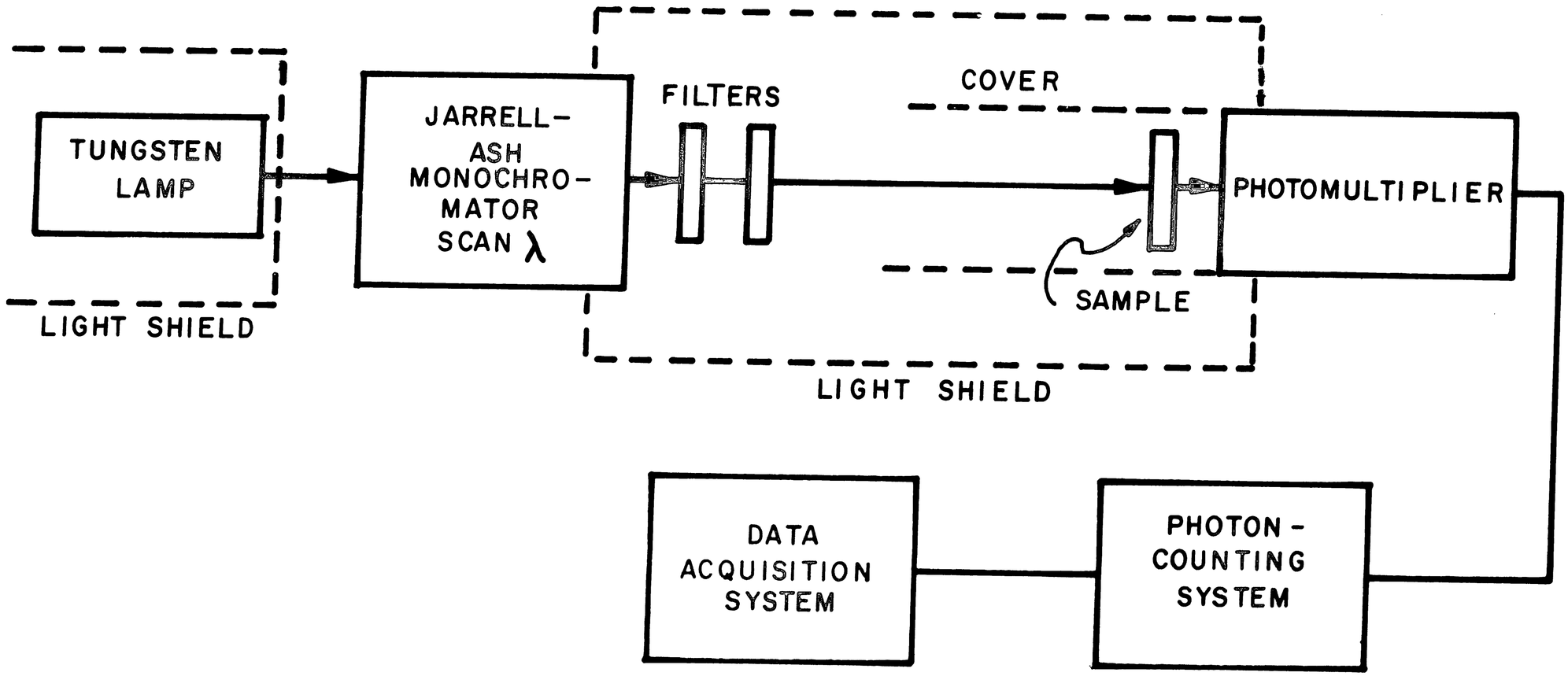

FIGURE 5

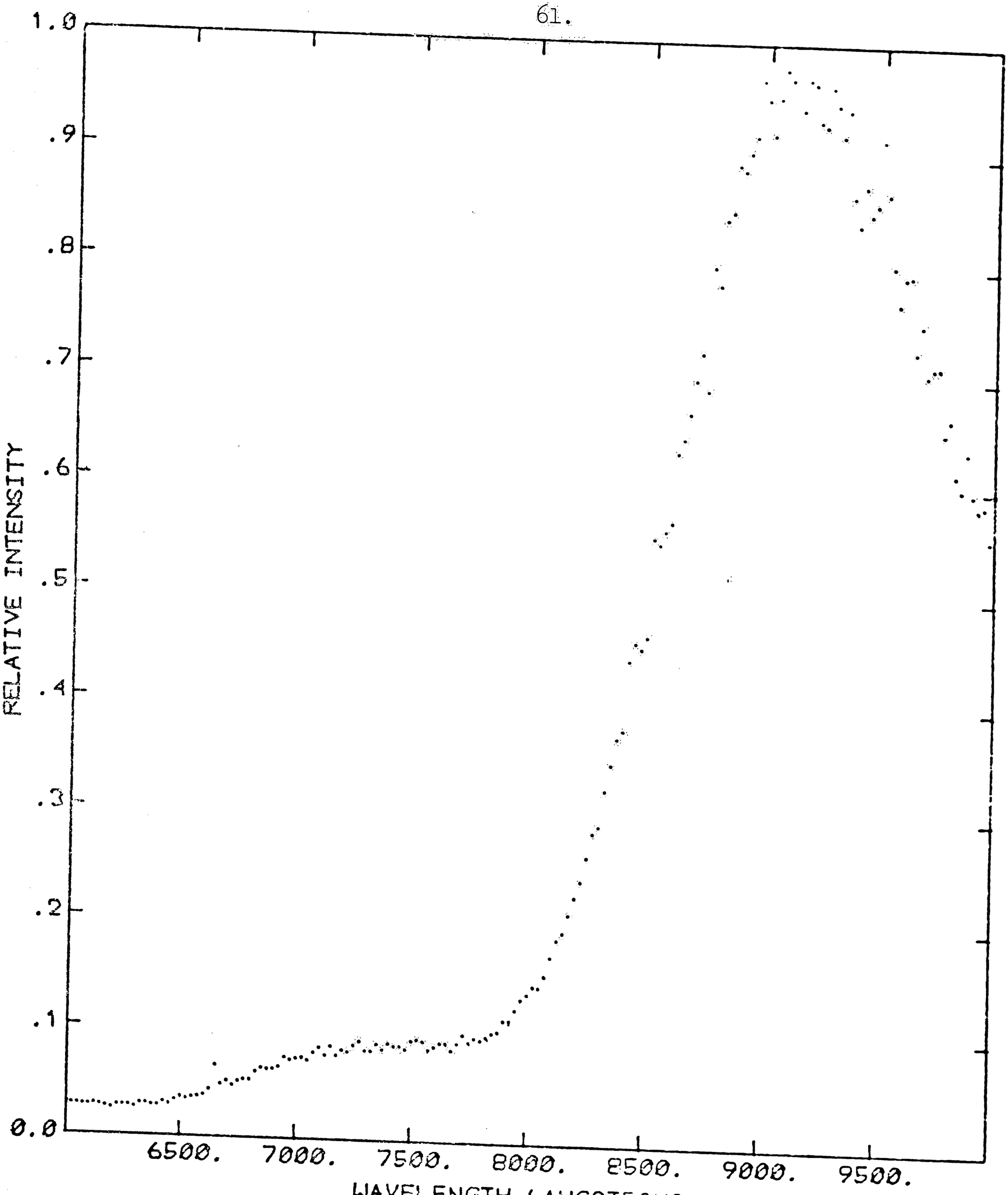

PHOTOLUMINESCENCE SPECTRUM: UNANNEALED (MS80503-1)
4880 EXCITATION: 10/20/70
SLIT WIDTH: 2500. MICRONS SLIT HT: 5. MM
PHOTONS COUNTED PER DATA POINT: 1000.
MAXIMUM SIGNAL: 3.24D 08 PHOTONS/SEC

FIGURE 6

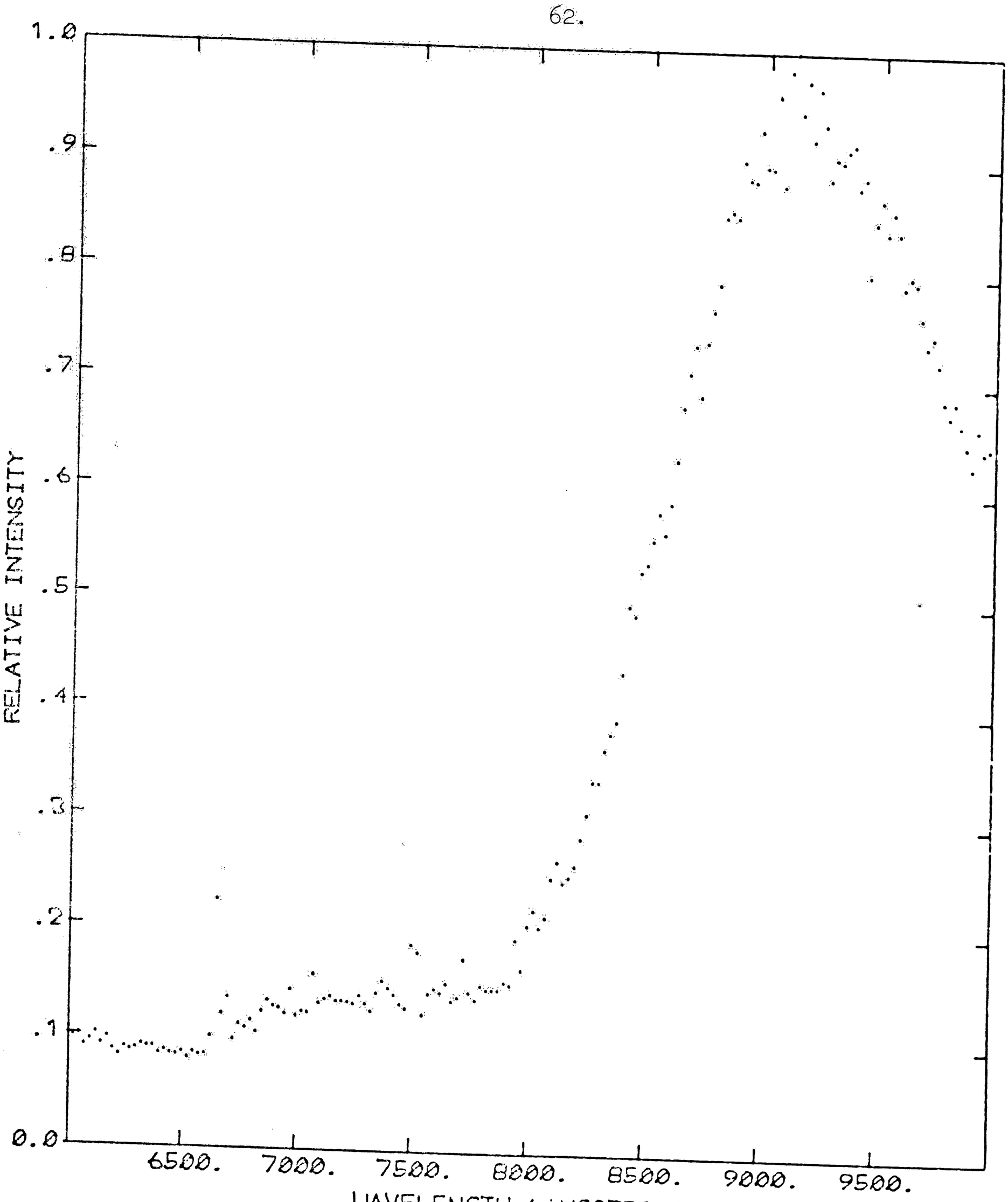

PHOTOLUMINESCENCE SPECTRUM: ANNEALED (MS80503-1)
4880 EXCITATION: 11/18/70
SLIT WIDTH: 2500. MICRONS SLIT HT: 5. MM
PHOTONS COUNTED PER DATA POINT: 1000.
MAXIMUM SIGNAL: 2.40D 03 PHOTONS/SEC

FIGURE 7

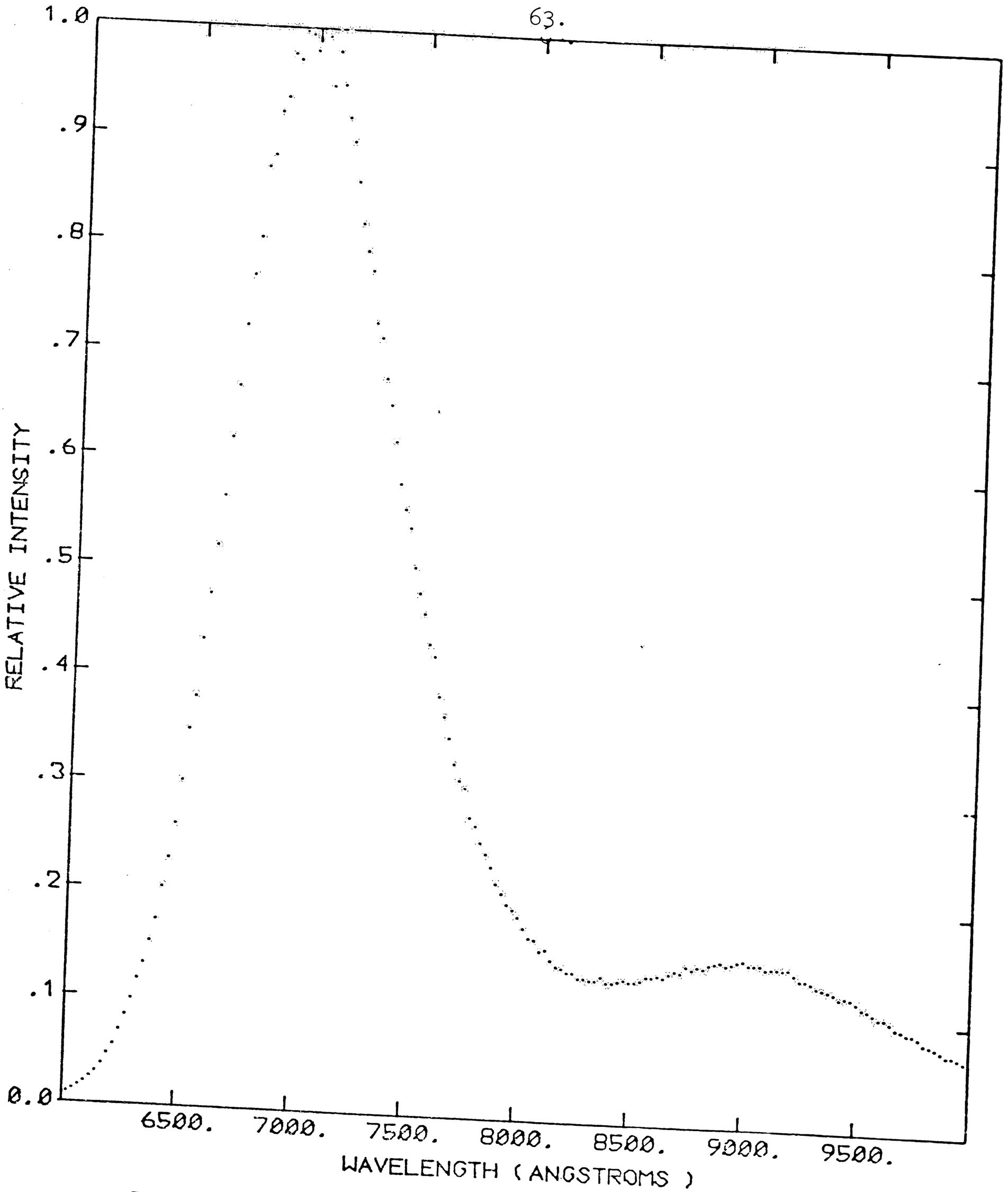

PHOTOLUMINESCENCE SPECTRUM: UNANNEALED (MS80815-2)
4880 EXCITATION: 9/16/70
SLIT WIDTH: 2500. MICRONS SLIT HT: 5. MM
PHOTONS COUNTED PER DATA POINT: 10000.
MAXIMUM SIGNAL: 2.82D 09 PHOTONS/SEC

FIGURE 8

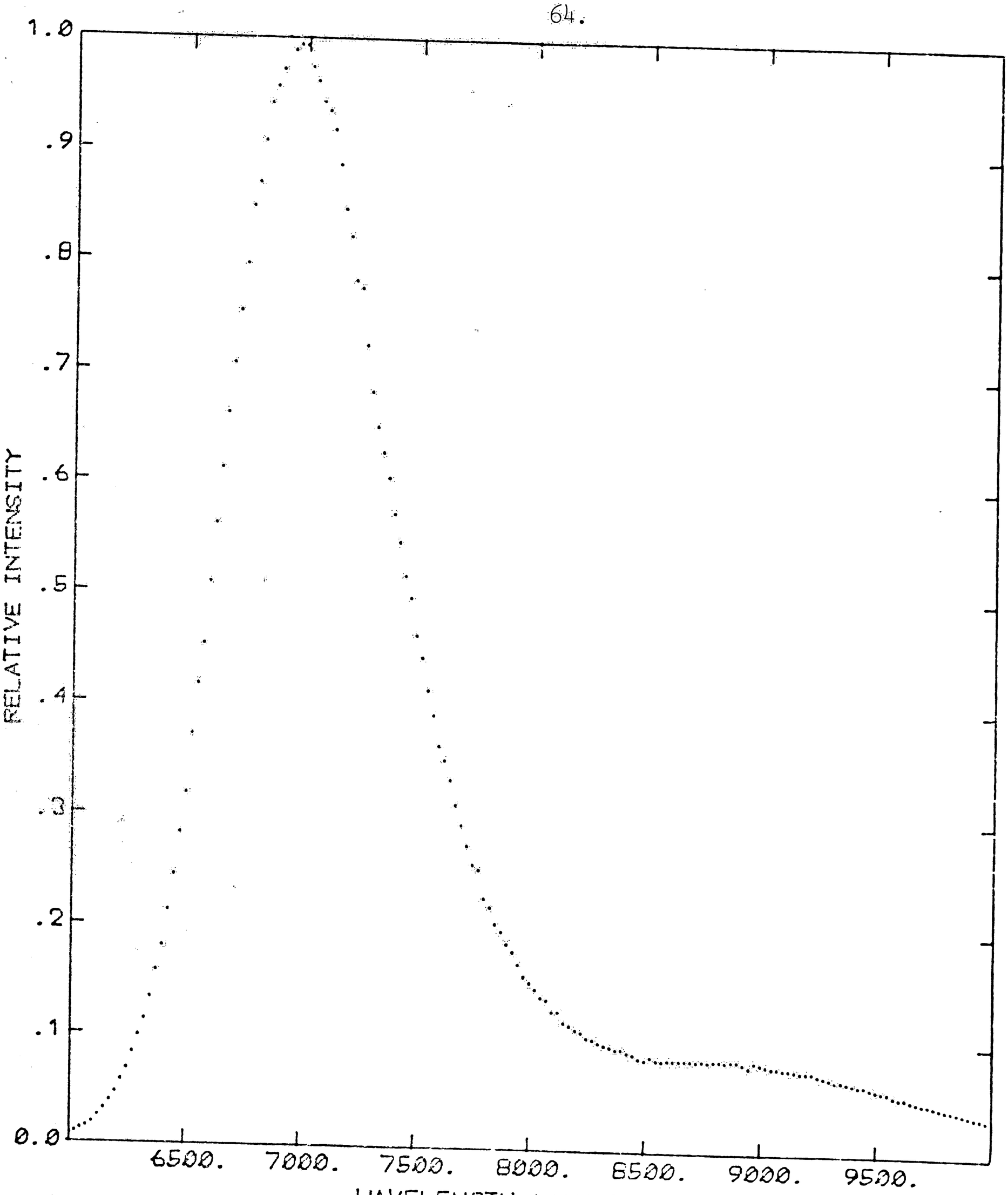

PHOTOLUMINESCENCE SPECTRUM: ANNEALED (MS80815-2)
4880 EXCITATION: 11/16/70
SLIT WIDTH: 2500. MICRONS SLIT HT: 5. MM
PHOTONS COUNTED PER DATA POINT: 10000.
MAXIMUM SIGNAL: 3.02D 09 PHOTONS/SEC

FIGURE 9

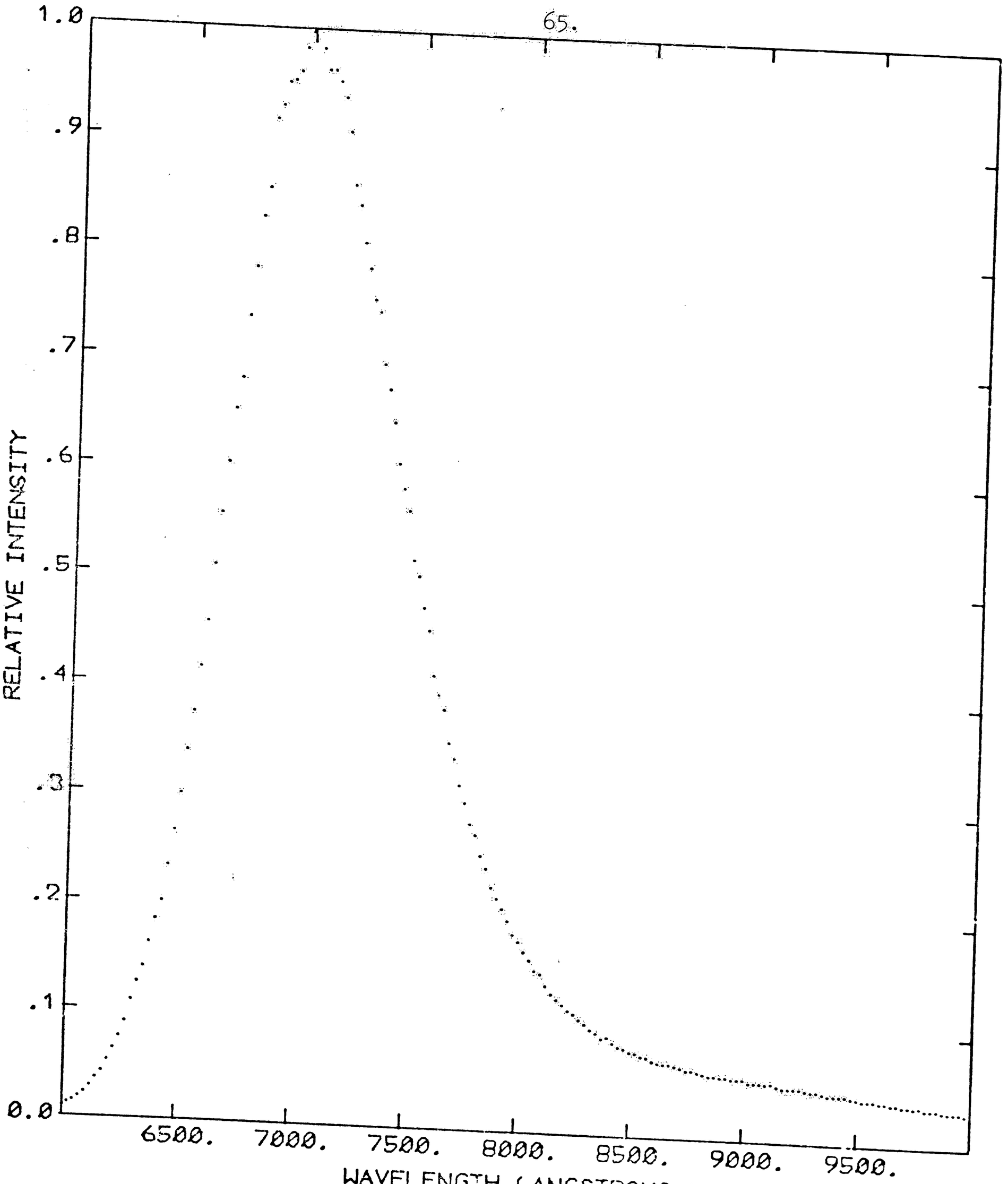

PHOTOLUMINESCENCE SPECTRUM: UNANNEALED (MS80524-1)
4880 EXCITATION: 9/16/70
SLIT WIDTH: 2500. MICRONS SLIT HT: 5. MM
PHOTONS COUNTED PER DATA POINT: 10000.
MAXIMUM SIGNAL: 2.74D 09 PHOTONS/SEC

FIGURE 10

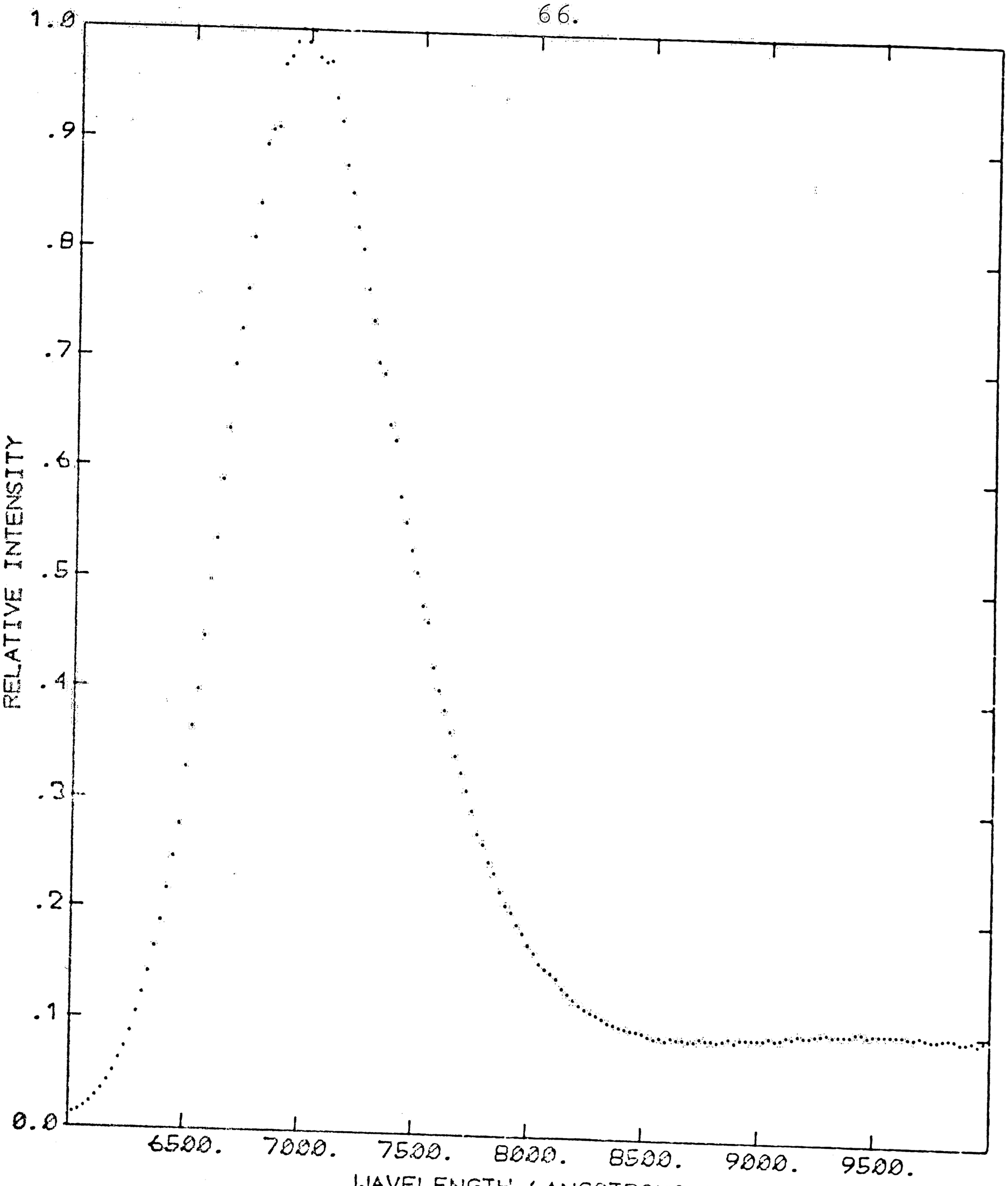

PHOTOLUMINESCENCE SPECTRUM: ANNEALED (MS80524-1)
4880 EXCITATION: 11/18/70
SLIT WIDTH: 2500. MICRONS SLIT HT: 5. MM
PHOTONS COUNTED PER DATA POINT: 10000.
MAXIMUM SIGNAL: 1.37D 09 PHOTONS/SEC

FIGURE 11

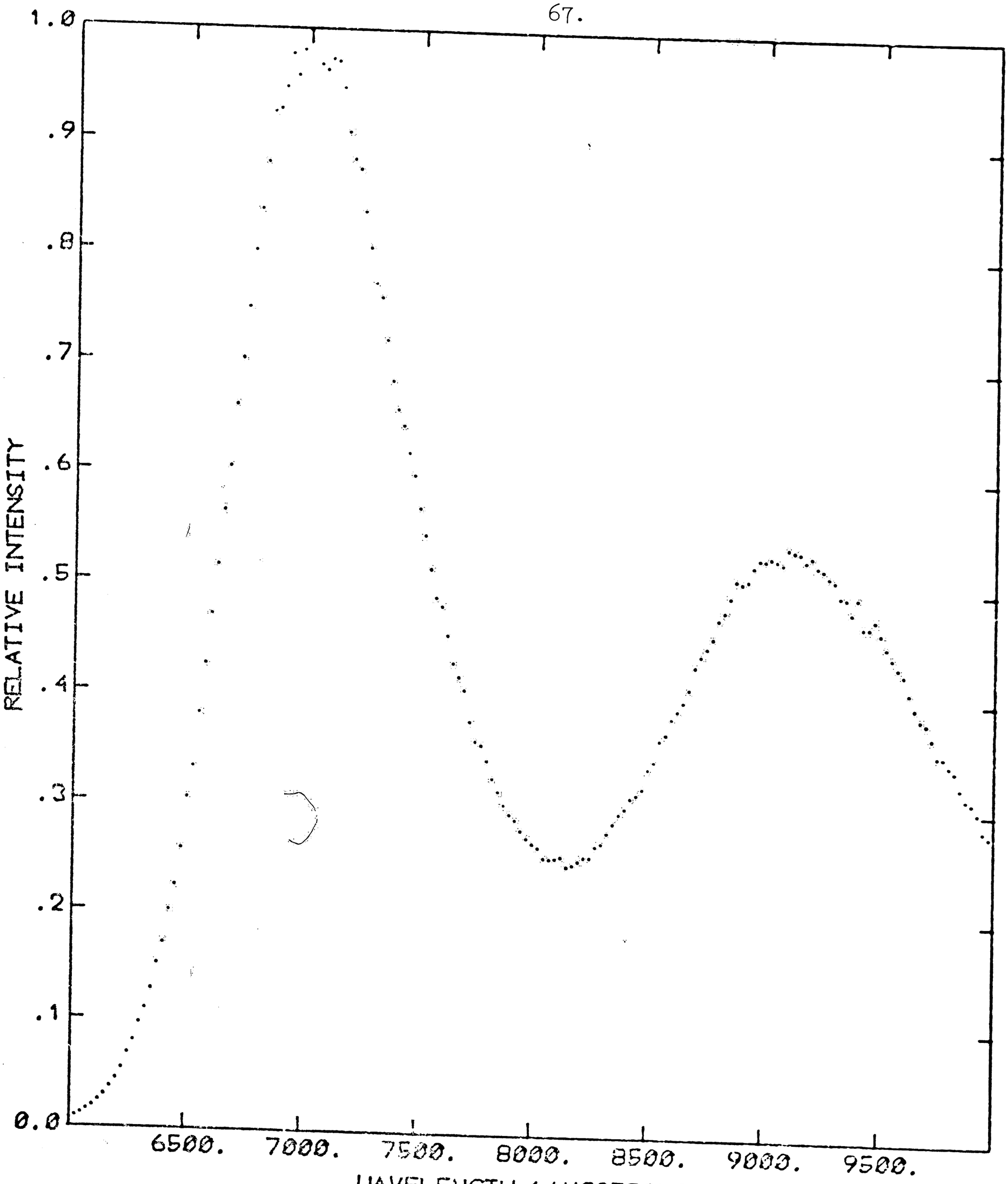

PHOTOLUMINESCENCE SPECTRUM: UNANNEALED (MS80722-1)
4880 EXCITATION: 10/20/70
SLIT WIDTH: 2500. MICRONS SLIT HT: 5. MM
PHOTONS COUNTED PER DATA POINT: 10000.
MAXIMUM SIGNAL: 2.45D 07 PHOTONS/SEC

FIGURE 12

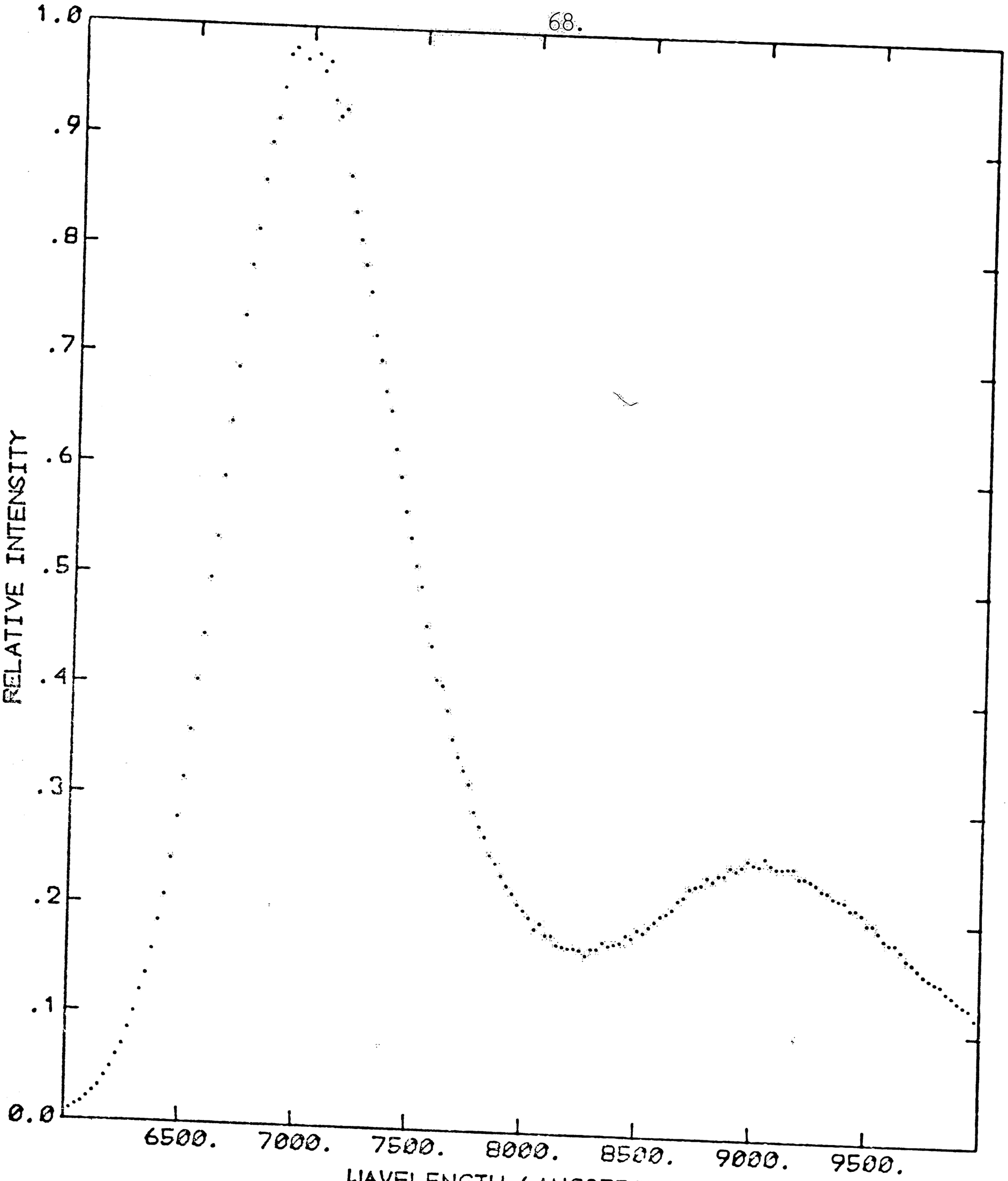

PHOTOLUMINESCENCE SPECTRUM: UNANNEALED (MS80722-2)
4880 EXCITATION: 10/20/70
SLIT WIDTH: 2500. MICRONS SLIT HT: 5. MM
PHOTONS COUNTED PER DATA POINT: 10000.
MAXIMUM SIGNAL: 3.00D 09 PHOTONS/SEC

FIGURE 13

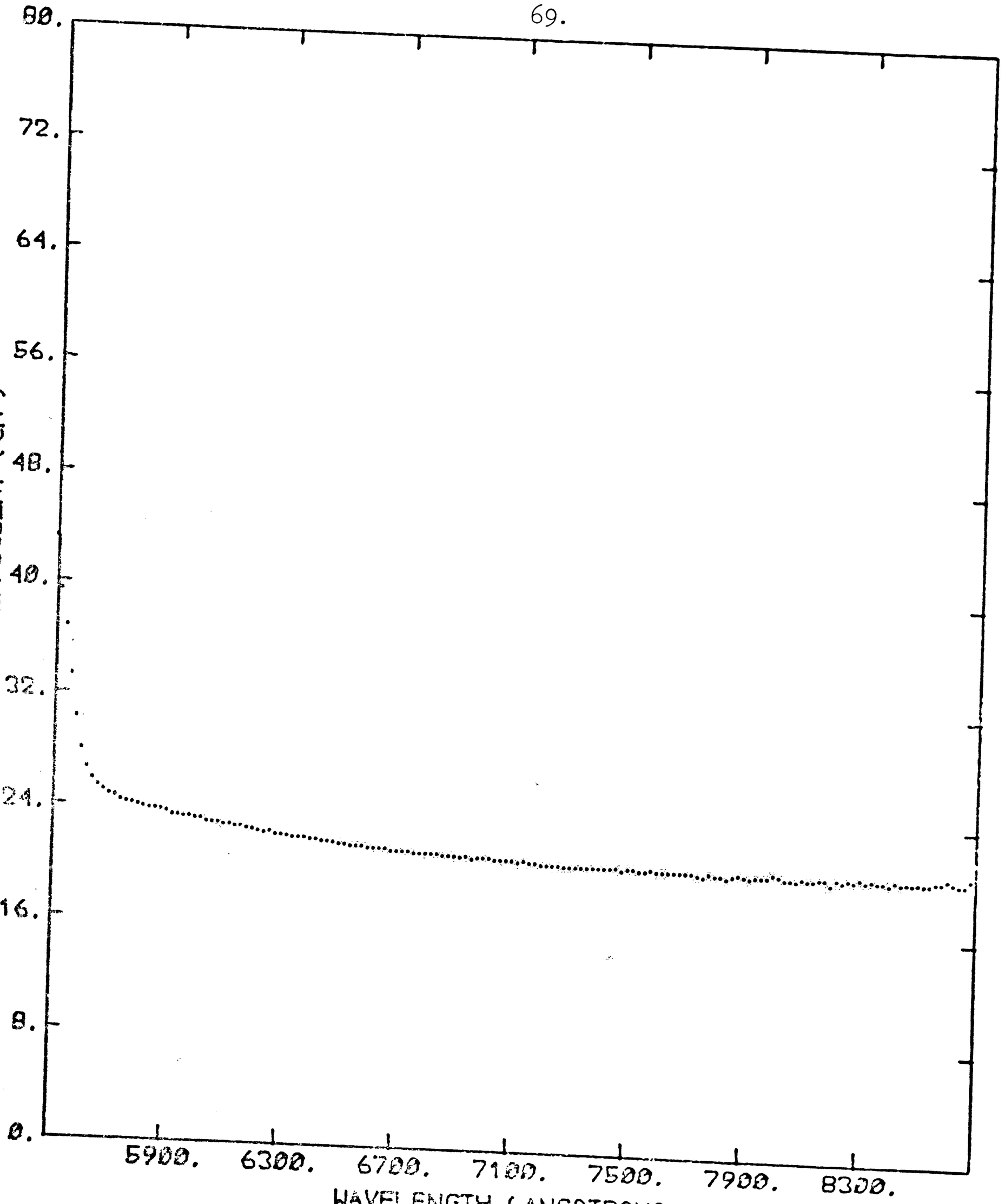

ABSORPTION SPECTRUM : UNANNEALED (MSB0503-1)
FW130 PMT DETECTOR @ 2200 VOLTS: 10/27/70
BANDPASS: 16.50 ANGSTROMS

FIGURE 14

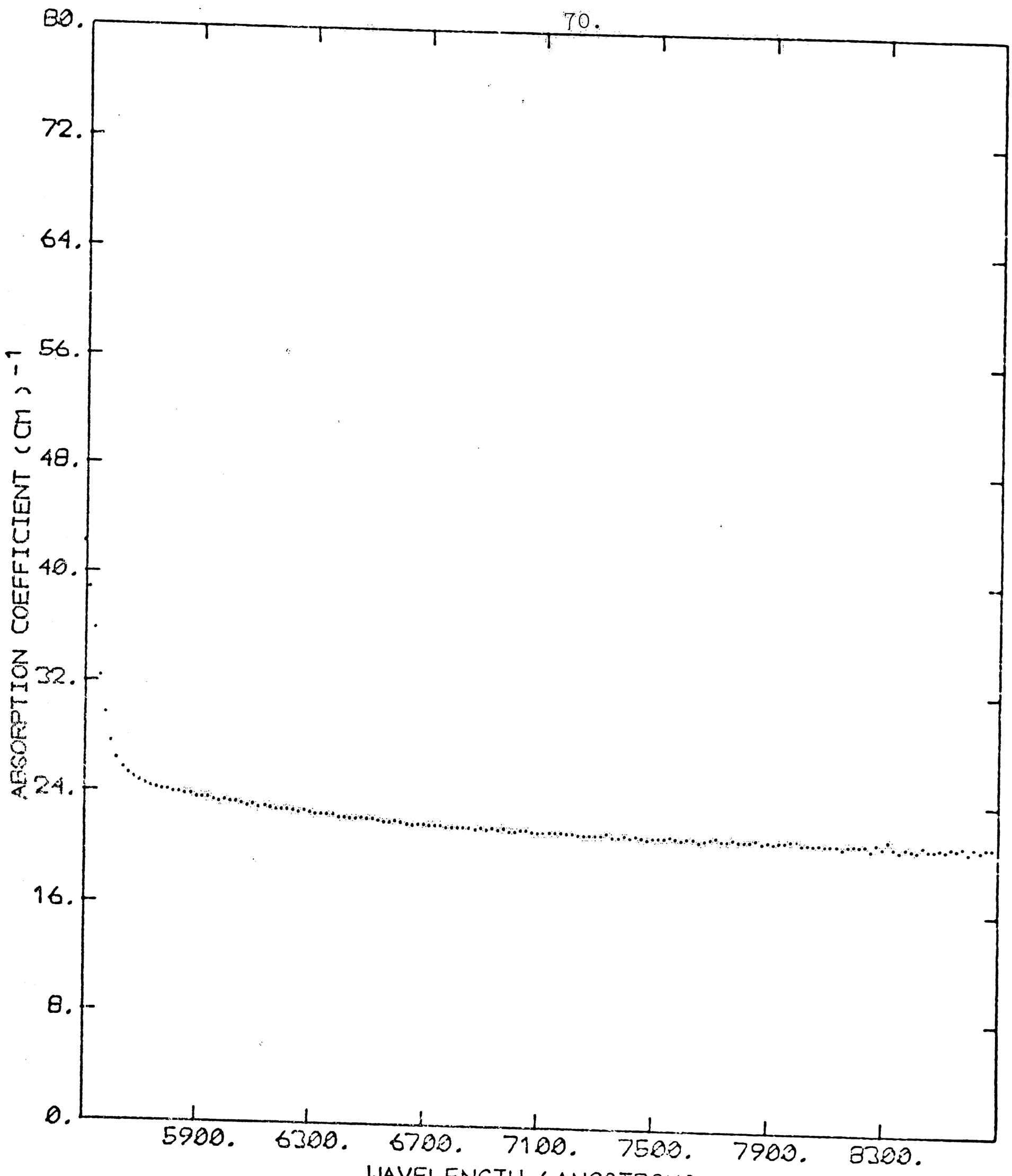

ABSORPTION SPECTRUM : ANNEALED (MS80503-1)
FW130 PMT DETECTOR @ 2200 VOLTS: 11/17/70
BANDPASS: 16.50 ANGSTROMS

FIGURE 15

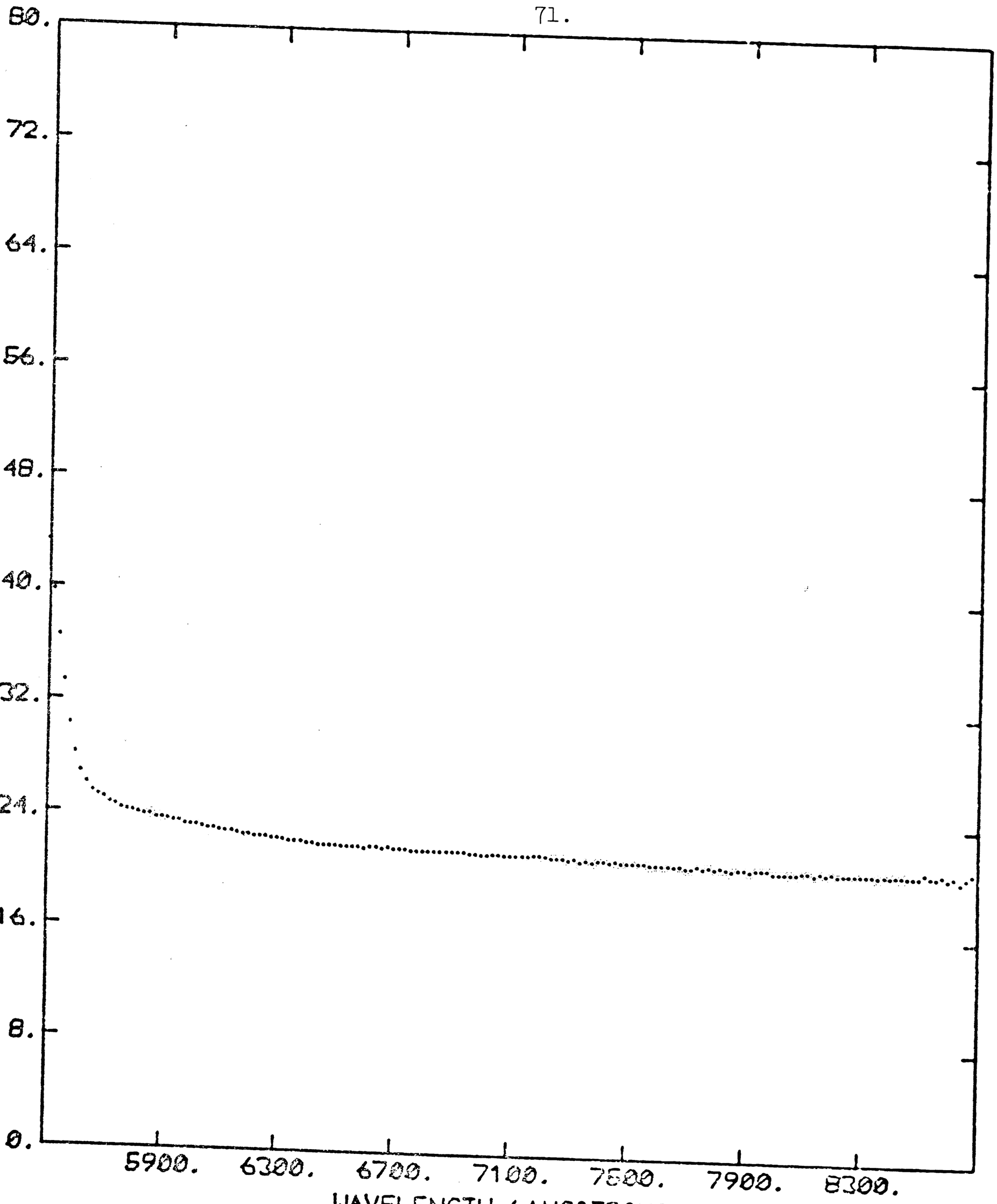

ABSORPTION SPECTRUM : UNANNEALED (MS80815-2)
FW130 PMT DETECTOR @ 2200 VOLTS: 11/4/70
BANDPASS: 16.50 ANGSTROMS

FIGURE 16

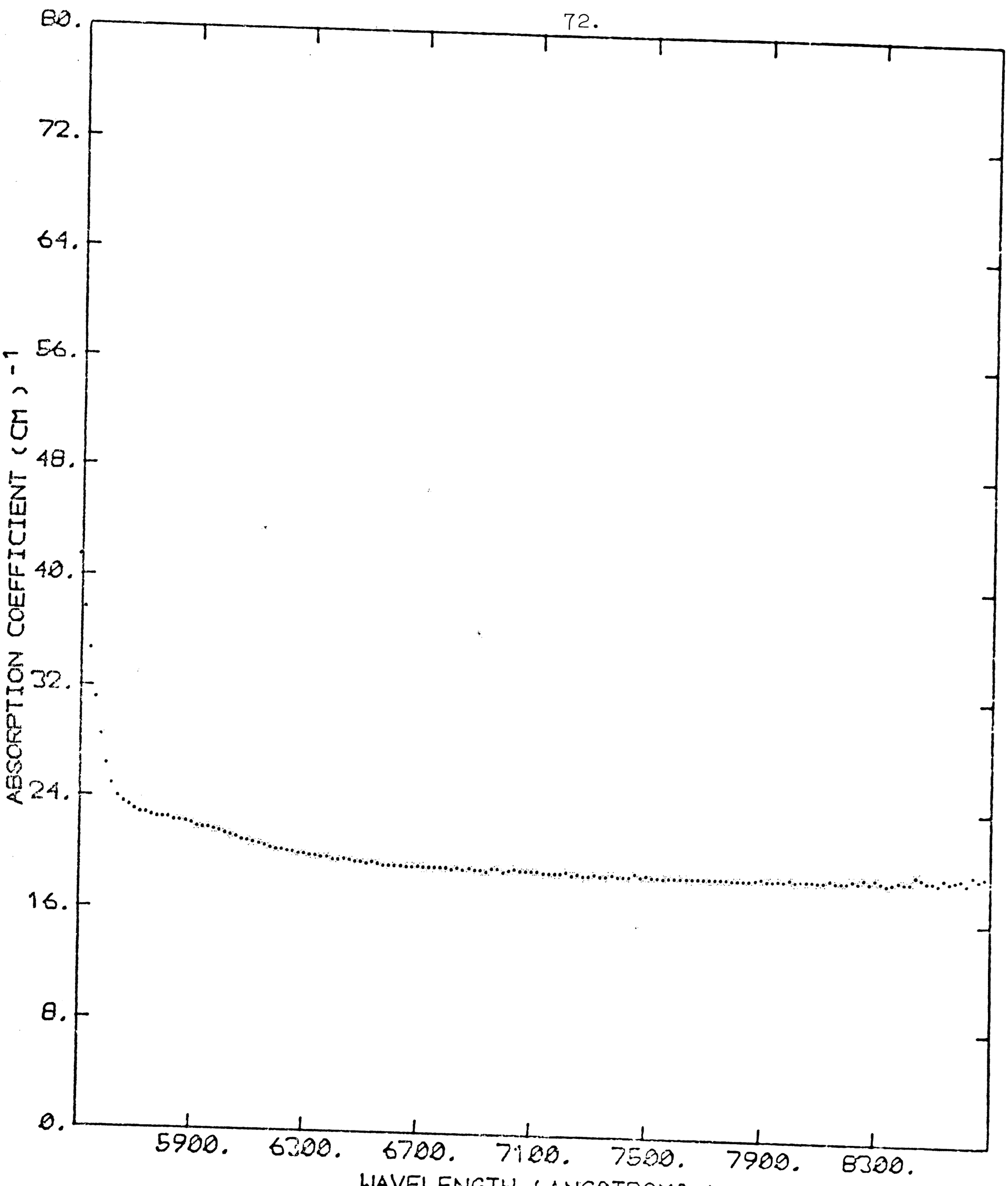

ABSORPTION SPECTRUM : ANNEALED (MS80815-2)
FW130 PMT DETECTOR @ 2200 VOLTS: 11/17/70
BANDPASS: 16.50 ANGSTROMS

FIGURE 17

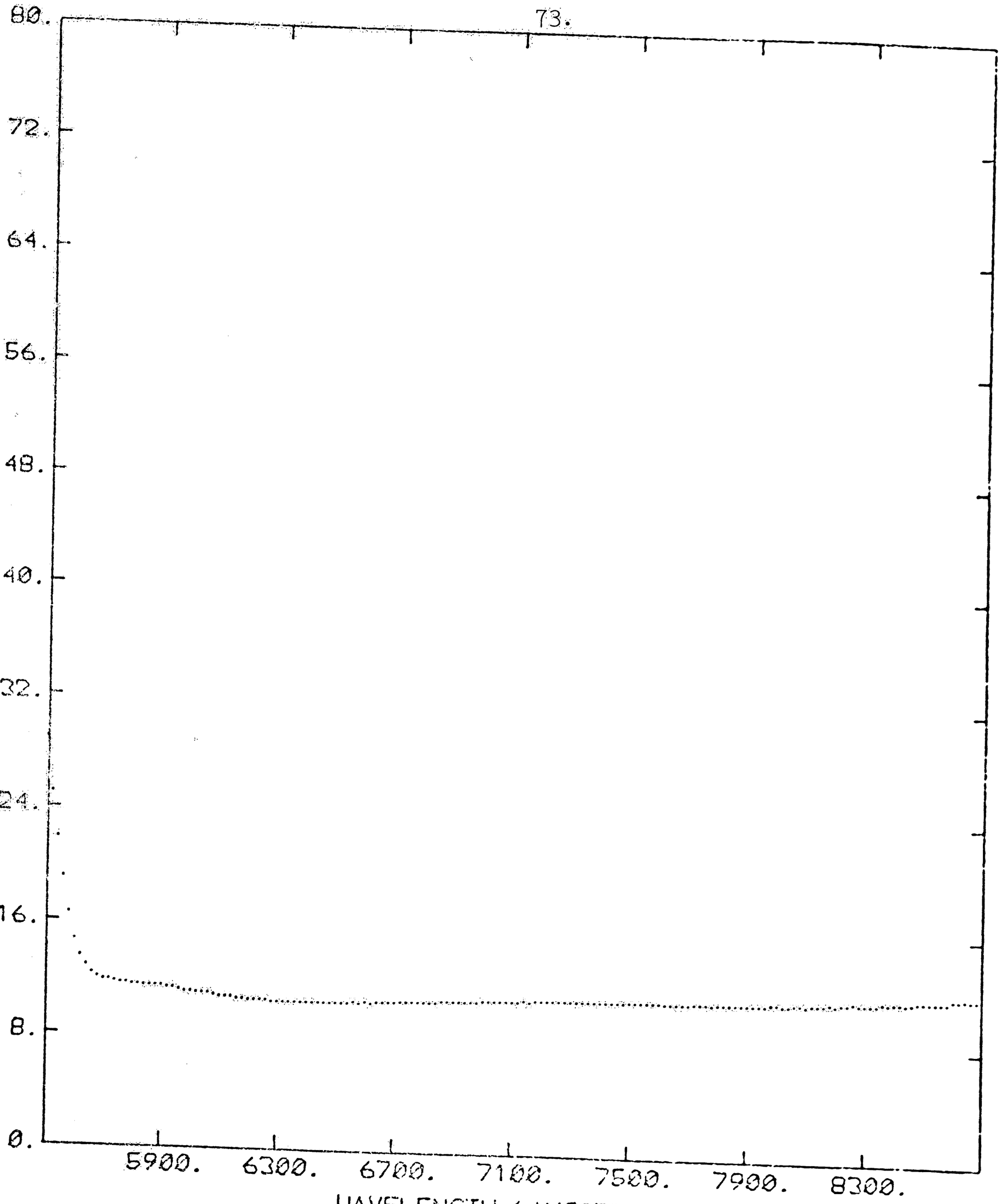

ABSORPTION SPECTRUM : UNANNEALED (MS80516-2)
FW130 PMT DETECTOR @ 2200 VOLTS: 10/27/70
BANDPASS: 16.50 ANGSTROMS

FIGURE 18

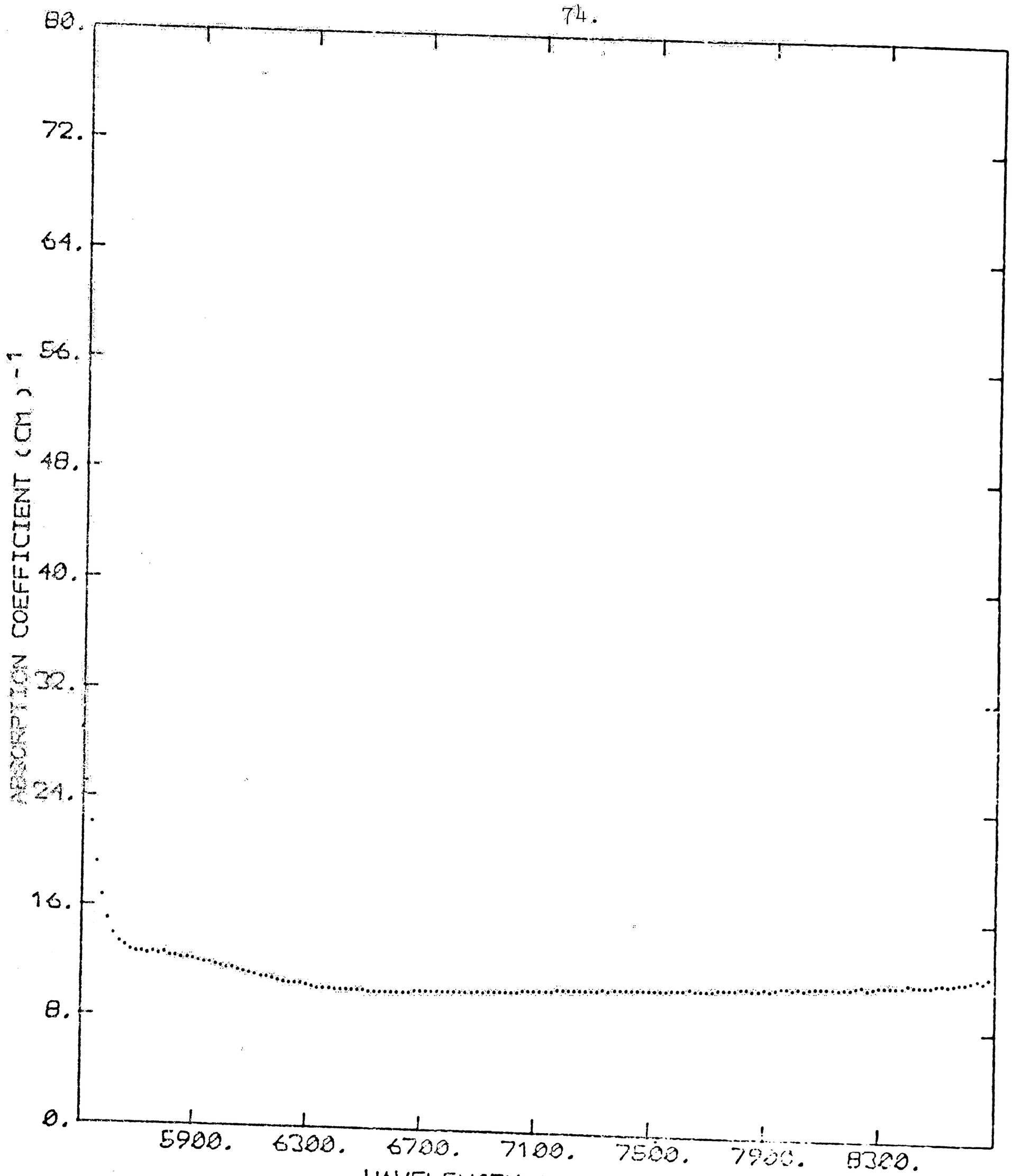

ABSORPTION SPECTRUM : ANNEALED (MSB0516-2)
FW130 PMT DETECTOR @ 2200 VOLTS: 11/17/70
BANDPASS: 16.50 ANGSTROMS

FIGURE 19

DIFFERENCE IN ABSORPTION COEFFICIENTS AFTER ANNEALING AS A FUNCTION OF WAVELENGTH

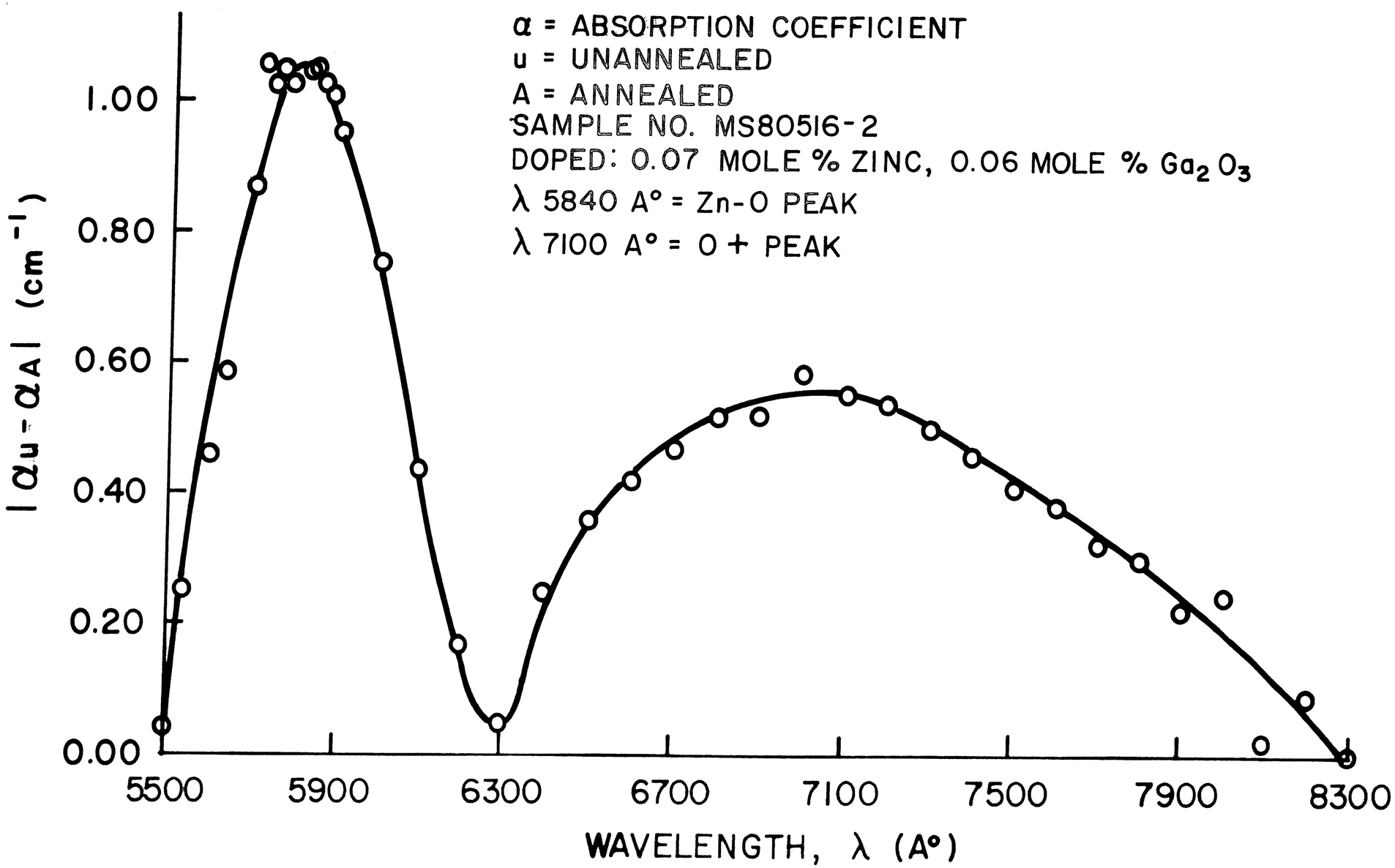

α = ABSORPTION COEFFICIENT
u = UNANNEALED
A = ANNEALED
SAMPLE NO. MS80516-2
DOPED: 0.07 MOLE % ZINC, 0.06 MOLE % Ga_2O_3
λ 5840 A° = Zn-O PEAK
λ 7100 A° = O + PEAK

FIGURE 20

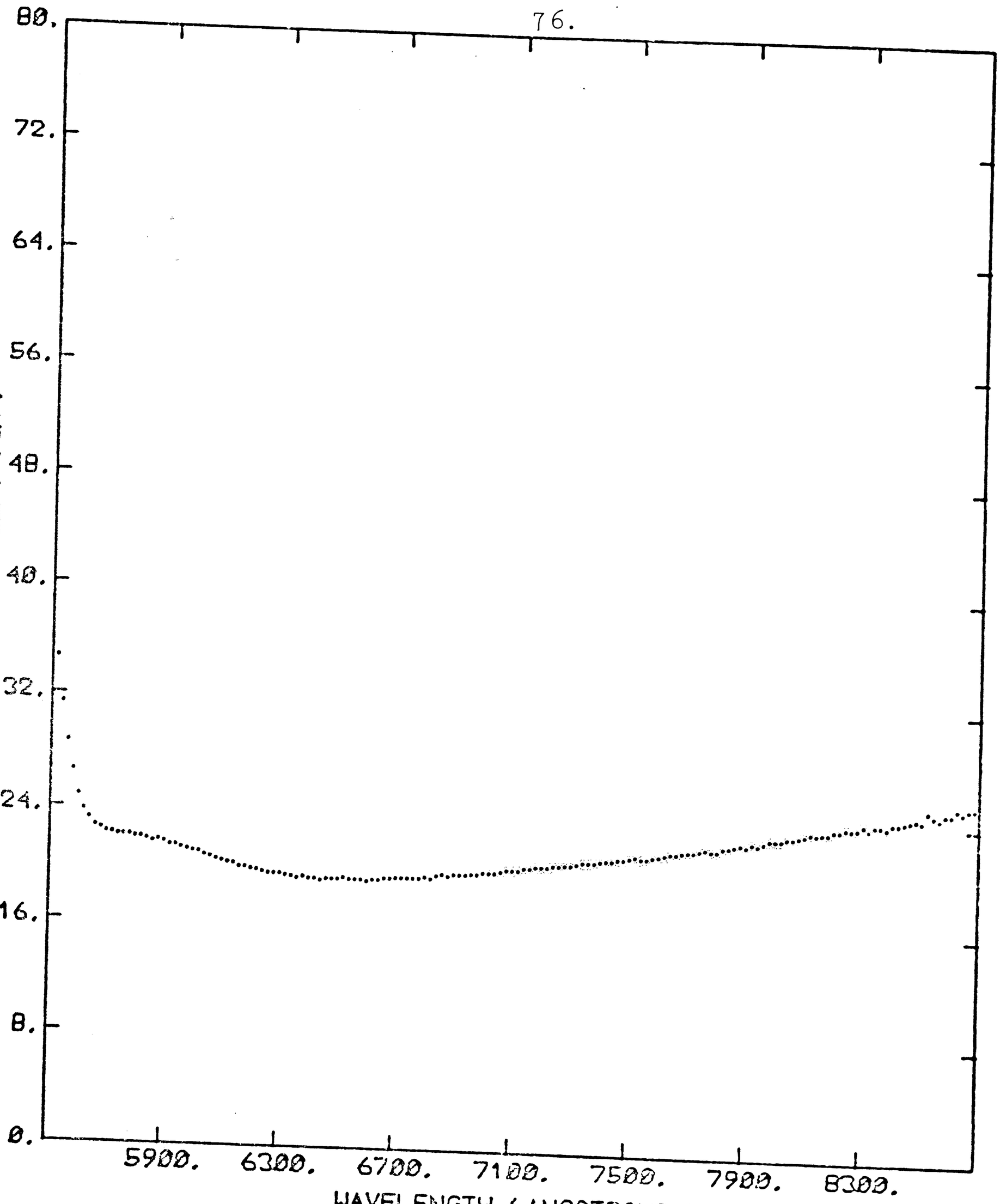

ABSORPTION SPECTRUM : UNANNEALED (MS80524-1)
FW130 PMT DETECTOR @ 2200 VOLTS: 10/27/70
BANDPASS: 16.50 ANGSTROMS

FIGURE 21

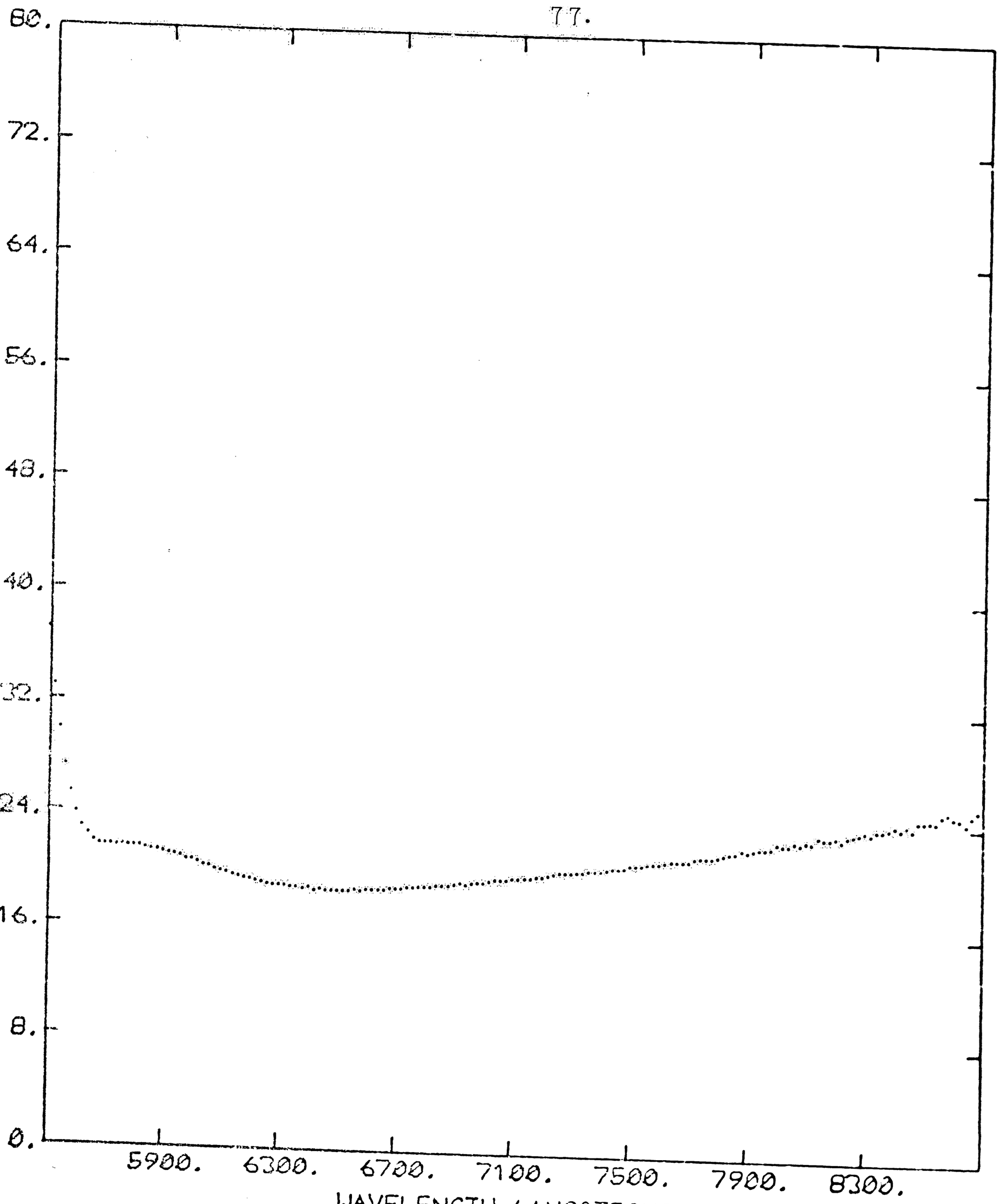

ABSORPTION SPECTRUM : ANNEALED (MS80524-1)
FW130 PMT DETECTOR @ 2200 VOLTS: 11/17/70
BANDPASS: 16.50 ANGSTROMS

FIGURE 22

TOTAL EFFICIENCY vs. ZINC DOPING CONTENT

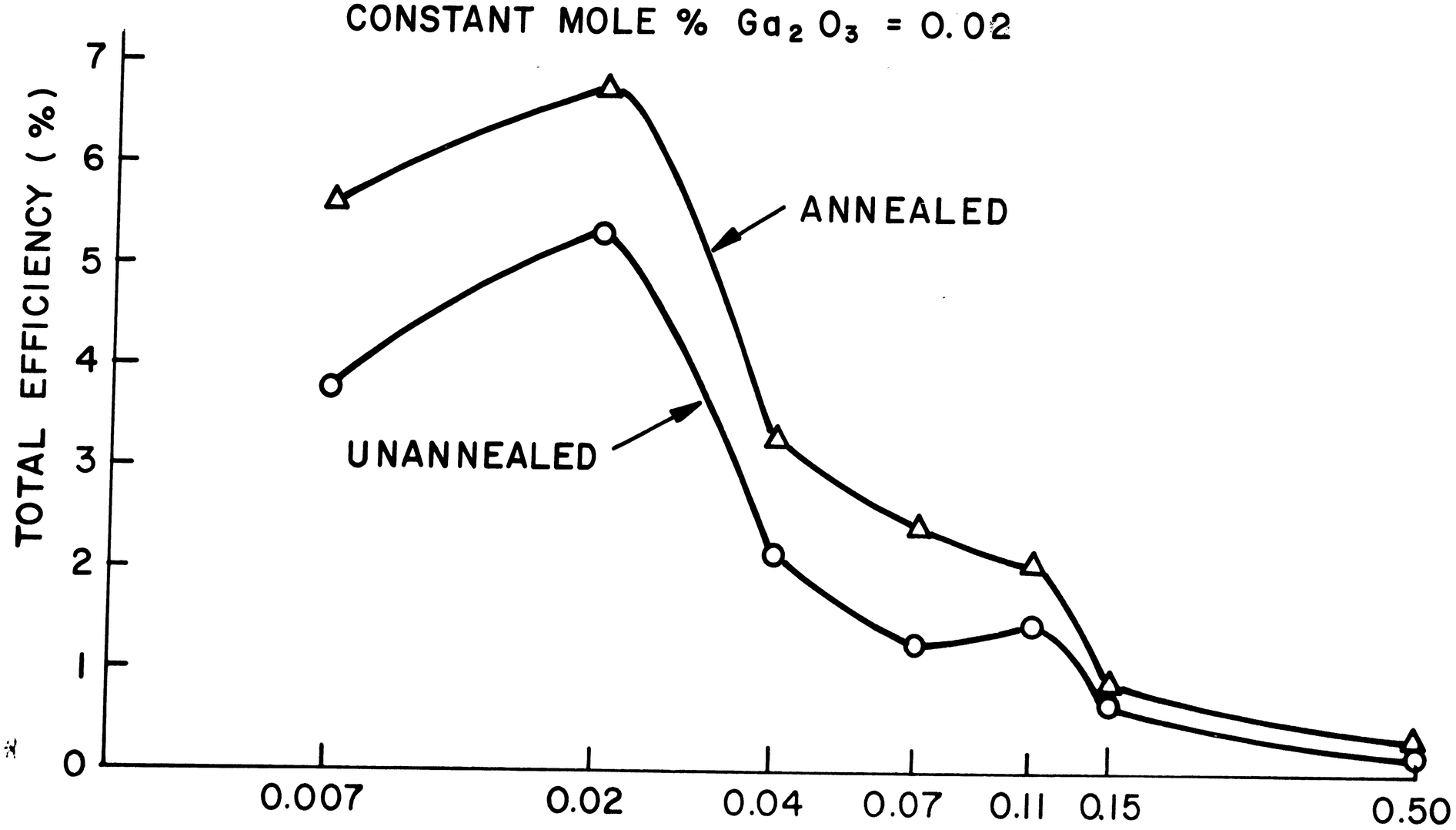

FIGURE 23

RED-TO-INFRARED INTEGRATED INTENSITY RATIO vs. ZINC DOPING CONTENT

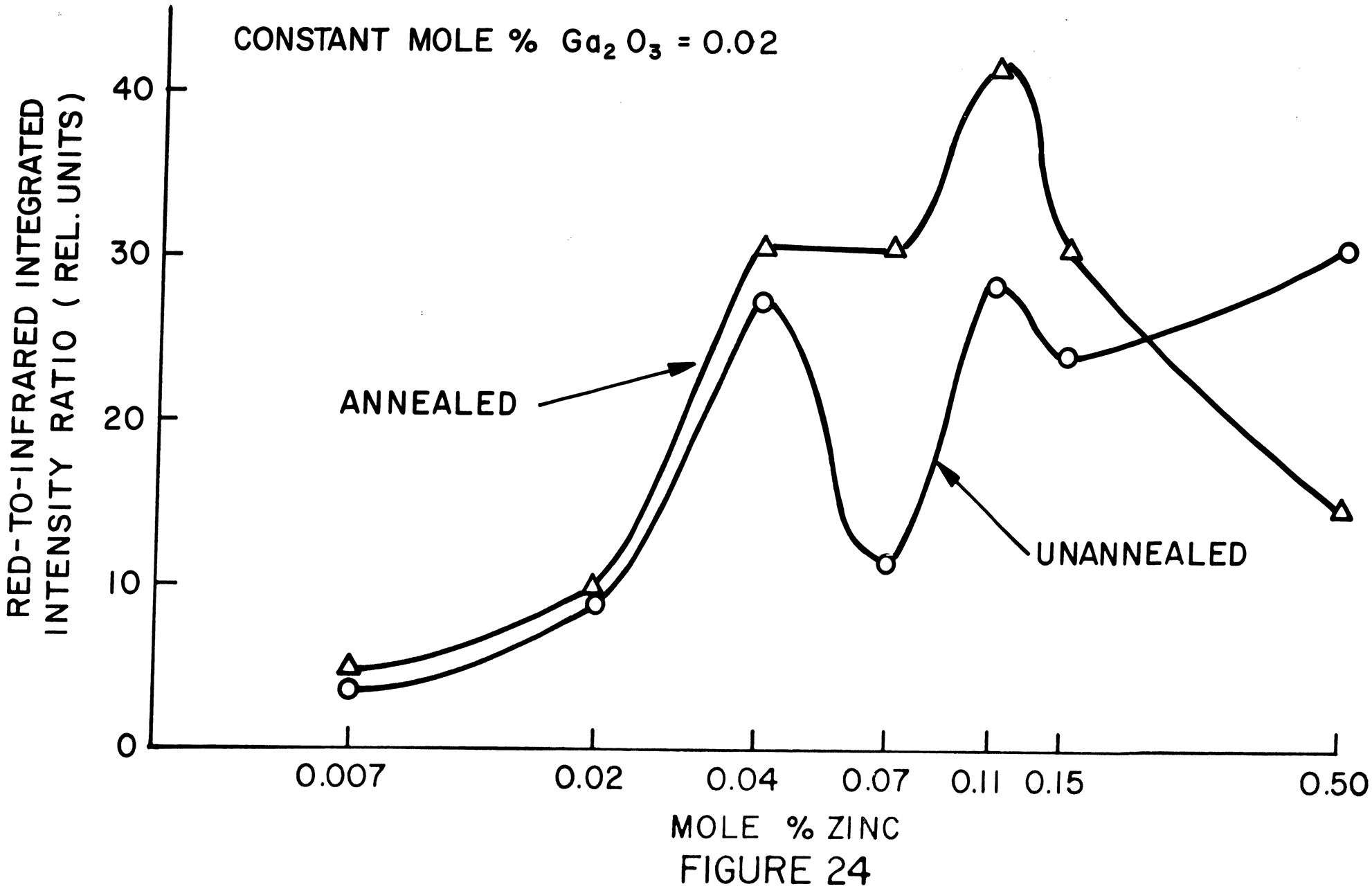

FIGURE 24

RED EXTERNAL EFFICIENCY vs. ZINC DOPING CONTENT

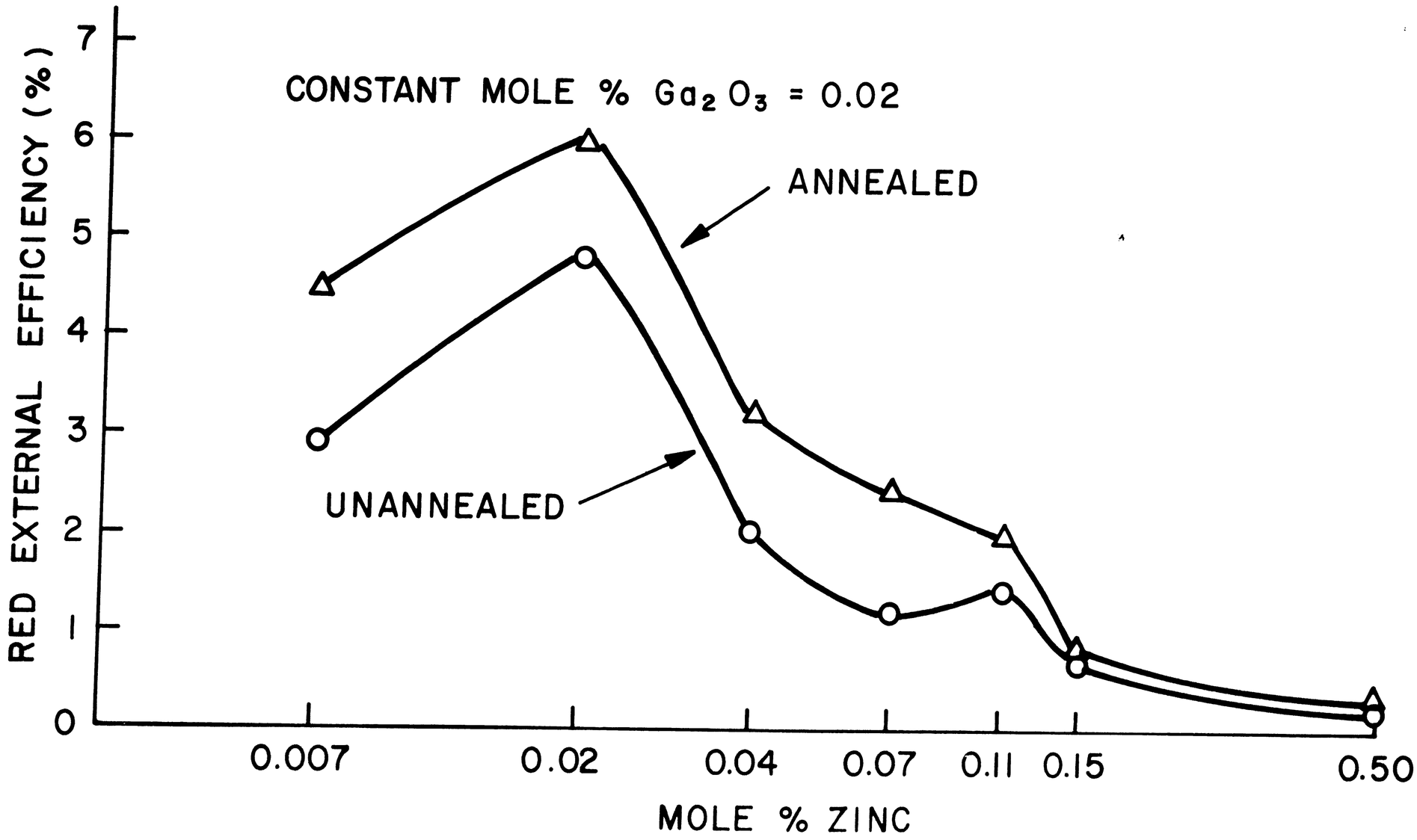

FIGURE 25

INFRARED EXTERNAL EFFICIENCY VS. ZINC DOPING CONTENT

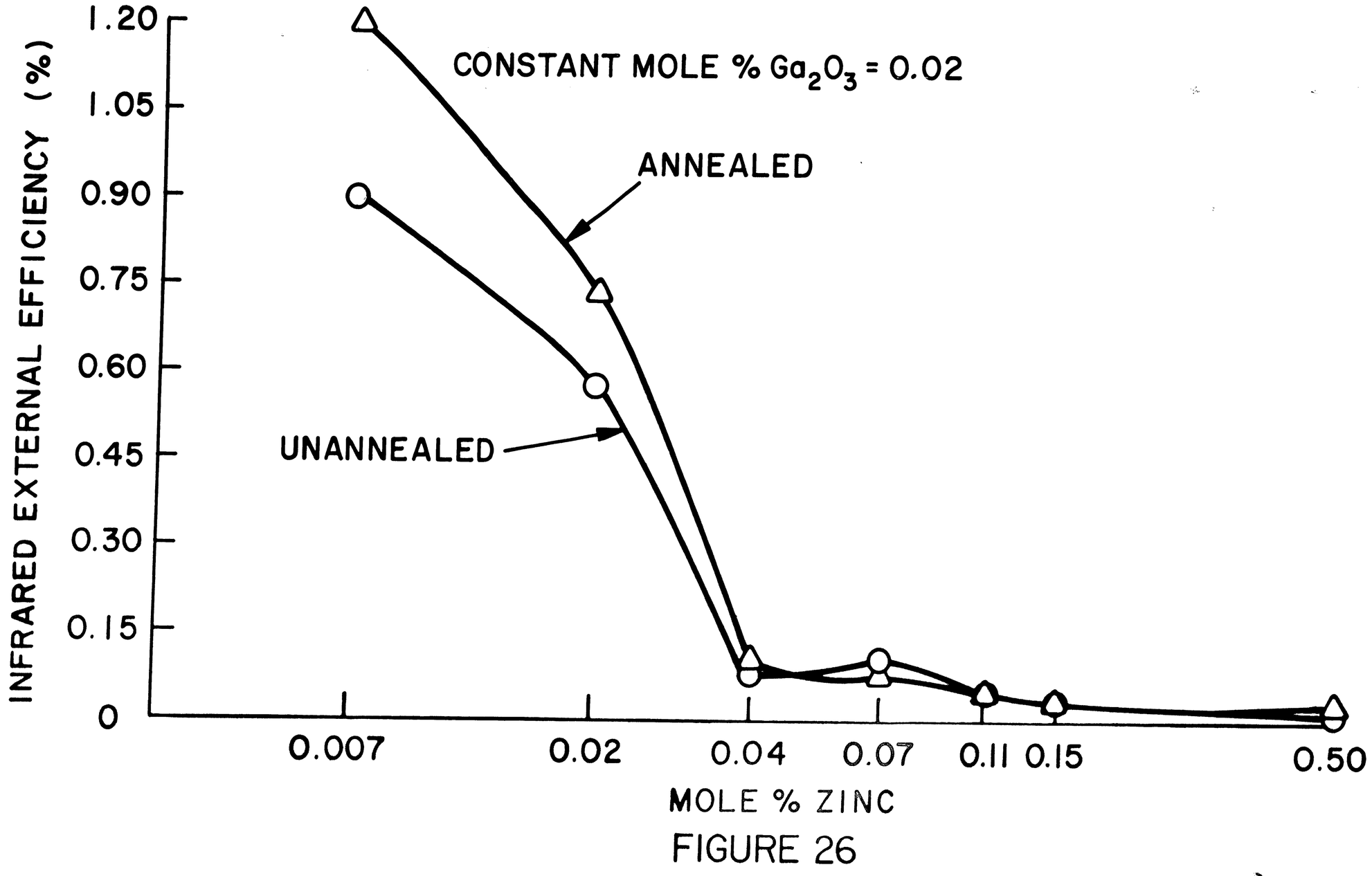

FIGURE 26

PEAK ABSORPTION COEFFICIENT AT 5840 A° vs. ZINC DOPING CONTENT

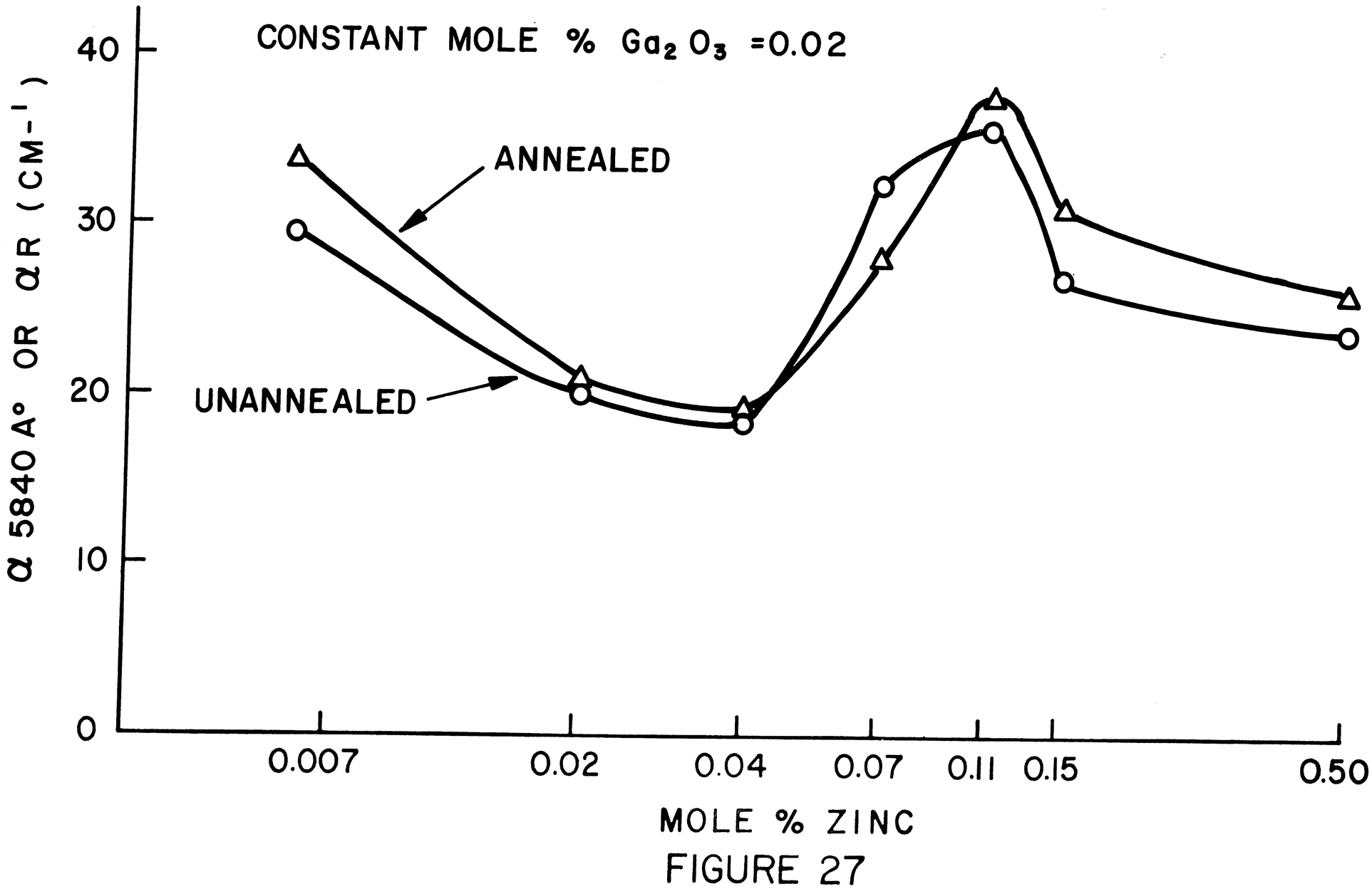

FIGURE 27

PEAK ABSORPTION COEFFICIENT AT 7100 A° vs. ZINC DOPING CONTENT

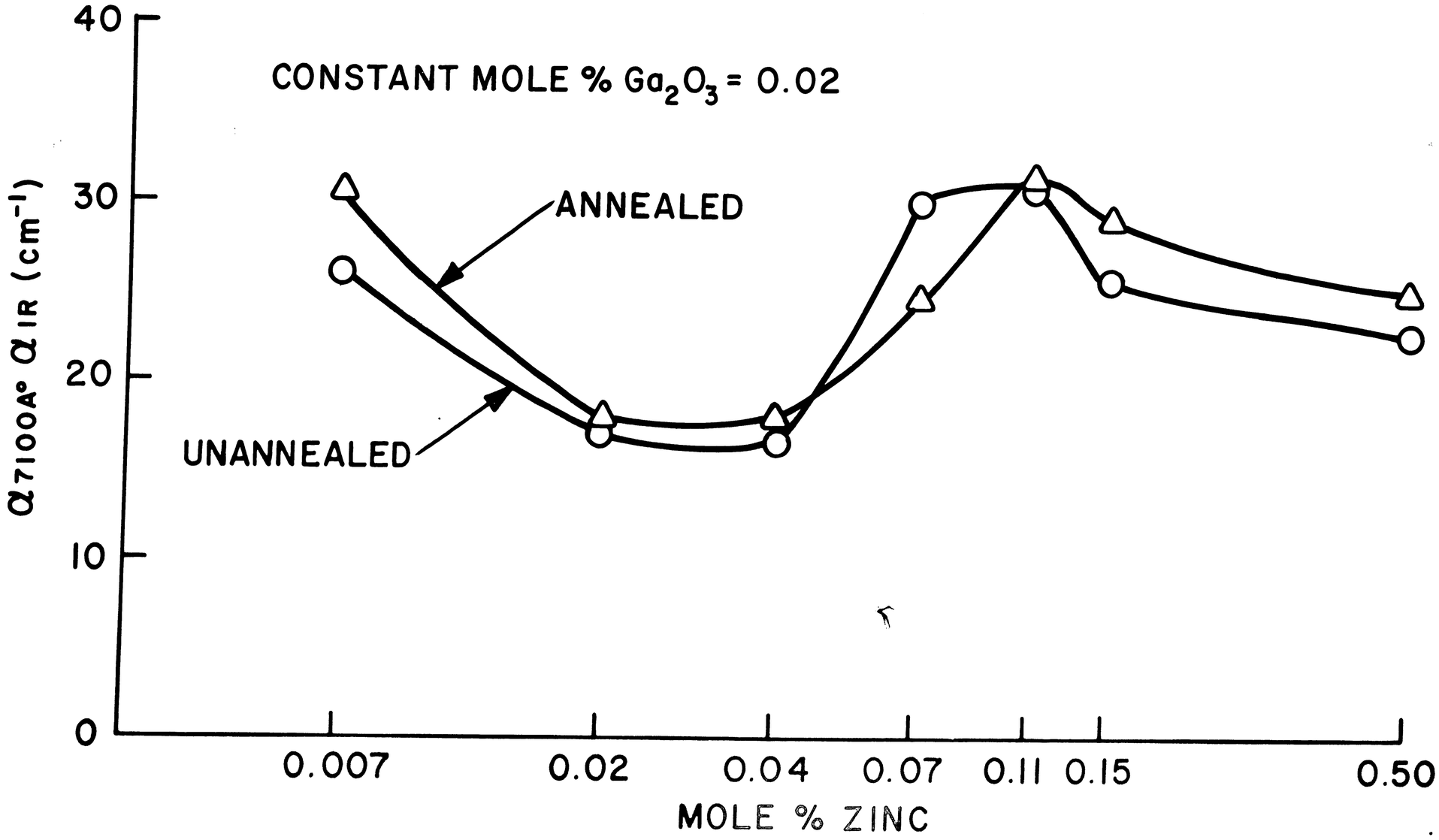

FIGURE 28

RATIO OF PEAK ABSORPTION COEFFICIENTS AT 5840 A° AND 7100 A° VS. ZINC DOPING CONTENT

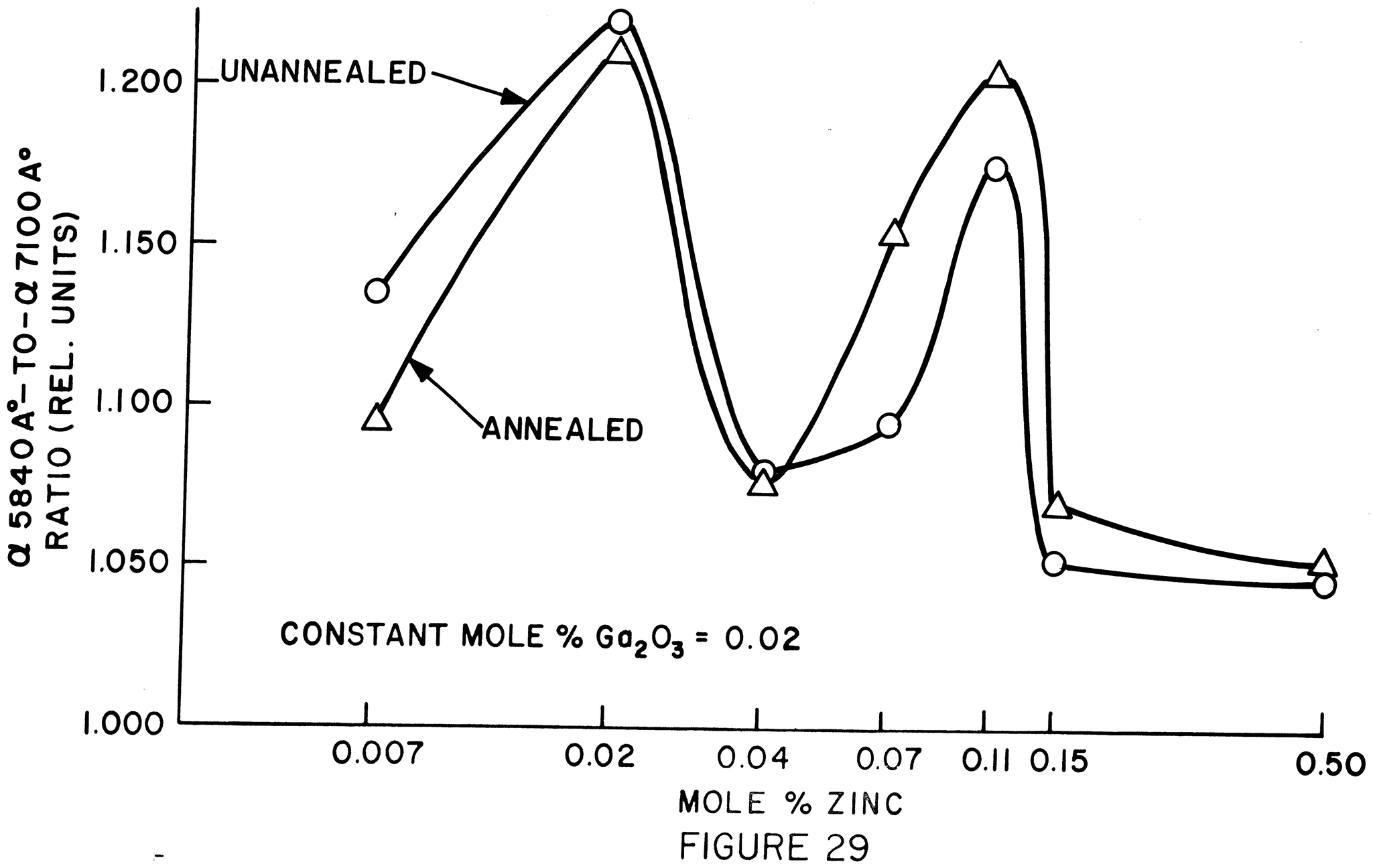

FIGURE 29

TOTAL EFFICIENCY VS. OXYGEN DOPING CONTENT

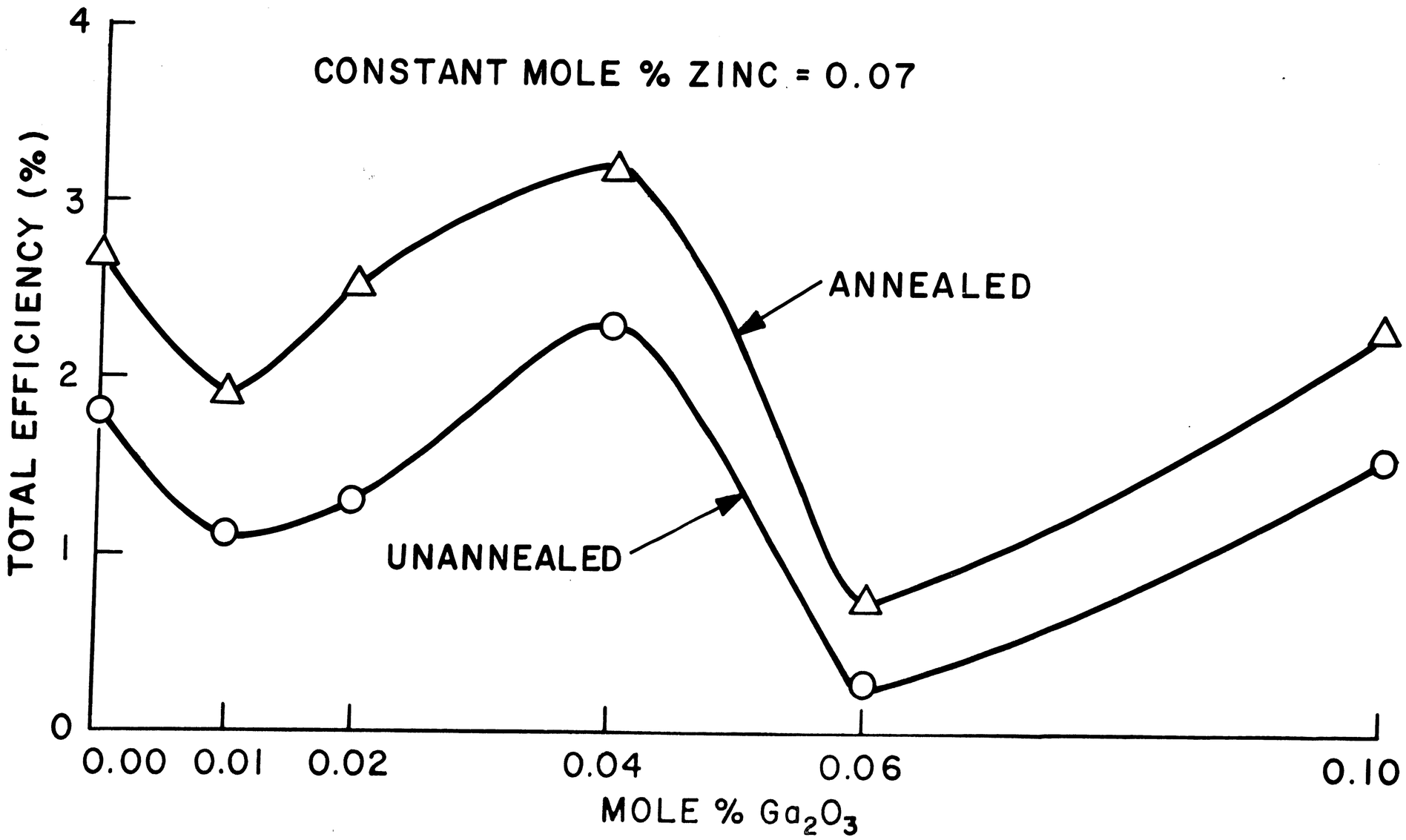

FIGURE 30

RED-TO-INFRARED INTEGRATED INTENSITY RATIO VS. OXYGEN DOPING CONTENT

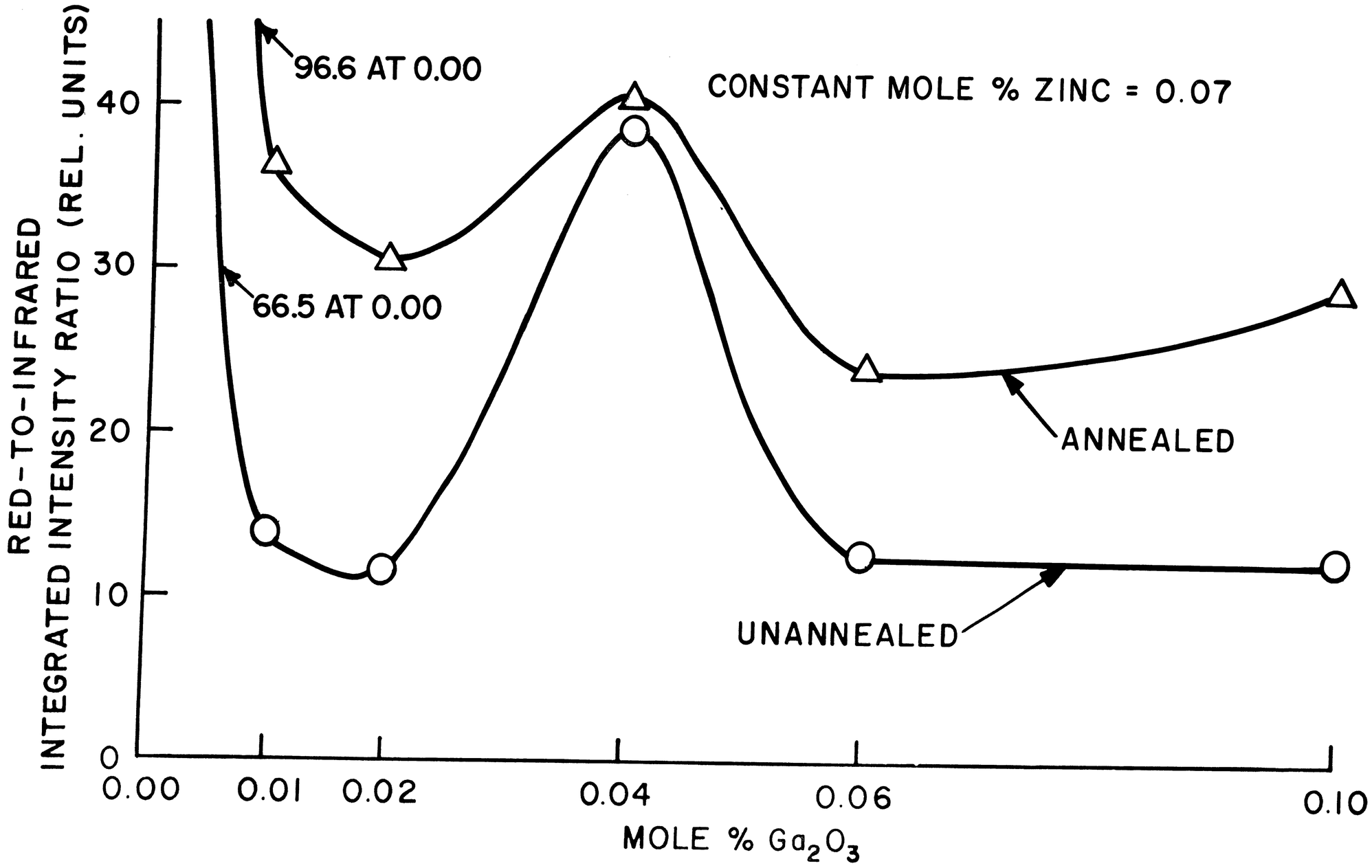

FIGURE 31

RED EXTERNAL EFFICIENCY VS. OXYGEN DOPING CONTENT

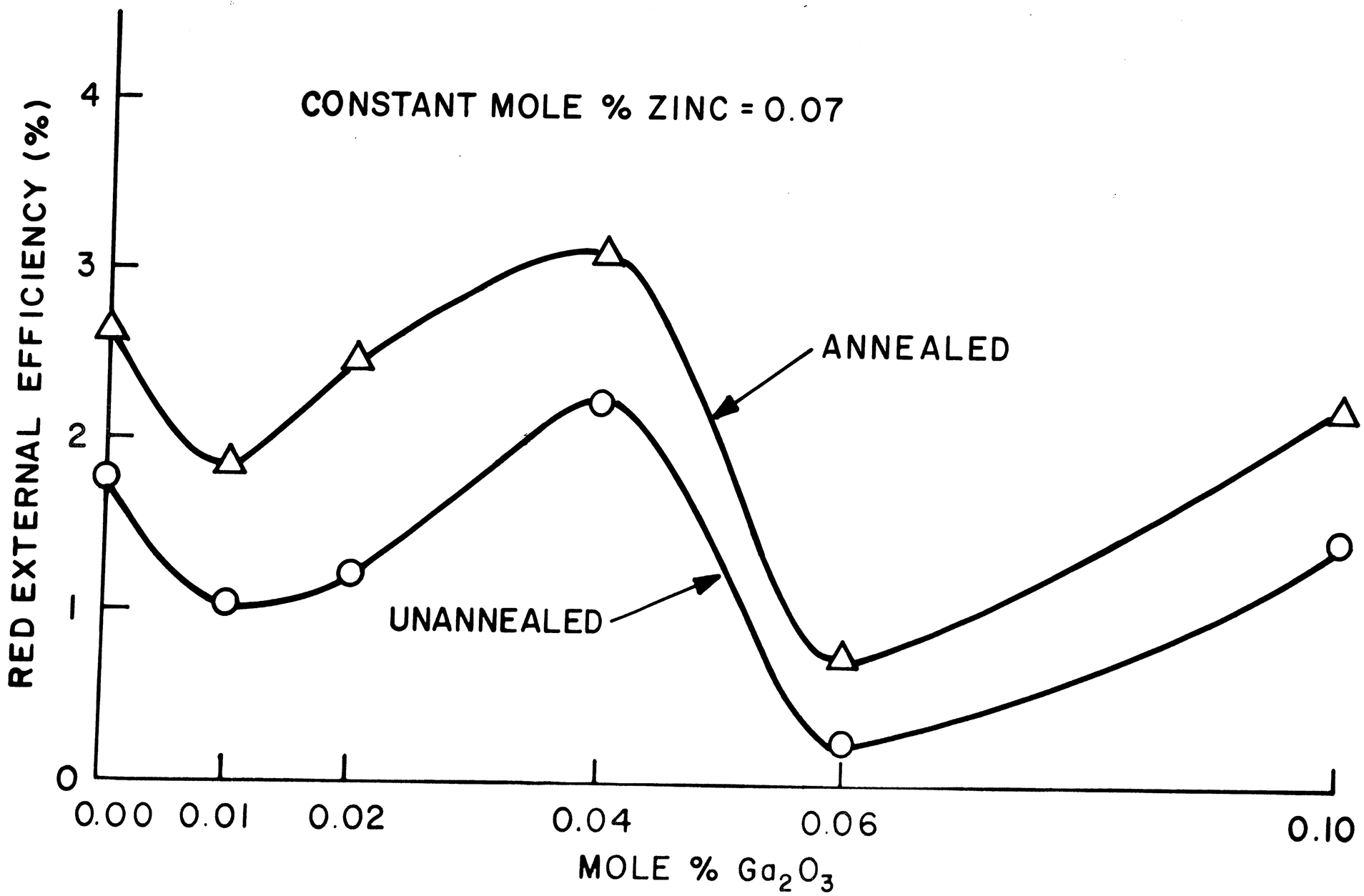

FIGURE 32

INFRARED EXTERNAL EFFICIENCY VS. OXYGEN DOPING CONTENT

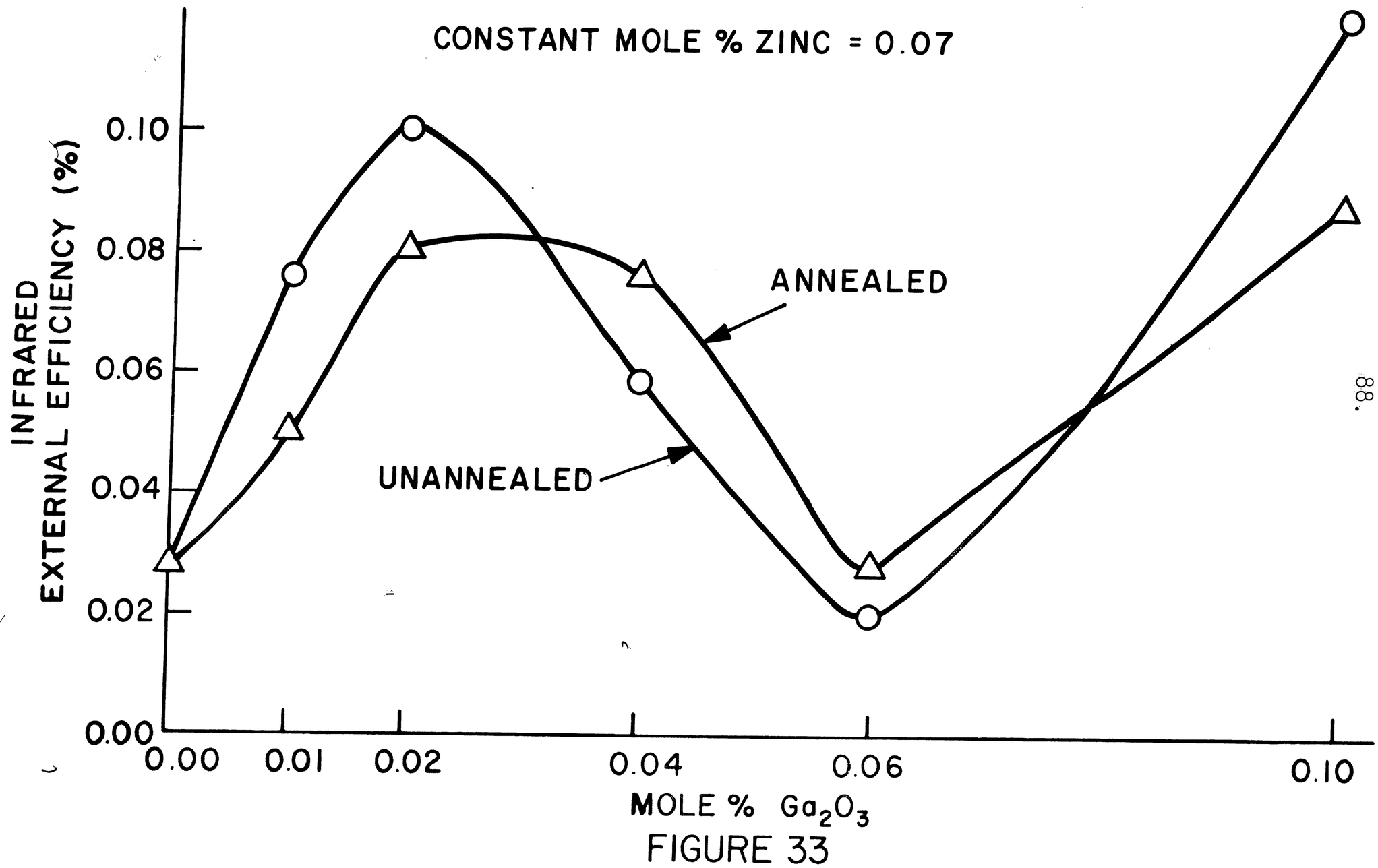

FIGURE 33

PEAK ABSORPTION COEFFICIENT AT 5840 A°
VS. OXYGEN DOPING CONTENT

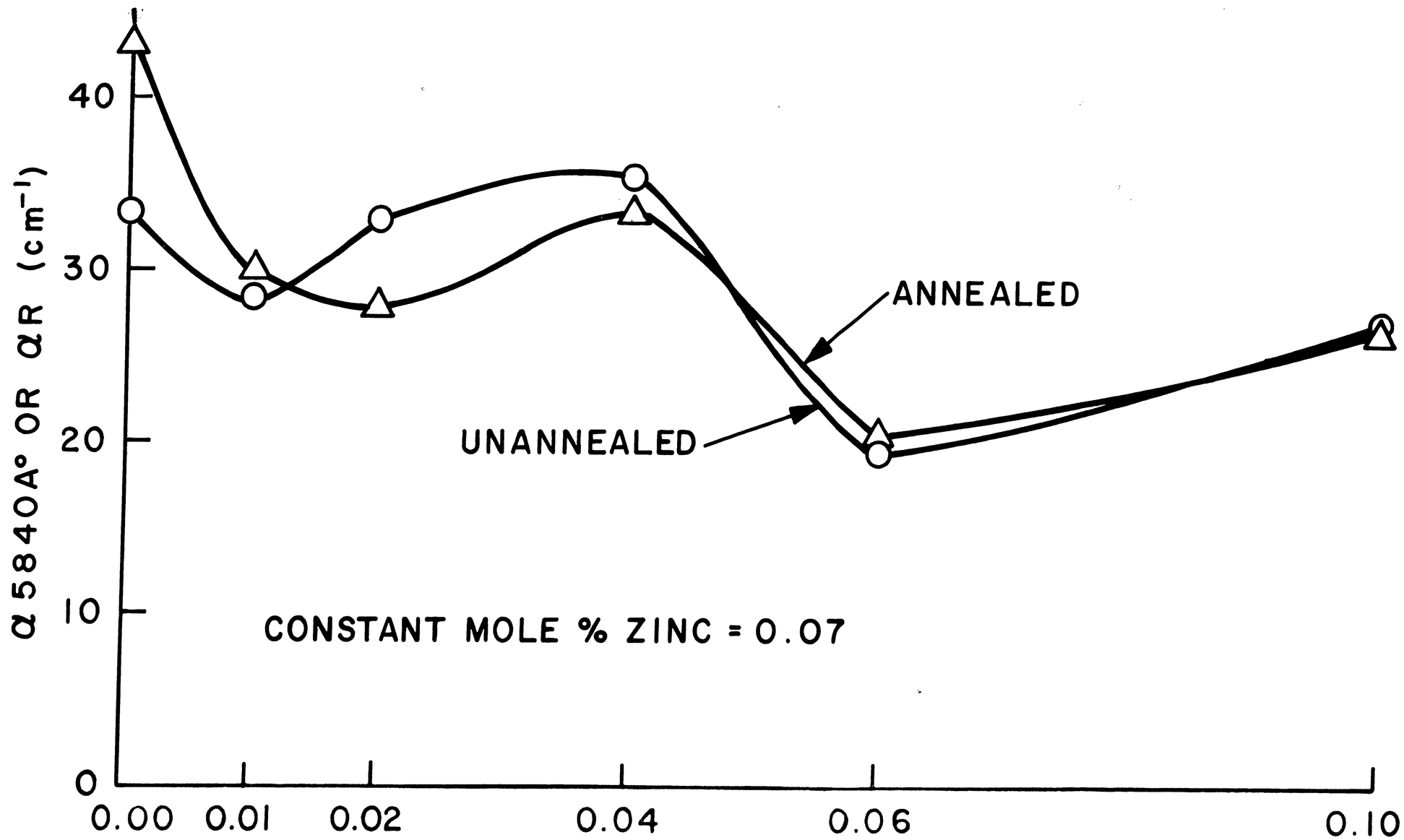

FIGURE 34

PEAK ABSORPTION COEFFICIENT AT 7100 A° vs OXYGEN DOPING CONTENT

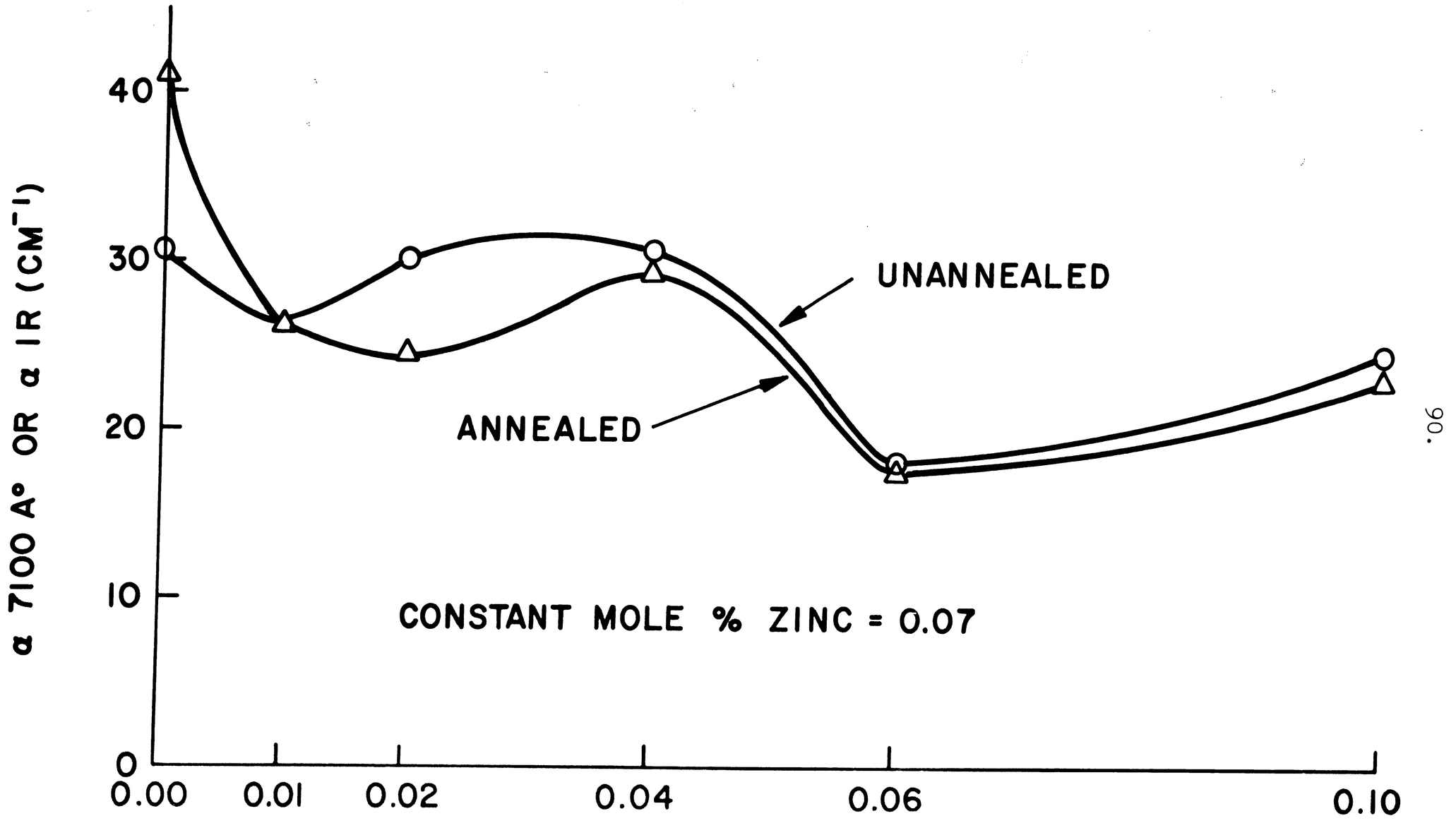

FIGURE 35

RATIO PEAK ABSORPTION COEFFICIENTS AT 5840 A° AND 7100 A° VS. OXYGEN DOPING CONTENT

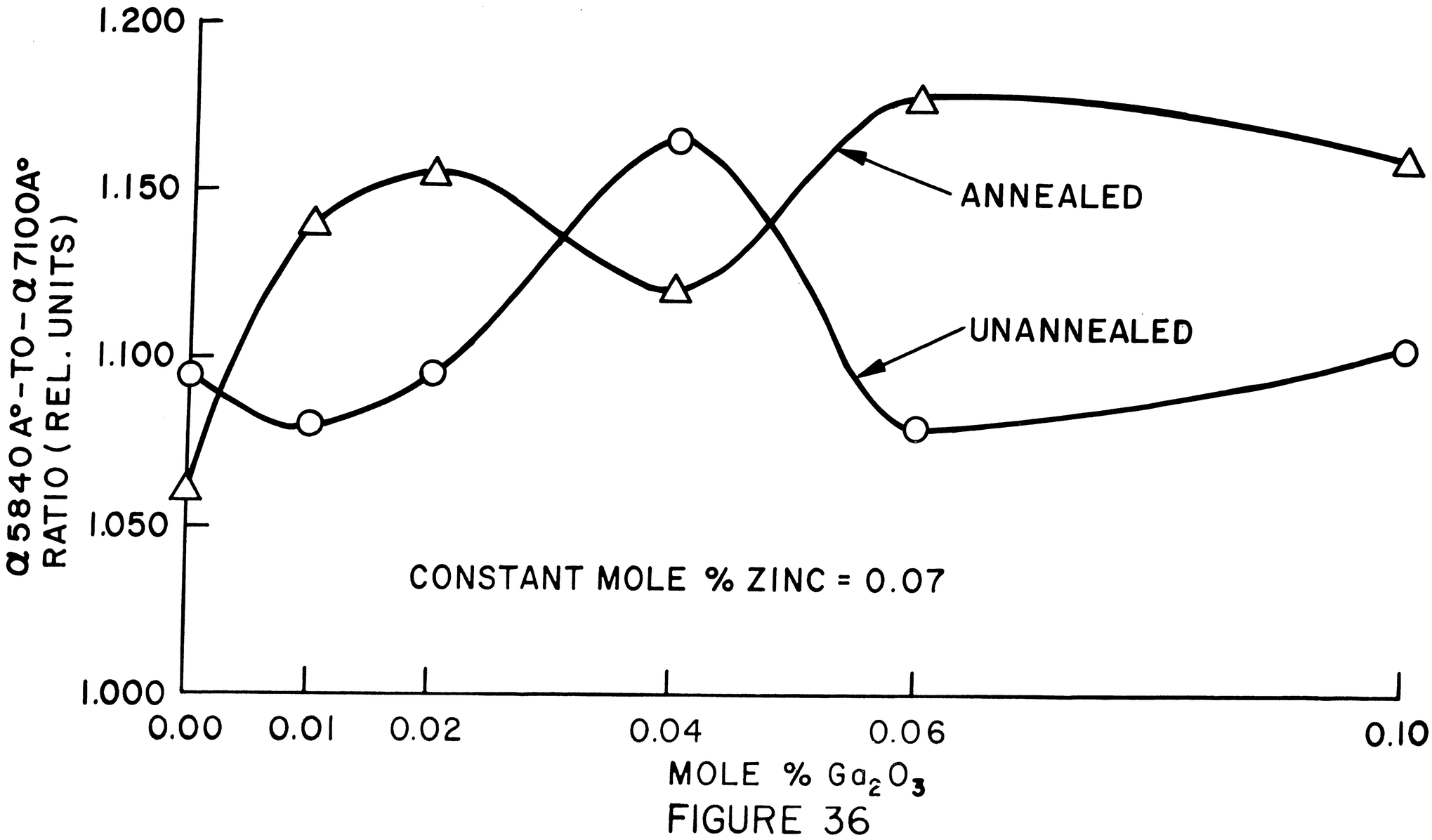

FIGURE 36

Table I

Variable Zinc Doping

U = Unannealed
A = Annealed

SAMPLE NUMBER	MOLE % Zn	MOLE % Ga_2O_3	η_x^T U	η_x^T A	η_i^R/η_i^{IR} U	η_i^R/η_i^{IR} A	η_x^R U	η_x^R A	η_x^{IR} U	η_x^{IR} A
MS80722-1	0.007	0.02	2.84	5.86	2.12	2.88	1.93	4.35	0.91	1.51
MS80722-2	0.007	0.02	4.76	5.50	4.62	5.66	3.92	4.68	0.848	0.825
MS80905-1	0.02	0.02	5.63	6.44	11.5	12.9	5.18	5.97	0.45	0.463
MS80905-2	0.02	0.02	5.07	6.98	6.26	6.30	4.37	6.02	0.70	0.956
MS80912-1	0.04	0.02	2.09	3.01	23.9	30.5	2.01	2.91	0.083	0.095
MS80912-2	0.04	0.02	2.10	3.51	30.5	30.5	2.03	3.40	0.066	0.111
MS80725-1	0.07	0.02	1.30	2.52	11.5	30.5	1.20	2.44	0.104	0.080
MS80916-1	0.11	0.02	1.48	2.10	29.3	41.5	1.43	2.05	0.048	0.049
MS80729-1	0.15	0.02	0.725	0.785	23.9	30.5	0.695	0.760	0.029	0.025
MS80524-1	0.50	0.02	0.213	0.259	30.3	12.9	0.206	0.241	0.007	0.018
MS80524-2	0.50	0.02	0.218	0.275	30.5	16.7	0.211	0.260	0.007	0.015

Table II

Variable Ga_2O_3 Doping

U = Unannealed
A = Annealed

SAMPLE NUMBER	MOLE % Zn	MOLE % Ga_2O_3	η_x^T		η_i^R/η_i^{IR}		η_x^R		η_x^{IR}	
			U	A	U	A	U	A	U	A
MS80715-1	0.07	0.00	1.80	2.67	66.5	96.6	1.77	2.64	0.027	0.027
MS80520-1	0.07	0.01	0.942	1.65	13.7	30.5	0.878	1.60	0.064	0.052
MS80520-2	0.07	0.01	1.26	2.11	13.7	42.1	1.17	2.06	0.086	0.049
MS80725-1	0.07	0.02	1.30	2.52	11.5	30.5	1.20	2.44	0.100	0.080
MS80415-1	0.07	0.04	0.426	1.18	12.8	30.3	0.395	1.14	0.031	0.038
MS80716-1	0.07	0.04	2.06	2.73	40.8	30.5	2.01	2.64	0.049	0.087
SG20424-1	0.07	0.04	2.44	3.50	42.0	42.0	2.38	3.42	0.057	0.081
SG20424-2	0.07	0.04	2.44	3.74	40.8	67.5	2.38	3.69	0.058	0.055
SG20424-3	0.07	0.04	2.22	2.69	30.5	30.5	2.15	2.60	0.070	0.085
MS80516-1	0.07	0.06	0.305	0.493	13.7	19.2	0.284	0.469	0.021	0.024
MS80516-2	0.07	0.06	0.229	0.991	11.4	29.3	0.211	0.958	0.018	0.033
MS80815-1	0.07	0.10	1.62	2.54	12.6	40.8	1.50	2.48	0.120	0.061
MS80815-2	0.07	0.10	1.48	2.03	11.8	16.7	1.36	1.92	0.116	0.115

Table III

Carrier Concentrations

Mole % Zn in Melt	$N_A - N_D$ (cm^{-3})
0.007	2.0×10^{17}
0.02	4.2×10^{17}
0.04	8.0×10^{17}
0.07	1.2×10^{18}
0.11	1.7×10^{18}
0.15	2.0×10^{18}
0.50	3.4×10^{18}

Notes:

1. $N_A - N_D$ = NET acceptor concentration.
2. All samples contain 0.02 mole % Ga_2O_3.
3. These values were supplied by Dr. J. M. Dishman of Bell Telephone Laboratories.

BIBLIOGRAPHY

1. Thomas, D. G., "Electroluminescence," Physics Today, V. 21, No. 2, p. 43, (February, 1968)

2. Epstein, A. S., and Holonyak, N., "Solid State Light," Science Journal, p. 69, (January, 1969)

3. Lorenz, M. R., "Visible Light from Semiconductors," Science, V. 159, No. 3822, p. 1419, (March, 1968)

4. Lorenz, M. R., "The Generation of Visible Light from p-n Junctions in Semiconductors," Transactions of the Metallurgical Society of AIME, V. 245, p. 539, (March, 1969)

5. Dishman, J. M., DiDomenico, Jr., M, and Caruso; R., "Luminescence and Minority Carrier Recombination in P-Type GaP (Zn,O), Physical Review B, V. 2, No. 6., (September, 1970)

6. Dean, P. J., Henry, C. H., and Frosch, C. J., "Infrared Donor-Acceptor Pair Spectra Involving the Deep Oxygen Donor in Gallium Phosphide," Physical Review, V. 168, No. 3., p. 812, (April, 1968)

7. Bhargava, R. N., "Role of Oxygen in (Zn,O) Doped GaP," Physical Review B, V. 2., No. 2., p. 387, (July, 1970)

8. Morgan, T. N., Welber, B., and Bhargava, R. N., "Optical Properties of Cd-O and Zn-O Complexes in GaP," Physical Review, V. 166, No. 3, p. 751, (February, 1968)

9. Cuthbert, J. D., Henry, C. H., and Dean, P. J., "Temperature-Dependent Radiative Recombination Mechanisms in GaP (Zn,O) and GaP (Cd, O)," Physical Review, V. 170, No. 3, p. 739, (June, 1968)

10. Casey, Jr., H. C. and Trumbore, F. A., "Single Crystal Electroluminescent Materials," Material Science and Engineering, V. 6., p. 69, (1970)

11. Sinha, K. P., and DiDomenico, Jr., M., Physical Review B1, V. 2623, (1970)

12. Bhargava, R. N., "Time Decay and Temperature Dependence of Radiative Recombination in (Zn-O) - Doped GaP," Journal of Applied Physics, V. 41, No. 9, p. 3698, (August, 1970)

13. Foster, L. M., and Scardefield, J., "Oxygen Doping of Solution Grown GaP," Journal of Electrochemical Society: Solid State Science, V. 116, p. 494, (1969)

14. Thomas, D. G., Gershenzon, M., and Trumbore, F. A., "Pair Spectra and Edge Emission in Gallium Phosphide," Physical Review, V. 133, No. 1A, p. A269, (January 6, 1964)

15. Logan, R. A., White, H. G., and Trumbore, F. A.,"p-n Junctions in Compensated Solution-Grown GaP," Journal of Applied Physics, V. 38, No. 6, p. 2500, (May, 1967)

16. Logan, R. A.,White, H. G., and Trumbore, F. A., "p-n Junctions in GaP with External Electroluminescence Efficiency 2% at 25°C," Applied Physics Letters, V. 10, No. 7, p. 206, (April 1, 1967)

17. Onton, A., and Lorenz, M. R., "Dependence of Radiative Efficiency in GaP Diodes on Heat Treatment," Applied Physics Letters, V. 12, No. 4, p. 115, (February 16, 1968)

18. Toyama, M., Kasamic, A., Naito, M., and Maeda, K., "Effect of Heat Treatment of Diffused Gallium Phosphide Electroluminescent Diodes," Transactions ofthe Metallurgical Society of AIME, V.245, p. 551, (March, 1969)

19. Gershenzon, M., Trumbore, F. A., Mikulyok, R. M., and Kowalchik, M., "Radiative Recombination Between Deep Donor-Acceptor Pairs in GaP," Journal of Applied Physics, V. 36, No. 5, p. 1528, (1965)

20. Cuthbert, J. D., Henry, C. H., and Dean, P. J., "Temperature-Dependent Radiative Recombination Mechanisms in GaP (Zn,O) and GaP (Cd, O)," Physical Review, V. 170, No. 3, p. 739, (June 15, 1968)

21. Lorenz, M. R., and Pettit, G. D., "Internal Quantum Efficiency of GaP Diodes," Journal of Applied Physics, V. 38, No. 10, p. 3893, (September, 1967)

22. Cheroff, G., Stern, F., and Triebwasser, S., Applied Physics Letters, V. 2., p. 173, (1963)

23. Moser, F., and Urback, F., "Optical Absorption of Pure Silver Halides," Physical Review, V. 102, No. 6, p. 1519, (June, 1956)

24. Hindle, P. H., and Ibbett, R. N., "A Digitization System For a Scanning Spectrometer," Journal of Scientific Instruments, V. 43, p. 209, (1966)

25. Kleinman, D. A., and Spitzer, W. G., "Infrared Lattice Absorption of GaP", Physical Review, V. 118, No. 1, p. 110, (April, 1960)

26. Dean, P. J., and Thomas, D. G., "Intrinsic Absorption - Edge Spectrum of Gallium Phosphide," Physical Review, V. 150, No. 2, p. 690, (October, 1966)

27. Lacey, S. D., "The Absorption Coefficient of Gallium Phosphide in the Wavelength Region 530 to 1100 nm," Solid State Communications, V. 8, pp. 1115 - 1118, (1970)

28. Schulman, J. H., and Compton, W. D., Color Centers in Solids, New York: Macmillan Co., 1962.

29. The presence of Ga_2O_3 in p-type LPE layers was initially observed by M. Kowalchik using optical microscopy. See M. Kowalchik, A. S. Jordan, and M. H. Read, RNP 250, presented at the Atlantic City meeting of the Electrochemical Society, October 4-8, 1970.

30. Angelova, L. A., Bindemann, R., et al., "Photoluminescence of Gallium Phosphide Doped with Zinc and Oxygen," Soviet Physics-Semiconductors , V. 3., No. 2, p. 269, (August, 1969)

31. Miyauchi, T., Sonomura, H., and Yamamoto, N., "Note on Impurity Oxygen in Gallium Phosphide," J. Journal of Applied Physics, V. 8, No. 7, p. 886, (July, 1969)

32. Hughes, D. L., "Annealing Effects on the Photoluminescence of GaP Crystals," Lehigh University Master's Thesis, (June, 1970).

VITA

The author was born on December 29, 1939 in Mount Carmel, Illinois. He completed elementary school and high school in Evansville, Indiana, from which he graduated in 1957.

After graduation, he joined the U.S. Marine Corps, where he served a four-year enlistment ending in 1961. From 1961 to 1962, the author attended Santa Ana College in California, then returned to Indiana and enrolled at the University of Evansville. He graduated in 1966 with the degree of Bachelor of Science in Electrical Engineering.

The first year after receiving his degree, he was employed by Union Carbide Nuclear Division as an Instrumentation Design Engineer. He then joined the Western Electric Company in Indianapolis and worked on the design of test equipment until June, 1969. During the two-year period in Indianapolis, he studied electrical engineering at the Graduate School of Purdue University.

In June, 1969, the author was transferred from Indianapolis to Princeton, New Jersey as a member of the Western Electric - Lehigh University Fellowship Program, while employed at the Western Electric Engineering Research Center.

The author is a member of Kappa Mu Epsilon (mathematics) and the Institute of Electrical and Electronics Engineers.